TECHNISCHE UNIVERSITÄT MÜNCHEN

Lehrstuhl für Biochemische Pflanzenpathologie

Effect of Nitric Oxide on the Growth and Development of *Arabidopsis thaliana*

Gitto Thomas Kuruthukulangarakoola

Vollständiger Abdruck der von der Fakultät Wissenschaftszentrum Weihenstephan für Ernährung, Landnutzung und Umwelt der Technischen Universität München zur Erlangung des akademischen Grades eines

Doktors der Naturwissenschaften

genehmigten Dissertation.

Vorsitzender: Univ.- Prof. Dr. Ralph Hückelhoven

Prüfer der Dissertation:

1. Univ.- Prof. Dr. Jörg Durner
2. Univ.- Prof. Dr. Claus Schwechheimer

Die Dissertation wurde am 20.12.2012 bei der Technischen Universität München eingereicht und durch die Fakultät Wissenschaftszentrum Weihenstephan für Ernährung, Landnutzung und Umwelt am 28.02.2013 angenommen.

PUBLICATIONS

Gaupels F, Kuruthukulangarakoola G T and Durner J (2010) Upstream and downstream signals of nitric oxide in pathogen defence. *Current opinion in plant biology* 16: (707-714). (Review article – Results from my PhD thesis work is not published in this article)

Kuruthukulangarakoola G T and Lindermayr C (2012) Regulation and function of protein S-nitrosylation in plant stress. Stress Signaling in Plants: The Genomics and Proteomics Perspective. *Springer publishing group*. ***In press***. (Book Chapter – Results from my PhD thesis work is not published in this book)

Kuruthukulangarakoola G T, Durner J, Werner H, Hebelstrup K, Michalke B, Sarioglu H, Lang H, Schnitzler J, Albert A and Lindermayr C (2013) Nitric oxide-fixation pin plants: A new pathway for nitrogen assimilation in *Arabidopsis thaliana*. ***Manuscript prepared for submission***.

INDEX

SUMMARY

Nitric oxide (NO) is a signaling molecule that regulates various biological processes in plants. NO accumulation and downstream NO signaling plays an important role in plant defense responses. S-nitrosoglutathione reductase (GSNOR) is an enzyme that can metabolize the physiological NO donor S-nitrosoglutathione (GSNO). However, an exact enzymatic source for NO production during the defense response in plants is not known. Hence most of the studies to understand NO mediated signaling in the plants have made use of chemicals that can donate NO moiety. Reports on fumigating plants with NO gas to understand its effect on plant physiology and NO signaling are limited. In this context, we have performed a long-term fumigation of *Arabidopsis thaliana* wild type (WT) and *GSNOR* knock-out mutant (*atgsnor-KO*) plants with different NO concentrations (up to 3 ppm) to study its impact on plant physiology and to investigate the role of GSNOR in regulating phytotoxic effects of NO fumigation. Rosettes of the plants grown under ambient conditions developed red senescence phenotype due to anthocyanin accumulation. Accumulation of anthocyanin was associated with the nitrogen (N) deficiency in the soil. Plants fumigated with NO showed delayed red senescence and reduced anthocyanin accumulation in both WT and *atgsnor-KO* plants. Though there was an increase in the nitrosothiol content after NO fumigation, GSNOR accumulation and its activity remained unaffected suggesting that this enzyme has no regulatory role under these conditions. Analyses of transcriptome, proteome and metabolites showed that the plants fumigated with 3 ppm NO used exogenous NO gas to compensate for the declining N metabolites received from the soil. Class 1 non-symbiotic hemoglobin (GLB1) is known to oxidize NO into nitrate during hypoxic stress. Our studies showed that not only GLB1 but also class 2 non-symbiotic hemoglobin (GLB2) can mediate oxidation of NO to nitrate during NO fumigation. Moreover, generated nitrate was used by the plants for N-assimilation which resulted in enhanced growth and development. After NO fumigation, plants overexpressing *GLB1* and *GLB2* genes showed enhanced growth of rosette and vegetative shoot compared to WT controls.

To summarize, our studies suggested a new pathway for the plants termed as NO-fixation pathway wherein NO accumulation is used for the growth and development of the plants via improved N-assimilation. Careful engineering of plants can probably raise NO-fixation pathway to an economically important trait for the biomass production and improved crop yield.

ABBREVIATIONS

2D-DIGE	Two dimensional difference gel electrophoresis
ANOVA	Analysis of variance
AP	Alkaline phosphatase
atgsnor-KO	T-DNA insertion mutant of S-nitrosoglutathione reductase
BSA	Bovine serum albumin
C	Carbon
βCA1	Beta-carbonic anhydrase 1
βCA2	Beta-carbonic anhydrase 2
cDNA	Complementary deoxyribonucleic acid
CO_2	Carbon dioxide
Col-0	Columbia-0
DAG	Days after germination
DMF	Dimethylformamide
DNA	Deoxyribonucleic acid
FDR	False discovery rate
FW	Fresh weight
GLB	Non-symbiotic hemoglobin
GLB1	Class 1 non-symbiotic hemoglobin
GLB2	Class 2 non-symbiotic hemoglobin
GLB1-Ox	Plants overexpressing class 1 non-symbiotic hemoglobin
glb1-RNAi	RNAi silenced mutant plants of class 1 non-symbiotic hemoglobin
glb2-KO	Knock-out mutant plants of class 2 non-symbiotic hemoglobin
GLB2-Ox	Plants overexpressing class 2 non-symbiotic hemoglobin
GO	Gene Ontology
GSH	Glutathione
GSNO	S-nitrosoglutathione
GSNOR	S-nitrosoglutathione reductase
HPLC	High-performance liquid chromatography
IS	Internal standard
JA	Jasmonic acid
MDHAR	Monodehydroascorbate reductase
N	Nitrogen
NEM	N-ethylmaleimide
NIA2	Nitrate reductase 2

NiR1	Nitrite reductase 1
NO	Nitric oxide
NO_2	Nitrogen dioxide
NOA	Nitric oxide analyzer
NOD	Nitric oxide degrading dioxygenase
NO_x	Nitrogen oxides
O_2	Oxygen
PAL	Phenylalanine ammonia lyase
PAR	Photosynthetically active radiation
PAP1	Production of anthocyanin pigment 1
PAP2	Production of anthocyanin pigment 2
PBS	Phosphate buffered saline
PCR	Polymerase chain reaction
PFD	Photon flux density
ppb	Parts-per-billion
ppm	Part-per-million
RIN	RNA integrity number
RNA	Ribonucleic acid
ROI	Reactive oxygen intermediate
RSNO	Nitrosothiol
RT	Room temperature
SA	Salicylic acid
SAG12	Senescence-associated gene 12
SDS-PAGE	Sodium dodecyl sulfate polyacrylamide gel electrophoresis
WAG	Weeks after germination
TF	Transcription factor
UV	Ultraviolet
Ws	Wassilewskija
WT	Wild type

LIST OF FIGURES AND TABLES

LIST OF FIGURES

LIST OF TABLES

LIST OF SUPPLEMENTARY FIGURES

LIST OF SUPPLEMENTARY TABLE

1 INTRODUCTION

1.1 Nitric oxide signaling in plants

Nitric oxide (NO) is a gaseous free radical involved in many diverse biological pathways mediating multitude of physiological functions in plants and animals. Until late 1980's NO was considered only as an air pollutant, however in 1987 for the first time it was reported as a signaling molecule in animals (Ignarro et al., 1987a, Ignarro et al., 1987b, Palmer et al., 1987). On the other hand, in plants, NO was merely considered as a by-product during nitrate assimilation. Nevertheless, in 1996 for the first time it was detected as a gas emitted from pea foliage. The rate of emission of NO was found to be close to that of ethylene. Interestingly, both NO and ethylene affect the rate of senescence and maturation in plants (Leshem & Haramaty, 1996). First evidences for the signaling function of NO in plants came in simultaneously from two independent works involving plant defense responses (Durner et al., 1998, Delledonne et al., 1998). Since then, studies have revealed the ubiquitous signaling nature of NO in regulating variety of physiological processes in plants like germination (Bethke et al., 2004b), stomatal closure (Neill et al., 2002, Garcia-Mata et al., 2003), flowering (He et al., 2004), senescence (Corpas et al., 2004, Guo & Crawford, 2005), wounding responses (Huang et al., 2004), and abiotic stresses (Corpas et al., 2011). This astonishingly ubiquitous signaling behavior of NO is scrutinized by plants through controlled regulation of NO bioactivity at different levels ranging from controlled NO production to site-specific reactivity and finally, the NO turnover.

1.1.1 Upstream signaling and induction of NO synthesis in plants

Signaling pathways involving extracellular adenosine triphosphate, phosphatidic acid, cyclic nucleotide phosphate, calcium and mitogen-activated protein kinases are all known to act as upstream regulators of endogenous NO production in plants during various stress-related responses (Sueldo et al., 2010, Gaupels et al., 2011, Ma & Berkowitz, 2011). However, efforts to identify the mechanism through which these upstream signaling events regulate NO production are hampered due to the fact that an exact enzymatic source of NO production is yet to be revealed in plants. Recently, Gaupels et. al. have speculated the possible upstream cellular signaling processes with respect to NO production based on their position in relation to NO production in the signaling cascade and their influence on NO production (Gaupels et al., 2011).

Though an exact enzymatic source for NO production in not known, several oxidative and reductive pathways have been suggested (Gupta et al., 2011a).

1.1.2 Unique nitric oxide biochemistry of NO

Stress related responses are often associated with an increase in the steady-state levels of cellular NO in plants. The unique chemistry of NO allows it to exist in three redox-related forms, all with different biochemical properties; the reduced nitroxyl anion (NO^-), the NO radical ($^{\cdot}NO$) and the oxidized nitrosonium cation (NO^+) each with different oxidation state for the nitrogen atom i.e. +1, +2 and +3, respectively (Arnelle & Stamler, 1995). NO can react with thiols in the cellular thiol pool covalently and reversibly to from S-nitrosothiols (RSNO) in a process generally termed as S-nitrosylation. S-nitrosylation is the main means of mediating NO signaling. Cellular cysteine thiol pool comprises of free cysteine, glutathione (GSH), peptides and proteins with redox-sensitive cysteine residue that are susceptible to NO modification. Upon S-nitrosylation, they yield S-nitrosocysteine (CySNO), S-nitrosoglutathione (GSNO) and S-nitrosylated peptides and proteins respectively (Gow et al., 1997, Keszler et al., 2010). An exact *in vivo* reaction mechanism describing the formation of RSNO from NO is yet unknown. However, the intrinsic biochemistry of NO suggests multiple reaction pathways for S-nitrosylation mechanisms with evidences supported by various *in vitro* studies. NO^- (reduced form of $^{\cdot}NO$) can exist in two chemical forms; high energy singlet form and low energy triplet form, with zero or two unpaired electrons respectively (Lipton et al., 1998). In mammals, neuronal nitric oxide synthase produces high energy singlet NO^- that reacts with thiols to form S-nitrosothiols (Schmidt et al., 1996). However, it is not clear whether this is one step process that leads to direct RSNO formation. Conversely, low energy triplet NO^- may react with dioxygen to form peroxynitrite (Lipton et al., 1998) which can indirectly influence S-nitrosylation (Balazy et al., 1998, van der Vliet et al., 1998). Various pathways that have been suggested based on the *in vitro* studies are summarized in Figure 1. In oxidative pathway, a pH dependent conversion of nitrite (NO_2^-) into dinitrogen trioxide (N_2O_3) (Figure 1 - pathway marked in red) that facilitates RSNO formation (Guikema et al., 2005) has been suggested. The apoplast of plants is acidic in nature and therefore it might be mediating this pathway in RSNO formation (Yu et al., 2000, Bethke et al., 2004a). Direct oxidation of $^{\cdot}NO$ by oxygen (O_2) depends on the concentration of available $^{\cdot}NO$ and O_2 (Figure 1A – reactions highlighted with green arrows) (Wink et al., 1994, Goldstein & Czapski, 1996). $^{\cdot}NO$ burst is a typical stress-associated phenomenon in plants (Desikan et al., 2002, Zeidler et al.,

2004) and thus it is possible that under these conditions oxidation of ˙NO to $^{\cdot}NO_2$ occurs to counteract exceeding levels of cellular ˙NO. There are many mechanisms proposed in Radical-mediated pathway (see the legend of Figure 1B). Peroxynitrite ($OONO^-$) mediated RSNO formation is interesting because it is often formed during stress conditions from accumulating free radicals ˙NO and $O_2^{\cdot -}$. RSNO formation from $OONO^-$ is possible by a direct electrophilic attack on the thiolate anion (Figure 1B – reactions highlighted with black arrow) (van der Vliet et al., 1998) or through an intermediate thiyl radical formation (Figure 1B – reactions highlighted with blue arrow) (Goldstein et al., 1996, Keszler et al., 2010).

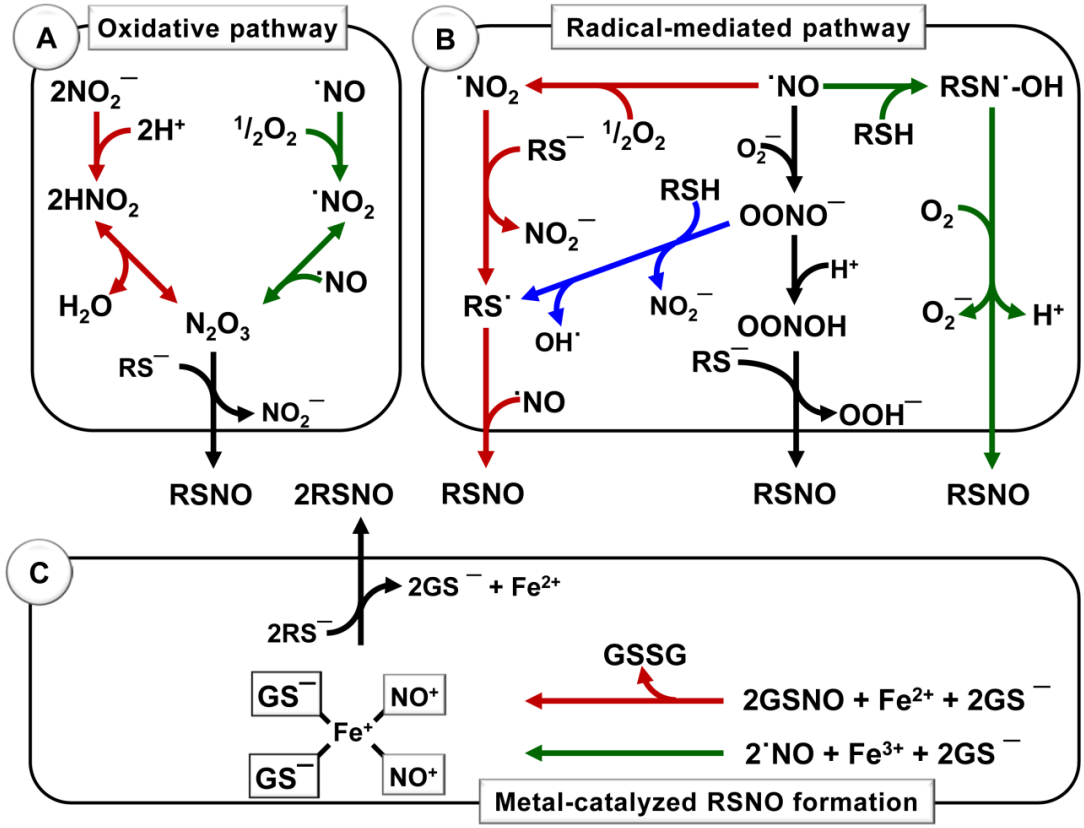

Figure 1 - Pathways leading to S-nitrosothiol (RSNO) formation.
(A) N_2O_3 can be formed from protonated nitrite at very low pH (red arrows) and by the auto-oxidation of ˙NO in an O_2 rich environment (green arrows). N_2O_3 provides NO^+ equivalence to nucleophilic thiols to form RSNO (black arrows). (B) $RS^{\cdot}$ radicals are produced either by peroxynitrite radical (blue arrows) or by the auto-oxidation products of ˙NO. $RS^{\cdot}$ formed directly reacts with ˙NO radical to form RSNO (red arrows). In the presence of thiolate anions (RS^-) protonation of peroxynitrite can also result in the formation of RSNO (black arrows). Furthermore, ˙NO can form an intermediate radical with thiols which then oxidizes to form RSNO (green arrows). (C) Chelatable iron pool can mediate the formation of dinitrosyl iron complexes (red and green arrows) that yields NO^+ equivalence to form RSNO (black arrows).

Due to the high affinity of iron for NO they form coordinate complexes known as iron-nitrosyl complexes. Though they are known to mediate RSNO formation in animals, a similar pathway is yet to be revealed in plants (Figure 1C) (Kim et al., 2000, Simontacchi et al., 2012).

1.1.3 Protein-S-nitrosylation and its impact on plant physiology as a signaling process

NO mediates majority of its signaling processes via S-nitrosylation of proteins. Analysis of GSNO-treated cell cultures, NO-treated plants, infected plants and plants undergoing HR showed that most of the physiologically important proteins in plants are targets of S-nitrosylation (Lindermayr et al., 2005, Romero-Puertas et al., 2008, Maldonado-Alconada et al., 2011, Yun et al., 2011). Until now, majority of the identified proteins were those involved in stress related defense responses. Figure 2 shows some of the important S-nitrosylated proteins involved in stress-related responses and the potential role of this modification in regulating biological processes.

In *Arabidopsis*, AtRBOHD (NADPH-oxidase) activity is required for the pathogen-induced reactive oxygen intermediates (ROI) production and disease resistance (Torres et al., 2002). Interestingly, during HR the activity of AtRBOHD is inhibited by S-nitrosylation of its cysteine residue (Cys890) (Yun et al., 2011) (Figure 2). Salicylic acid (SA) binds to SA-binding protein 3 (SAPB3) and activates its carbonic anhydrase activity and thereby positively regulates the plant defense response. S-nitrosylation of SABP3 is known to reduce its SA binding ability resulting in the reduction of the carbonic anhydrase (CA) activity of the enzyme (Wang et al., 2009) (Figure 2). Both the studies (S-nitrosylation of AtRBOHD and SABP3) emphasize the negative or a feed-back regulatory role of NO in defense response.

Non-expressor of pathogen related proteins 1 (*NPR1*) is a transcriptional co-activator of pathogen related gene 1 (PR1). Endogenous NPR1 is located in the cytoplasm in an oligomeric status. Upon SA-dependent activation NPR1 dissociates into its monomers, which are translocated into the nucleus (Mou et al., 2003, Pieterse & Van Loon, 2004). S-nitrosylation of NPR1 facilitates its oligomerization, which keeps it in the cytosol and is essential for NPR1 homeostasis upon SA induction (Tada et al., 2008). The monomerization of NPR1 is catalyzed by thioredoxin TRX-5h, which reduces NPR1 and allows its translocation into the nucleus. But surprisingly, in *Arabidopsis* mesophyll protoplasts nuclear localization of NPR1 is promoted by GSNO (Lindermayr et al., 2010). Together, these studies suggest that S-nitrosylation might be

serving as an intermediate of oligomeric and monomeric forms making their redox transition easier (Figure 2). Inside the nucleus NPRI interacts with the transcription factor TGA1 (TGACG motif binding factor) and activates *PR1* gene expression (Despres et al., 2003). Both NPR1 and TGA1 are S-nitrosylated when treated with GSNO resulting in enhanced DNA binding of the NPR1/TGA1 complex (Lindermayr et al., 2010).

Glycine decarboxylase complex (GDC) is a key enzyme involved in plant metabolic process. Upon inhibition it switches its function to ROI production that induces cell death (Palmieri et al., 2010). Inhibition of the GDC activity is a part of stress-related response of *Arabidopsis* to the bacterial elicitor hairpin and can result in ROI accumulation and cell death (Palmieri et al., 2010). S-nitrosylation/S-glutathionylation of GDC inhibited its metabolic enzyme activity (Palmieri et al., 2010) (Figure 2). Another important metabolic enzyme that was identified to undergo S-nitrosylation is Glyceraldehyde-3-phosphate dehydrogenase (GAPDH) (Lindermayr et al., 2005). In rat cells S-nitrosylated GAPDH interacts with the E3-ubiqitin-ligase Siah1, translocates into the nucleus and mediates cell death (Sen et al., 2008). Though the treatment of the enzyme with GSNO inhibited enzymatic activity of GAPDH in plants, its nuclear translocation function is not proven yet (Figure 2). S-adenosylmethionine synthetase (SAMS) is an enzyme that catalyzes the biosynthesis of S-adenosylmethionine (SAM), a precursor of ethylene. Among the three known isoforms of SAMS, SAMS1 can be regulated by S-nitrosylation (Lindermayr et al., 2006) (Figure 2).

Tyrosine nitration is another post translational mechanism mediated by NO. Interestingly, S-nitrosylation can also regulate tyrosine nitration. Defense related responses in plants are accompanied by $OONO^-$ accumulation (Saito et al., 2006, Gaupels et al., 2011). In plants however, detoxification of $OONO^-$ is carried out by peroxiredoxin II E (PrxII E). During HR response PrxII E gets S-nitrosylated and its activity are inhibited (Romero-Puertas et al., 2007) (Figure 2). This allows the accumulation of peroxynitrite which can mediate tyrosine nitration. Consequently, higher tyrosine nitrate levels can be found in plants undergoing biotic stress (Saito et al., 2006). In sunflower-mildew interaction, susceptible cultivars with increased levels of RSNO showed increased tyrosine nitrate levels whereas resistant cultivars did not (Chaki et al., 2009). Moreover, enhanced RSNO levels are accompanied by accumulation of nitrated tyrosine residues in sunflower after mechanical wounding (Chaki et al., 2011b). This correlation between

RSNO levels and tyrosine nitration is again seen in sunflower plants stressed with high temperature (Chaki et al., 2011a).

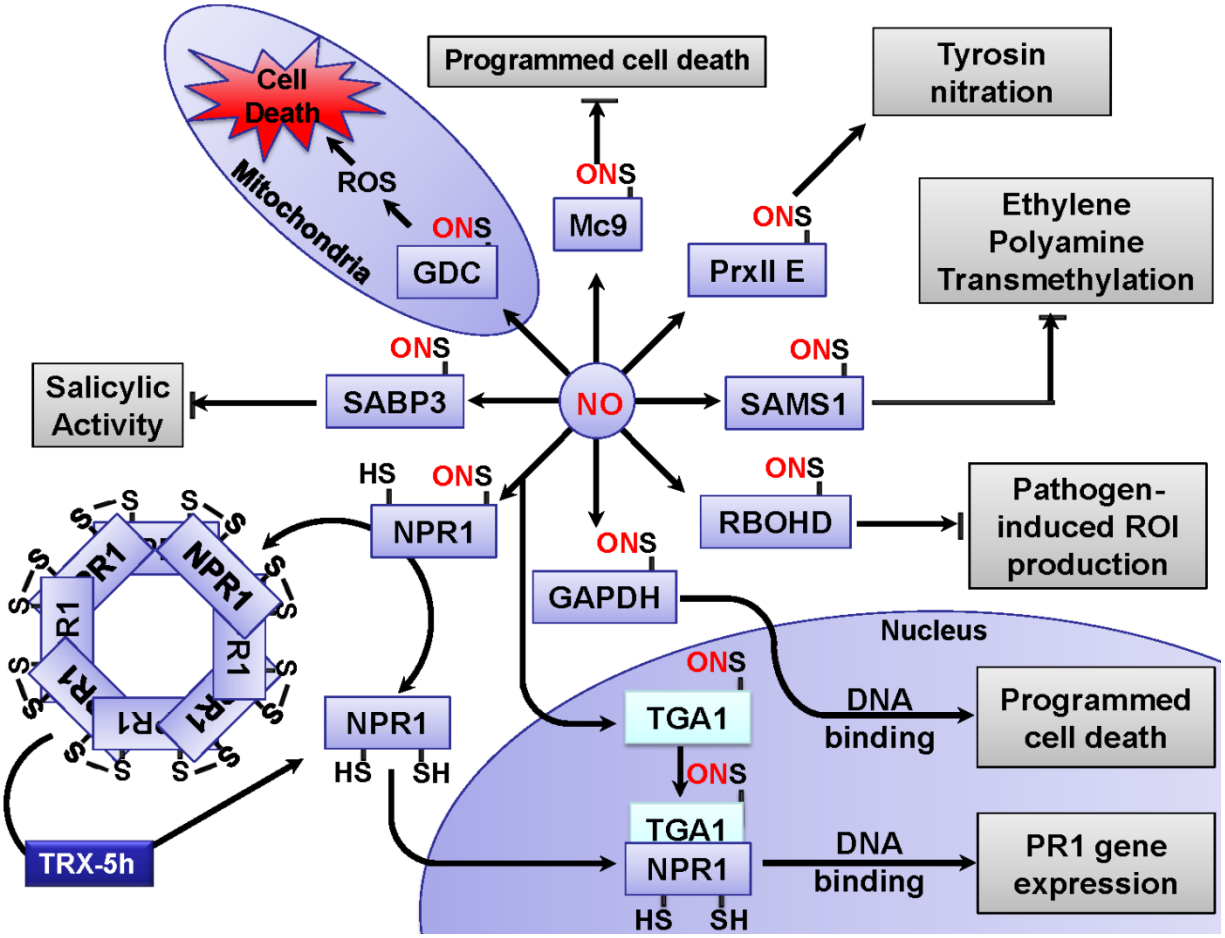

Figure 2 – Function of protein-S-nitrosylation in plant stress response
Stress-induced accumulation of nitric oxide species can inhibit, activate or alter the function of proteins through S-nitrosylation. The activity of SABP3 (important mediator of SA signaling), Mc9 (cysteine protease activity), PrxII E (detoxifying peroxynitrite – regulate tyrosine nitration), SAMS1 (enzyme involved in ethylene and polyamine synthesis and transmethylation reactions) and RBOHD (synthesis of pathogen-induced ROI) is inhibited by S-nitrosylation. Furthermore, GDC inhibition induces mitochondrial ROI production and cell death. S-Nitrosylation of mammalian GAPDH mediates its nuclear localization and induces cell death. Plant GAPDH can also be S-nitrosylated, but its role in cell death is not yet known. Monomer to oligomer transition of NPRI is proposed to be mediated by S-nitrosylation and reversible transition by thioredoxin and induce PR1 gene expression. Moreover, NO-treatment enhances the DNA binding activity of the NPR1/TGA1 complex.

Plant metacaspases are cysteine-dependent proteases, which contain a specific cysteine residue that can serve as a nucleophile for the substrate to mediate peptide bond hydrolysis. *Arabidopsis* has nine metacaspases groups that are classified into two types based on their difference in the N-terminal region (Coll et al., 2010). In Type II metacaspase 9 (MC9), the cysteine residues at

the active site are known to be S-nitrosylated. Consequently, autoprocessing and proteolytic activity of MC9 are suppressed (Belenghi et al., 2007) (Figure 2).

1.2 Regulation of NO signaling

Besides its signaling functions, NO can also be a deleterious free radical. With its unique chemistry, NO can react with a wide variety of other cellular free radicals (Figure 1), which in turn can modify unspecific cellular targets and dangerously affect the cellular processes. Thus, it is important to regulate NO levels through its metabolism. As a signaling mechanism, it is also important to regulate S-nitrosylation by reversing the modification. Removing NO moiety from the S-nitrosylated cysteine residue of the proteins, known as denitrosylation, is very important for proper regulation of protein S-nitrosylation. Although it is known that several enzymes can mediate denitrosylation, mainly S-nitrosoglutathione reductase (GSNOR) and thioredoxin/thioredoxin reductase are known to have significant role in mediating denitrosylation in animals (Figure 2) (Benhar et al., 2009, Lopez-Sanchez et al., 2010). A similar role of their counterparts in plants, especially that of GSNOR is merely emerging and is of considerable interest. Non-symbiotic hemoglobin in plants is shown to metabolize the accumulated NO in stressed plants (Igamberdiev et al., 2011).

1.2.1 Regulation of S-nitrosylation by GSNOR

Glutathione (GSH) is an important regulator of redox status and redox signaling processes in plants (Reviewed by Foyer and Noctor 2011). NO can S-nitrosylate the cysteine residue of GSH to form GSNO (Figure 3 – reaction pathway A). Though the reaction mechanism of GSNO formation is still debatable, it is now known that GSNO can function as a physiological NO donor and can mediate the transfer of NO group to modify proteins that are functionally important in plants (Figure 3 – reaction marked inside triangle). Search for an enzyme that can mediate metabolism of GSNO has led to the identification of GSNOR that is conserved in almost all the living systems including plants (Liu et al., 2001, Sakamoto et al., 2002, Diaz et al., 2003). GSNOR was classified to class III alcohol dehydrogenase (ADH) and was originally found to function as glutathione dependent-formaldehyde dehydrogenase (FALDH) in plants. FALDH has been a well characterized enzyme in several plant species (Uotila & Koivusalo, 1979, Martinez et al., 1996) before its GSNOR activity was discovered (Sakamoto et al., 2002, Achkor et al., 2003, Diaz et al., 2003). GSNOR metabolizes GSNO with NADH as an electron donor (Figure 3

– Reaction pathway B) (Wilson et al., 2008). Thus, GSNOR is associated with the removal of NO through GSNO metabolism. This is evident in the *GSNOR* knock-out (*atgsnor-KO*) and overexpression lines of *Arabidopsis* plant that showed increased and reduced nitrosothiol levels respectively (Feechan et al., 2005). GSNOR, however, cannot metabolize S-nitrosylated moiety of proteins or peptides (Liu et al., 2001).

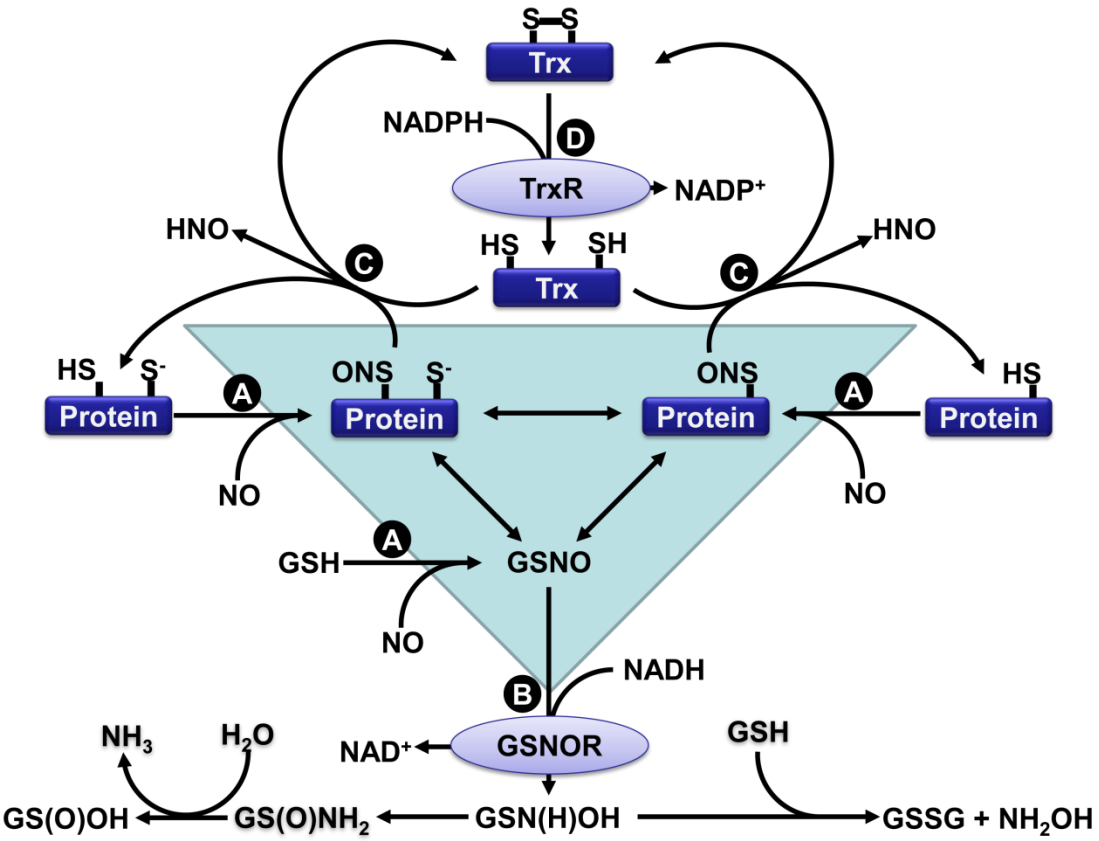

Figure 3 – Regulation of S-nitrosylation signaling mechanism.
RSNO pool comprises of S-nitrosylated proteins and GSNO (inside the triangle) formed by incorporation of NO to their thiol moiety (reactions marked A) and by transferring NO groups between each other through trans-nitrosylation. GSNO from the RSNO pool is metabolized and removed by GSNOR (reaction marked as B). S-nitrosylated proteins on the other hand might be regulated by denitrosylation mediated by Trx (reaction marked as C). Oxidized Trx is further recycled by TrxR (reaction marked as D).

There is an equilibrium that exists between low molecular weight S-nitrosothiols like GSNO and S-nitrosylated proteins and peptides (Seth & Stamler, 2011). This equilibrium allows regulation of GSNO metabolism by GSNOR to indirectly regulate S-nitrosylated proteins (Figure 3 – reaction marked inside the triangle). In *atgsnor-KO* mutant plants, an increase in low molecular weight nitrosothiols resulted in a corresponding increase in the levels of high molecular weight S-nitrosothiols that is assumed to include proteins which is a clear indication of indirect effect of

GSNOR regulation of protein S-nitrosylation (Liu et al., 2001, Liu et al., 2004, Yun et al., 2011). GSNOR is receiving increasing attention for its role in plant stress responses. Physiological role of GSNOR is evident from the *atgsnor-KO* plants that showed delayed and stunned growth phenotype and altered flower development (Lee et al., 2008, Holzmeister et al., 2011). *Atgsnor-KO* plants showed a reduced cell death phenotype after treatment with paraquat, a herbicide that is known to induce cell death phenotype in wild type plants via generation of reactive oxygen intermediates (ROI) (Chen et al., 2009). Interestingly, both wild type and *atgsnor-KO* plants showed same levels of ROI accumulation after paraquat treatment (Chen et al., 2009). Lack of sensitivity of the *atgsnor-KO* plants to increased ROI can be due to altered cellular ROI/NO homeostasis, which is very important for plant defense responses (Delledonne et al., 2001).

Atgsnor-KO mutants, challenged with avirulent *Pseudomonas syringae pv. tomato (Pst)* DC3000, showed low levels of salicylic acid accumulation that resulted in a compromised disease resistance (Feechan et al., 2005, Yun et al., 2011). However, these plants with high cellular RSNO levels showed an increased cell death induced by hypersensitive response (CDHR) through a pathway independent of SA and ROI production (Yun et al., 2011). On the other hand, even though SA-induced defense is compromised, increased CDHR rate prevented avirulent oomycete pathogens to complete its life cycle (Yun et al., 2011). These evidences highlight two different roles of GSNOR during defense response; positive regulator of SA-induced defense and negative regulator of CDHR-induced defense responses. Conversely, *GSNOR* transcripts and GSNOR activity in *Arabidopsis* and tobacco respectively were shown to be up regulated when treated with SA (Diaz et al., 2003). These studies indicate the possibility of a mutual regulation between GSNOR and SA during plant defense.

Interestingly, in another study on *atgsnor-KO* plants, there was no difference in the level of disease resistance against Pseudomonas *syringae pv. tomato (Pst)* DC3000 with respect to the wild type plants (Holzmeister et al., 2011). However, here the knock-out plants used were from different background ecotype of *Arabidopsis thaliana* plants and the procedures to inoculate them were also different. These contrary results have raised the questions on how GSNOR regulates disease resistance in various ecotypes. On the contrary, plants with reduced *GSNOR* expression (antisense technology) have affirmed the negative regulatory role of GSNOR during disease resistance against oomycetes (Rusterucci et al., 2007). Further studies are required to

show how this enzyme is regulated at transcript and protein levels during attempted pathogen invasions.

Transcripts of *GSNOR*, however, were down regulated transiently and systemically during wound-induced responses in *Arabidopsis* plants (Diaz et al., 2003). In tobacco plants, wound-induced down-regulation of *GSNOR* is mediated by jasmonic acid (JA) signaling pathway (Diaz et al., 2003). In *Arabidopsis*, GSNO accumulation is required to activate the JA-dependent wound responses, whereas the alternative JA-independent wound-signaling pathway did not involve GSNO. Furthermore, it was shown that GSNO acts synergistically with salicylic acid in systemic acquired resistance activation (Espunya et al., 2012). Plant stress responses induced by wounding are often associated with nitrosative stress and tyrosine-nitration (Chaki et al., 2011b). Stress experiments in sunflower plants have demonstrated that wound-induced nitrosative stress is mediated by down-regulation of *GSNOR* expression levels resulting in decreased activity and a corresponding increase in cellular RSNO levels (Chaki et al., 2011b). In pea plants wounding enhanced RSNO levels, but surprisingly GSNOR activity also increased (Corpas et al., 2008). The same phenomenon was observed during cold stress (Corpas et al., 2008). Although these results appear to be contradicting, they can perhaps explain the dual regulatory phases of cellular levels of GSNO by GSNOR; first, GSNO levels can be regulated by regulating *GSNOR* expression and second, increasing GSNO accumulation can induce higher *GSNOR* expression and its protein activity to counter the effect. Furthermore, GSNOR is regulated in pea plants during cadmium stress, both on activity and transcript level (Barroso et al., 2006). However, a pathway that regulates GSNOR under cadmium stress is not known. Cadmium treatment also induced SA, JA and ethylene levels in pea plants (Rodriguez-Serrano et al., 2006) accompanied by a decrease in the GSH content (Barroso et al., 2006).

Gene silencing studies in tobacco plants have demonstrated the significant role of GSNOR in plant-herbivore interaction (Wunsche et al., 2011). Silencing *GSNOR* compromised plant defense against herbivore with a decrease in the accumulation of JA and ethylene (Wunsche et al., 2011). However, this silencing did not affect transcriptional regulation of all the secondary metabolites that are regulated by JA signaling (Wunsche et al., 2011) implying the specificity of GSNOR in mediating defense response against the herbivore *Manduca sexta*. GSNOR is also required for thermo tolerance. It has been observed that *atgsnor-KO* were highly sensitive to hot temperatures (Lee et al., 2008). This heat sensitivity was associated with increased NO species in

these knock-out plants. NO-overproducing mutants and wild-type plants treated with NO donors were also sensitive to high temperatures (Lee et al., 2008). Consequently, thermo tolerance was restored in *atgsnor-KO* plants when treated with chemicals that scavenge NO. Furthermore, expression of heat-shock-proteins that are essential for thermo tolerance was not affected in *atgsnor-KO* plants (Lee et al., 2008). Interestingly, neither expression nor activity of GSNOR was altered in wild-type plants due to heat stress (Lee et al., 2008). This study suggests that though GSNOR do not regulate heat stress response in plants, its activity to regulate cellular RSNO levels is essential for thermo tolerance.

1.2.2 Denitrosylation mediated by Trx/TrxR system

The thioredoxin/thioredoxin reductase (Trx/TrxR) system, present in almost all organisms, consists of oxidized and reduced forms of Trx, TrxR and NADPH/$NADP^+$ (Lillig & Holmgren, 2007). In animals, Trx/TrxR system was recently proved to mediate denitrosylation (Benhar et al., 2008, Benhar et al., 2010) (Figure 3 – Reaction pathway C and D). Unlike GSNOR, Trx/TrxR system is proposed to mediate denitrosylation of S-nitrosylated proteins directly (Figure 3 – Reaction pathway C and D). In a recent review, it has been mentioned that Trx from plants possess in vitro denitrosylation activity (Spoel & Loake, 2011). Also, thioredoxin (TRX-5h) is a positive regulator of SA-induced defense response in plants (Tada et al., 2008), probably by denitrosylation.

1.2.3 Non-symbiotic hemoglobin: An enzyme that detoxify nitric oxide

Hemoglobins are proteins with globular structure containing heme as a prosthetic group. Heme is a large porphyrin ring with ferrous iron (Fe^{2+}) in the center that can bind to diatomic ligands such as O_2, NO, and carbon monoxide (CO) and also to membrane lipids (Gupta et al., 2011b, D'Angelo et al., 2004). Fe^{2+} contains six coordination sites, of which four are coordinated to pyrrole nitrogen atoms and the fifth site is coordinated to the proximal histidine residue (H_{prox}) of the protein. Sixth site is reversibly coordinated to a distal histidine residue (H_{dist}) (Figure 4A). Sixth coordination varies in the hemoglobins of different organisms and thus hemoglobins can be grouped pentacoordinated or hexacoordinated based on the occupied Fe^{2+} coordination sites (Igamberdiev et al., 2011). Pentacoordination leaves the sixth coordination site of Fe^{2+} free and facilitates the ligand binding (Figure 4A).

In plants, there are mainly three classes of hemoglobins, generally called as non-symbiotic hemoglobins (GLBs). Class 1 non-symbiotic hemoglobins (GLB1) have high affinity for oxygen because of the equilibrium (or low hexacoordinate equilibrium constant, K_H) between pentacoordinated and hexacoordinated GLBs (Igamberdiev et al., 2011). Upon binding, the coordination of O_2 is stabilized by protein conformational changes through the hydrogen bonds formed between H_{dist} and hydrogen atoms of porphyrin ring. This makes dissociation of the O_2 difficult and encourages reaction of NO with O_2 (Igamberdiev et al., 2011). Class 2 non-symbiotic hemoglobin (GLB2), on the other hand, has very low affinity for O_2 because it is completely hexacoordinated in the physiological conditions. This prevents the coordination between O_2 and Fe^{2+}. Interestingly, symbiotic hemoglobin that protect anaerobic nitrogen fixing bacteria from O_2 by scavenging it have evolved from GLB2 (Gupta et al., 2011b). The third class of GLB known as Class 3 hemoglobin is a truncated GLB version with least affinity for oxygen.

In plants, the primary function of GLB1 is related to NO detoxification rather than O_2 transport. Hypoxia induces NO burst in the plants and the resulting NO is oxidized to nitrate by oxy-GLB1 (Fe^{2+}), which in doing so is oxidized to GLB1 (Fe^{3+}) (Figure 4B) (Perazzolli et al., 2004). The rate limiting step in this process is the recycling of GLB1 (Fe^{3+}) to GLB1 (Fe^{2+}) by cytosolic monodehydroascorbate reductase (MDHAR) with ascorbate as a reducing agent and NADPH or NADH as the electron acceptor (Figure 4B) (Igamberdiev et al., 2006, Hebelstrup et al., 2007). NO metabolism of GLB1 is associated with conditions related to hypoxia like flooding, early stages of seed germination and in meristematic tissue with rapidly depleting oxygen (Igamberdiev et al., 2011). Nitrate formed is reduced to nitrite by hypoxia induced nitrate reductase. Under hypoxia plant mitochondria cannot support oxygenic respiration. Under these conditions they switch to anaerobic ATP synthesis with NADH and NADPH as electron donors and nitrite as a terminal electron acceptor producing NO. Resulting NO is recycled to produce nitrate by GLB1 (Stoimenova et al., 2007). Thus GLB1 can clearly respond to the NO accumulation during hypoxia and oxidize them to nitrate. Besides the NO metabolic function, the effect of direct coordination of NO to deoxyGLB1-Fe^{2+} in a process called NO scavenging and NO reaction with cysteine residue to form S-nitrosohemoglobin are still being investigated. These studies will enable one to further understand the influence of GLB1 in NO signaling in addition to NO metabolism during hypoxia. In *Arabidopsis thaliana*, overexpression of *GLB1* and *GLB2* reduced NO emission suggesting their role in NO detoxification (Hebelstrup et al.,

2012). The same plants lines also showed a reduced NO accumulation during pathogen induced defense responses (Mur et al., 2012). NO accumulation is essential for the pathogen induced NO signaling in plants. However, only GLB1 plant lines showed enhanced susceptibility to the pathogens (Mur et al., 2012). Wild type *Arabidopsis* plants downregulate *GLB1* expression during pathogen induced response (Mur et al., 2012). This is a clear indication of plants regulating NO signaling through the expression of *GLB1*.

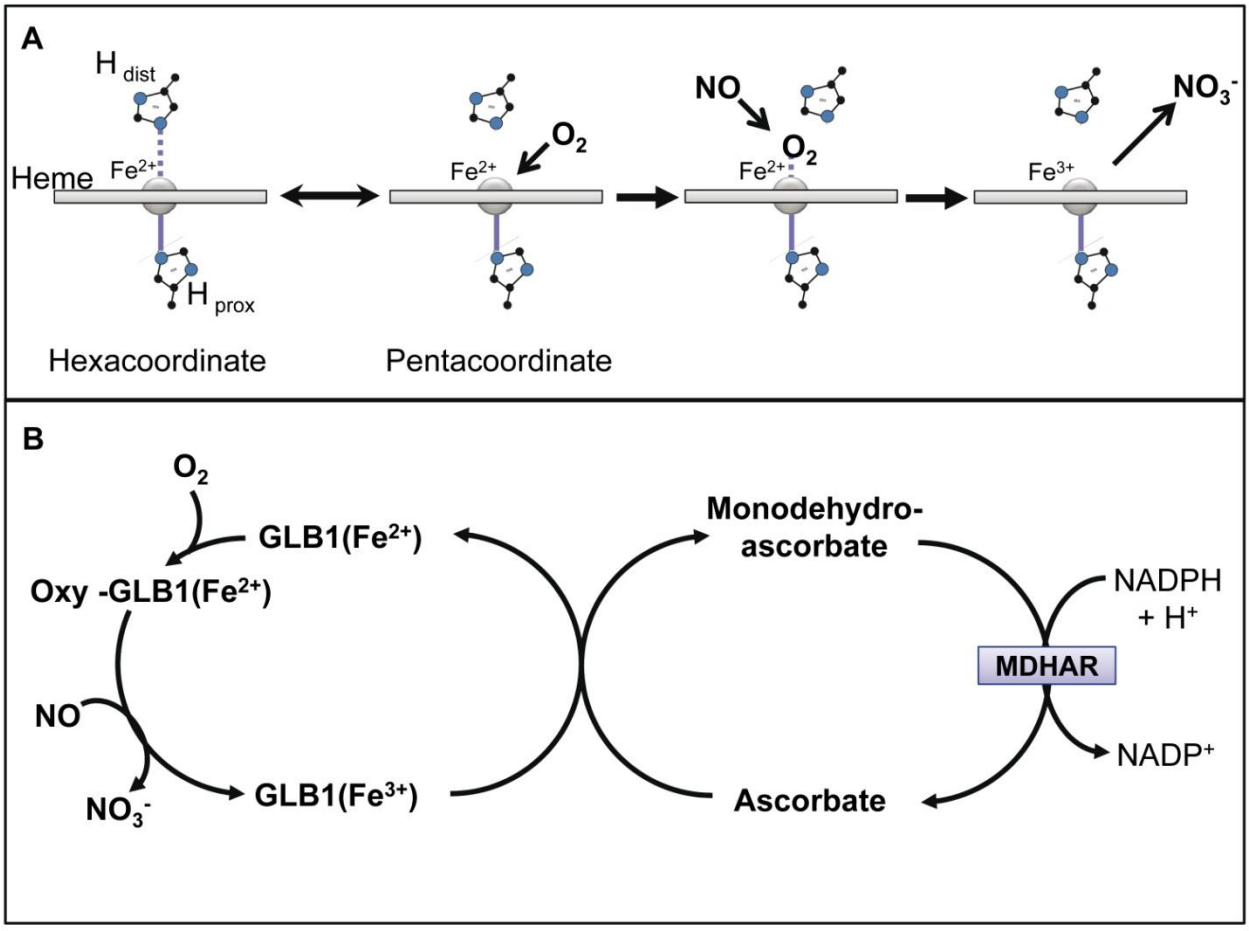

Figure 4 – NO-dioxygenase activity by GLB1.
(A) Hexacoordinated and pentacoordinated GLB1(Fe^{2+}) is in equilibrium. Pentacoordination enhances the ligand (oxygen) binding. Coordinated oxygen can react with NO resulting in nitrate formation thereby reducing GLB1(Fe^{2+}) to oxyGLB1(Fe^{3+}) (B) Reduced GLB1(Fe^{3+}) due to NO conversion to nitrate is oxidized to GLB1(Fe^{2+}) by ascorbate redox coupling.

1.3 Impact of nitrogen containing air pollutants in plants

NO, inside the plant has great physiological significance due to its signaling abilities, but outside it has varying effects on the plant physiology. The exhaust from industries and automobiles has resulted in the increase in concentration of nitrogen oxides (NO_x), mainly NO and NO_2 in the

atmosphere. Foliar uptake of atmospheric pollutants is suggested to have significant impact on plant physiology (Stulen et al., 1998). While the foliar uptake of nitrogen dioxide (NO_2) and ammonia is rapid through the leaf stomata, uptake of NO is rather very low. This is probably due to the internal resistance from plant and due to the lipophilic nature of NO (Stulen et al., 1998). However, accumulation of nitrite in the apoplast has been reported after fumigating plants with NO gas (Stulen et al., 1998). In addition, treatment of fruits vegetables and flowers with low NO concentrations has resulted in their delayed senescence and maturation (Leshem et al., 1998). Moreover, leaf disc expansion assay showed a concentration dependent expansion of pea leaf foliage disc upon NO exposure in an oxygen free environment (Leshem et al., 1998). It was observed that the expansion of the leaf disc started after fumigating it with NO gas of 10^{-7} M (3 – 4 ppb) concentration. It reached a maximum of 50% expansion at 10^{-6} M (30 ppb). However on further increase of NO concentration, the expansion decreased and reached 0% at 10^{-5} M (300 ppm) (Leshem et al., 1998). NO concentration above this limit reduced the leaf disc size (Leshem et al., 1998). Some of the earlier studies, however, have shown contrasting results on the effect of exposing plants to NO gas. Continuous exposure of the plants to 200 ppb NO gas induced phytotoxic effects in their leaves (Wellburn, 1990). Additionally, NO as an air pollutant exhibited inhibitory effects on plant growth and development (Neighbour et al., 1990). Fumigation of *Arabidopsis thaliana* plants expressing bacterial NO degrading dioxygenase (NOD) with 4 ppm NO gas initiated senescence process in the early growth and developmental stages of the plant. Interestingly, fumigation of plants with NO gas in the late growth and developmental stages attenuated the senescence process suggesting NO as a negative regulator of senescence (Mishina et al., 2007). However, not much is known about the impact of NO fumigation on plants at molecular levels, especially on the endogenous NO signaling processes.

1.4 Aim of this study and strategy

Nitric oxide is an inorganic biomolecule with major signaling functions in plants. An exact enzymatic source that produces NO inside the plants is not known yet. This has caused lot of limitations to study the signaling mechanisms induced by NO accumulation during stress-related responses. Use of chemical NO donors like GSNO and sodium nitroprusside to compliment controlled NO production and to induce NO signaling have faced the challenge of unspecific side effects from these chemicals. There are no reports so far on effects of NO accumulation by fumigating plants with NO gas. However, some of the earlier studies to see the effect of NO gas

fumigation on plant physiology have produced mixed results from beneficial antioxidant effects to deleterious phytotoxic effects.

The first aim of this study was to investigate the effect of controlled and continuous NO gas fumigation on plant physiology. NO is known to be involved in almost all the physiological processes in plants and the bottom line of the above strategy was to study the general effects of the exogenously applied NO (stress) on these processes. *Arabidopsis thaliana* plants were selected for our study because most of the NO-related mechanisms known till date have resulted from the studies based on this dicotyledonous model plant.

Our second aim was to study the role of GSNOR in regulating physiological processes during NO stress. *GSNOR* is a single copy gene in *Arabidopsis* that encodes for an enzyme capable of metabolizing GSNO. GSNO is a physiological NO donor that accumulates and mediates NO signaling when there is an accumulation of NO inside the plants. Plants carrying a T-DNA insertion in the *GSNOR* coding region (*atgsnor-KO*) encoded a defective enzyme that failed to metabolize GSNO. We fumigated both WT and *atgsnor-KO* plants from Wassilewskija background. Such experiment would help us to understand the toxic effects of NO during its accumulation in the absence of GSNOR (in *atgsnor-KO* plants) and effectively compare them with WT plants to study the protective function of GSNOR through controlled GSNO metabolism.

The strategy was to fumigate plants with different concentrations of NO gas throughout their growth period and to study their differential effects at phenotypic and molecular level. At the molecular level, we designed the experiments to analyze the changes in the transcriptomic level (microarray), proteomic level (two dimensional difference gel electrophoresis) and metabolic level (targeted metabolites and secondary metabolites) of the NO fumigated plants.

2 MATERIALS

2.1 Plant material

The plants used in this study and their sources have been summarized in the Table 1. The seeds were sowed on soil mixed with sand (5:1 proportion) in 5.5 cm x 6 cm x 5.5 cm (length x breadth x height) plastic pots. Five seeds per pot were sowed and the pots were arranged in rectangular trays. The trays were covered with thin plastic foils and were subjected to seed stratification (incubation at 4°C for at least 72 hours in the dark) before moving them to the growth chambers.

Table 1 – List of plant lines used in this study

Species	Ecotype	Plant line	Source of the seed
Arabidopsis thaliana	Wassilewskija	Wild-type	Lindermayr C, HMGU, BIOP
Arabidopsis thaliana	Wassilewskija	*atgsnor*-KO	Lindermayr C, HMGU, BIOP
Arabidopsis thaliana	Columbia-0	Wild-type	Lindermayr C, HMGU, BIOP
Arabidopsis thaliana	Columbia-0	*atgsnor*-KO	Lindermayr C, HMGU, BIOP
Arabidopsis thaliana	Columbia-0	*glb1*-RNAi	Hebelstrup K, MBG, Aarhus Univ.
Arabidopsis thaliana	Columbia-0	*GLB1*-Ox	Hebelstrup K, MBG, Aarhus Univ.
Arabidopsis thaliana	Columbia-0	*glb2*-KO	Hebelstrup K, MBG, Aarhus Univ.
Arabidopsis thaliana	Columbia-0	*GLB2*-Ox	Hebelstrup K, MBG, Aarhus Univ.
Arabidopsis thaliana	Columbia-0	*NIA2*-KO	SALK_088070c
Arabidopsis thaliana	Columbia-0	*NiR1*-KO	SALK_046068c

2.2 Chemicals and solutions

Name/Description	Company
Acetic acid (glacial)	Merck (Darmstadt)
Acetone	Merck (Darmstadt)
Acetonitrile	Carl Roth GmbH, Karlsruhe, Germany
Agar	Difco Laboratories, Detroit, Germany
Agarose	Biozym, Oldendorf, Germany
Ammonium bicarbonate	Carl Roth GmbH, Karlsruhe, Germany
Ammonium persulfate	GE Healthcare, Munich, Germany
Ascorbic acid	Sigma, Taufkirchen, Germany
β-Mercaptoethanol	Merck, Darmstadt, Germany

BCIP	Sigma, Taufkirchen, Germany
Bio-Rad protein assay (Bradford-Reagent)	Bio-Rad Laboratories, Munich, Germany
Bovine serum albumin	Sigma, Taufkirchen, Germany
Brij 35 (30%)	Skalar, Germany
Bromophenol blue	Merck, Darmstadt, Germany
2-Butanol	Merck, Darmstadt, Germany
CHAPS	Sigma, Taufkirchen, Germany
Complete mini EDTA-free protease inhibitor cocktail	Sigma, Taufkirchen, Germany
Coomassie Brilliant Blue G250	Merck, Darmstadt, Germany
Dipotassium hydrogen phosphate	Merck, Darmstadt, Germany
Dimethylformamide (DMF)	Sigma, Taufkirchen, Germany
Disodium hydrogen phosphate	Merck, Darmstadt, Germany
DMSO	Sigma, Taufkirchen, Germany
dNTPs	Invitrogen, Germany
DryStrip Cover Fluid	GE Healthcare, Munich, Germany
DTT	GE Healthcare, Munich, Germany
EDTA	Sigma, Taufkirchen, Germany
Ethanol	Merck, Darmstadt, Germany
Formaldehyde (37%)	Sigma, Taufkirchen, Germany
Glycerol	Carl Roth GmbH, Karlsruhe, Germany
Glycine	GE Healthcare, Munich, Germany
GSNO	Enzo life sciences, USA
Iodine	Sigma, Taufkirchen, Germany
Iodoacetamide	Bio-Rad Laboratories, Munich, Germany
IPG Buffer pH 3-11 NL	GE Healthcare, Munich, Germany
IPG Buffer pH 4-7 NL	GE Healthcare, Munich, Germany
Isopropanol	Merck, Darmstadt, Germany
Lysine	Serva, Heidelberg, Germany
Magnesium chloride. hexahydrate	Merck, Darmstadt, Germany
Methanol	Merck, Darmstadt, Germany
NADH	Sigma, Taufkirchen, Germany
NADPH	Sigma, Taufkirchen, Germany

NBT	Sigma, Taufkirchen, Germany
NO gas (15% - NO, 85% Nitrogen)	Air Liquide, Duesseldorf, Germany
Nitrogen gas	Linde, Munich, Germany
Oxygen gas	Linde, Munich, Germany
PageRuler® prestained protein ladder	Fermentas, UK
Phenylalanine	Sigma, Taufkirchen, Germany
Ponceau	Sigma, Taufkirchen, Germany
Potassium chloride	Sigma, Taufkirchen, Germany
Potassium ferricyanide	Merck, Darmstadt, Germany
Potassium iodide	Sigma, Taufkirchen, Germany
Potassium sodium tartrate	Merck, Darmstadt, Germany
Rotiphorese acrylamide gel solution (30 % (w/v) acrylamide, 0,8 % (w/v) bisacrylamide)	Carl Roth GmbH, Karlsruhe, Germany
Skim milk powder	Sigma, Taufkirchen, Germany
Sodium carbonate	Merck, Darmstadt, Germany
Sodium chloride	Merck, Darmstadt, Germany
Sodium dodecyl sulfate	GE Healthcare, Munich, Germany
Sodium nitrate	Merck, Darmstadt, Germany
Sodium nitrite	Merck, Darmstadt, Germany
Sodium nitroprusside	Sigma, Taufkirchen, Germany
Sodium thiosulfate pentahydrate	Sigma, Taufkirchen, Germany
Silver nitrate	Merck, Darmstadt, Germany
Sulphanilamide	Sigma, Taufkirchen, Germany
TEMED	Merck, Darmstadt, Germany
Thiourea	GE Healthcare, Munich, Germany
Tris	GE Healthcare, Munich, Germany
Triton^{TM} X-100	Sigma, Taufkirchen, Germany
TRIZOL	Invitrogen, Hilden, Germany
Tryptone	Difco Laboratories, Detroit, Germany
Urea	GE Healthcare, Munich, Germany

2.3 Kits, enzymes, antibodies and reaction systems used

Name/Description	Company
Extract-N-Amp™ Plant Kits, No. XNAP2	Sigma-Aldrich, Germany
RNeasy® Plant Mini Kit, No. 74903	Qiagen GmbH, Hilden, Germany
RNeasy® Mini Kit, No. 74104	Qiagen GmbH, Hilden, Germany
RNase-free® DNase set, No. 79254	Qiagen GmbH, Hilden, Germany
Low Input Amp Labeling Kit, One-Color, No. 51902305	Agilent Technologies, Germany
RNA Spike-In Kit, One-Color, No. 51885282	Agilent Technologies, Germany
Gene Expression Hybridization Kit, No. 51885242	Agilent Technologies, Germany
Gene Expression Wash Buffer Kit, No. 51885327	Agilent Technologies, Germany
RNA 6000 Nano Assay Kit, No. 50671511	Agilent Technologies, Germany
Stabilization and Drying Solution, No. 5185-5979	Agilent Technologies, Germany
Superscript II Reverse Transcriptase, No. 18064014	Invitrogen, Karlsruhe, Germany
RiboLock™ RNase Inhibitor, No. EO0381	Thermo Scientific, Bonn, Germany
Taq DNA Polymerase	Agrobiogen, Hilgertshausen, Germany
Phusion® High Fidelity DNA Polymerase, No. M0530S	New England Biolabs, Frankfurt, Germany
6x Loading Dye	MBI Fermentas, St Leon-Rot, Germany
Disposible P-10 Desalting Columns, No. 17085101	GE Healthcare, Germany
2-D Clean-Up Kit, No. 80648451	GE Healthcare, Germany
CyDye DIGE Fluor, minimal labeling kit (5 nmol), No. 25801065	GE Healthcare, Germany
Anti-GSNOR-IgG (rabbit), polyclonal, No. AS09647	Agrisera AB, Vännäs, Sweden
Anti-Rabbit IgG (Fc)-AP, S3731	Promega, Mannheim, Germany
Anti-biotin, HRP-linked Antibody, No. 7075	Cell Signaling Technology, Frankfurt, Germany .
SuperSignal® West Pico Chemiluminescent Substrate, No. 34077	Thermo Scientific, Bonn, Germany

2.4 Buffers and solutions

For DNA gel electrophoresis

50x TAE running buffer

2.0 M Tris base
5.71% (v/v) glacial acetic acid
50 mM EDTA

For Glycine-SDS polyacrylamide gel electrophoresis according to Laemmli

Protein extraction buffer

100 mM Tris/HCl (pH - 8.0)
10 mM EDTA
1 mM $MgCl_2.H_2O$
1 mM L-Ascorbic acid
12 mM 2-mercaptoethanol (freshly added)
1 Complete mini EDTA-free protease inhibitor/ 10 ml buffer (freshly added)

Coomassie R-250 staining solution

0.25% (w/v) Coomassie Brilliant Blue R-250
0.50% (v/v) Ethanol
10% (v/v) Glacial acetic acid

Coomassie R-250 destaining solution

0.50% (v/v) Ethanol
10% (v/v) Glacial acetic acid

10x SDS running buffer

0.25 M Tris
2 M Glycine
1% (w/v) SDS

Resolving gel buffer

1.5 M Tris/HCl (pH - 8.8)
0.4% (w/v) SDS

Resolving gel buffer

1.5 M Tris/HCl (pH - 6.8)
0.4% (w/v) SDS

6x sample loading buffer

0.1 M Tris (pH - 6.8)
20% (v/v) Glycerin
4% (w/v) SDS

4 mM DDT
0.2% (w/v) BPB

For transfer and immunodetection of proteins

TBST buffer

0.5% (w/v) Tween 20 in TBS buffer

TBS buffer

10 mM Tris/HCl (pH 7.4)
150 mM Sodium chloride
1 mM Magnesium chloride

Coomassie R-250 destaining solution

0.50% (v/v) Ethanol
10% (v/v) Glacial acetic acid

Blocking buffer

4% (w/v) Skim milk powder
1% (w/v) BSA
in TBST buffer

Alkaline phosphate buffer

0.1 M Tris/HCl (pH 9.5)
0.1 M Sodium chloride

Blotting buffer

40 mM Tris base
40 mM Tricine
0.04% (w/v) SDS
20% (v/v) methanol

BCIP solution

5% (w/v) BCIP in 100% DMF

NBT solution

5% (w/v) NBT in 70% DMF

Ponceau-S-staining

1% Ponceau stain powder
2% glacial acetic acid

For two dimensional difference gel electrophoresis (2D-DIGE)

Protein extraction buffer

100 mM Tris/HCl (pH - 8)
10 mM EDTA

1 mM Magnesium chloride hexahydrate
1 mM L-Ascorbic acid
12 mM 2-mercaptoethanol (freshly added)
1 Complete mini EDTA-free protease inhibitor/ 10 ml buffer (freshly added)

Labeling Buffer

7 M Urea
2 M Thiourea
30 mM Tris/HCl (pH - 8.5)
4% CHAPS

Rehydration Buffer

7 M Urea
2 M Thiourea
2% (w/v) CHAPS
0.5% (v/v) IPG Buffer (pH 4-7)
0.8% (w/v) DDT
0.002% (w/v) Bromophenol blue

2x Lysis Buffer

7 M Urea
2 M Thiourea
4% (w/v) CHAPS
0.04% (w/v) Bromophenol blue
2% (w/v) DTT (freshly added)
2% (v/v) IPG Buffer (pH 4-5) (freshly added)

4x SDS Gel Buffer Tris-HCl (Tris-HCl pH 8.8)

1.5 M Tris/HCl (pH 8.8)
0.4% (w/v) SDS

Homogenous Monomer Solution (12.5%)

Acrylamide solution (30% (w/v) acrylamide, 0,8% (w/v) bisacrylamide) - 209 ml
0.375 M Tris-HCl (pH 8.8) - 125 ml
TEMED - 250 µl
Milli-Q water - 164 ml
10% (w/v) Ammonium persulfate - 2 ml (Added just before gel casting)

Equilibration Buffer for Immobiline DryStrips

6 M Urea
2% (w/v) SDS
50 mM Tris/HCl (pH - 8.8)

0.02% (w/v) Bromophenol blue
30% (v/v) Glycerol

10x SDS Running Buffer

0.25 M Tris
1.92 M Glycine
1% (w/v) SDS

Agarose sealing solution

0.5% (w/v) Agarose NA
0.02% (w/v) Bromophenol blue
10% (v/v) 10x SDS running buffer

For Silver staining and mass spectrometric analysis (MS MALDI TOF)

Fixation solution

50% (v/v) Methanol
12% (v/v) Acetic acid

Sensitizing solution

0.8 mM Sodium thiosulfate

Silver staining solution

11.8 mM Silver nitrate
0.028% (v/v) Formaldehyde

Developer solution

0.57 M Sodium carbonate
0.03 mM Sodium thiosulfate
0.05% (v/v) of 37% Formaldehyde

Stop solution

0.5% (v/v) Glycine

Storage solution

20% (v/v) Ethanol
2% (v/v) Glycerol

Silver destaining solution

10 mM Potassium ferricyanide
100 mM Sodium Thiosulfate

Trypsin stock solution

0.1% (w/v) Trypsin
1 mM Hydrochloric acid

2.5mg/ml Matrix Solution

HCCA

70% (v/v) Acetonitrile
0.1% (v/v) Trifluoroacetic acid
Vortexed vigorously and ultrasonicated for several minutes.

Peptide Standard (for MALDI target calibration)

MALDI Peptide Calibration Standard II (Lyophilized)
30% (v/v)Acetonitrile
0.1% (v/v) Trifluoroacetic acid
Total volume 125µl

For nitric oxide analyzer (NOA)

Tri-iodide Solution (for nitrite and nitrosothiol estimation)

Glacial acetic acid	- 35ml
Iodine	- 325mg
Milli-Q water	- 10ml
Potassium iodide	- 500mg

Vanadium Chloride (for nitrate estimation)

Vanadium chloride	- 400mg
1 M HCl	- 50ml

Filter sterilized

10x PBS Buffer

1.37 M Sodium chloride
268 mM Potassium chloride
809 mM Disodium hydrogen phosphate dihydrate
176 mM Potassium dihydrogen phosphate

For enzyme activity assay

GSNOR activity extraction buffer

0.1 M Tris/HCl (pH 7.8)
0.1 mM EDTA
0.2% (v/v) TritonX-100
20% (v/v) Glycerol

GSNOR activity buffer

20 mM Tris/HCL (pH 8)
0.5 mM EDTA

PAL activity extraction buffer

0.1 M Tris/HCl (pH 8.8)

0.1 mM EDTA

12 mM 2-mercaptoethanol

PAL activity buffer

100 mM Tris/HCl (pH 8.8)

0.5 mM EDTA

For Biotin switch assay

HENT buffer

100 mM HEPES

10 mM EDTA

0.1 mM Neocuproine

1% (v/v) Triton X-100

HENS buffer

225 mM HEPES

0.9 mM EDTA

0.1 mM Neocuproine

2.5% (w/v) Triton X-100

2.5 Oligonucleotide primers for the polymerase chain reaction

Oligonucleotides for polymerase chain reaction

SAG12-For	5' - AATGATGAGCAAGCACTGATG - 3' (von Saint Paul et al., 2011)
SAG12-Rev	5' - CGTAGTGCACTCTCCAGTGAA - 3' (von Saint Paul et al., 2011)
Actin-For	5' - TGGAATCCACGAGACAACCTA - 3'
Actin-Rev	5' - TTCTGTGAACGATTCCTGGAC - 3'
GLB1-For	5' - TCCAAAGCTCAAGCCTCACGCA - 3'
GLB1-Rev	5' - AGCCTGACCCCAAGCCACCT - 3'
GLB2-For	5' - ACTGGAGATAGCACCAGCAGCA - 3'
GLB2-Rev	5' - AGTGAGGGTCAATAACGCCGC - 3'
NIA2-For	5' - GCCGAACTCGCCGACGAAGA - 3'

NIA2-Rev	5' - CCGTGACCTCCACACGGGTC - 3'
NiR1-For	5' - AGTGGCTTGGTCTCTTTCACCGT - 3'
NiR1-Rev	5' - TCAGGCAACACAACACCACGGA - 3'
PAL1-For	5' - TGACCATTGGACAAGTGGCTGCG - 3'
PAL1-Rev	5' - CGGCTCTTGTGGCGGAGTGT - 3'
PAL2-For	5' - GTGAATCTTGGCGGAGAAACACTGA - 3'
PAL2-Rev	5' - CGGATTGCGGCAGTGTGTGA - 3'

2.6 Instruments and accessories

Name/Description	Company
Autoclave (D-150)	Systec
Balance (LC 620S)	Sartorius
Balance (A 210 P)	Sartorius
Balance (L 2200 P)	Sartorius
Bioanalyzer (2100)	Agilent
Camera (Powershot G2)	Canon
Centrifuge (Beckman J2-21)	Beckmann Coulter
Centrifuge (Beckman L7-65)	Beckmann Coulter
Centrifuge (5145 D)	Eppendorf
Centrifuge (5810 R)	Eppendorf
Centrifuge (Biofuge 28 RS)	Heraeus
Centrifuge (Microcentrifuge 220r)	Hettich
ChemStation 1100 HPLC gradient system	Agilent
Electrophoresis System SE250	Pharmacia
Ettan DALT cassette rack	GE Healthcare
Ettan DALT gel caster	GE Healthcare
Ettan DALT*six* Electrophoresis System	GE Healthcare
Ettan IPGphor 3	GE Healthcare
Ettan IPGphor 3 Isoelectric Focusing System	GE Healthcare
Gel Caster (SE215)	Hoefer
Gel Documentation (Benchtop 2UV Transilluminator & PhotoDocIT Imaging Scanner	UVP

Hamilton gas-tight syringe (250µl)	Hamilton
High Resolution Microarray Scanner	Agilent
Hybridization Chamber gasket slides	Agilent
Hybridization Chamber, stainless	Agilent
Hybridization oven	Agilent
Hybridization oven rotator	Agilent
Immobiline DryStrips pH 4-7 (24 cm)	GE Healthcare
Immobiline DryStrips Reswelling Tray (IEF)	GE Healthcare
Immobiline DryStrips, pH 4 - 7 (IEF)	GE Healthcare
Ion chromatography (ICS 1500)	Dionex
IPGphor Cup Loading Strip Holder	GE Healthcare
Paper electrode (IEF)	GE Healthcare
pH Meter (IKA-Combimag Ret)	Jahnke &Kunke
Power Supply (EPS 601)	GE Healthcare
Power Supply (E 802)	Consort
Protein Transfer Unit (SemiPhor semidry transfer unit)	Hoefer
Proteomics Analyzer with TOF/TOF 4700	The Applied Biosystems
Loading cup (IEF)	GE Healthcare
Low fluorescent glass plates	GE Healthcare
Low Input Quick Amp Labeling Kit, One-Color	Agilent
NA 1500	Carlo-Erba
NanoDrop-1000 UV-VIS Spectrophotometer	NanoDrop Technologies
Nitric oxide analyzer	Sievers 280i
Plastic containers for the equilibration of Immobiline DryStrips	GE Healthcare
Power supply EPS 601 (2D-DIGE electrophoresis)	GE Healthcare
Scanner (Image Scanner II)	GE Healthcare
SGE MicroVolume 100 µL syringes (26250-U)	Sigma
Shaker (Reax2)	Heidolph
Sieve 250 Micron (31.031.0031)	Retsch
Skalar colorimetric analyzer (1100105)	Skalar
Slide staining dish, with slide rack (121)	Thermo Shandon

Spectrophotometer (Ultrospec 3100 pro)	Amersham
Stabilization and Drying Solution (5185-5979)	Agilent
Thermal Cycler (Hybaid PCR express)	Thermo Life sciences
Thermoblock (Thermomix Comfort)	Eppendorf
Tin Container (3.3 x 5 mm)	IVA (SA76980502)
Typhoon trio 9100	Amersham Biosciences
Vernier Caliper	Kincrome
Vortexer (Vortex-Genie 2)	UniEquip

2.7 Software and website/webtools

DeCyder 2-D Differential Analysis Software v6.5 (GE Healthcare)	GE healthcare
DiscreteAccess software (Skalar)	Skalar
Agilent's Scan Control software (Agilent)	Agilent
Feature extraction software v10.7 (Agilent)	Agilent
GeneSpring GX	Agilent
2100 Expert	Agilent
Mascot Version: 2.2.06	Matrix Science
Mapman 3.5.1R2	GABI pd (MPI)
Genevestigator	NEBION and ETH Zurich
Sievers NOAnalysis	GE Healthcare (Sievers)
Vector NTI 9.1.0	Invitrogen
ProteinPilot	ABSciex
Gasanalytik	Ansyco
http://www.ncbi.nlm.nih.gov/tools/primer-blast/ - Primer designing	
http://www.arabidopsis.org/tools/bulk/go/index.jsp - GO enrichment analysis	
http://arabidopsis.info/ - Seed ordering	
http://www.currentprotocols.com/WileyCDA/ - Protocol search	
http://www.expasy.ch/ - Protein information and analysis	
http://www.ncbi.nlm.nih.gov/Structure/cblast/cblast.cgi - Protein structure blast	
http://scholar.google.com/ - Literature and patent search of scholarly articles	
http://www.protocol-online.org/ - Protocol search	

3 METHODS

3.1 Treatment of *Arabidopsis thaliana* plants with NO

Arabidopsis thaliana plants were treated with various concentrations of nitric oxide (NO) in specially designed exposure chambers (Figure 5) under controlled conditions (Table 2). The NO levels inside these chambers were continuously monitored using chemiluminescence detection method sensitive to as low as 1 ppb of NO. Trays carrying pots with sowed seeds were subjected to stratification at 4 °C for at least 72 hours in the dark. Trays were then covered with thin transparent plastic foils and transferred into NO exposure chambers. Covered trays provide high humidity which enables uniform seed germination. All the chambers were supplied with ambient air that was directly drawn from the campus of Helmholtz Zentrum Munich, Germany. After 5 days, plastic covers were removed and ambient air drawn into the chamber was mixed with gaseous NO of required concentrations. The chambers and NO treatment facilities were provided by the Research unit of Environmental Simulation in the Department of Biochemical Plant Pathology (BIOP) at Helmholtz Zentrum Munich, Germany.

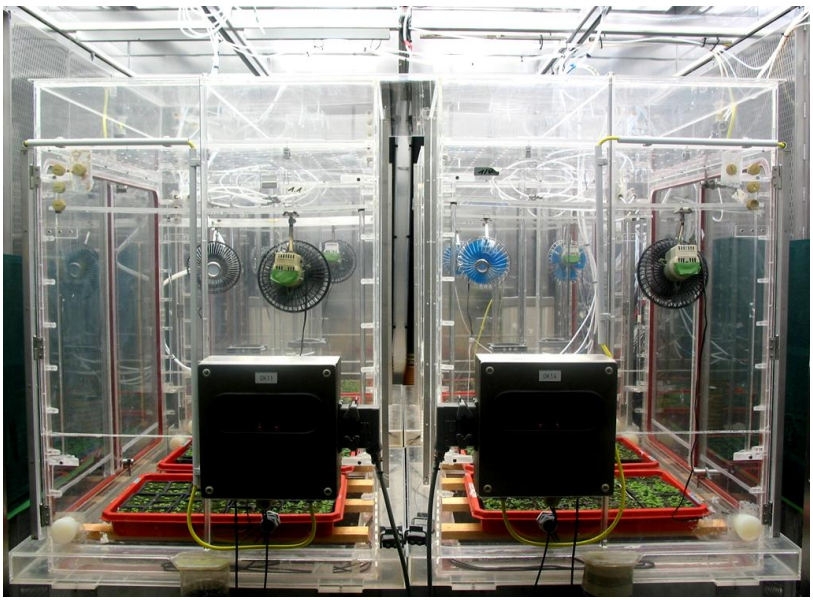

Figure 5 – Plant growth chambers for NO treatment.
A big plant growth chamber contains four small exposure chambers; each designed to provide specific gaseous environment for the plants. All the chambers were equipped with ventilators ensuring uniform circulation of air inside the chambers. Air was continuously withdrawn from all the chambers to detect NO and total nitrogen oxide (NOx) levels in the chamber.

Table 2 – Growth conditions for the plant growth chambers for NO treatment

Day Conditions (14 hours)	
Temperature	20 °C
Relative Humidity	80%
Light	300 μmol/m^2/s in PAR (400–700 nm)
UV-B	17 mWm^{-2}
Night Conditions (10 hours)	
Temperature	16 °C
Relative Humidity	80%

3.2 Analysis of plant growth parameters

To analyze the differences in growth in *Arabidopsis thaliana* among the various treatment groups - rosette size, rosette fresh and dry weights, shoot length, thickness of the stem and number of lateral shoots were measured. Rosette size was measured by measuring the diameter (in cm) of the biggest circle that was occupied by the 4 weeks old rosette in at least two opposite directions. Fresh weight (in g) was measured by weighing the freshly processed 4 weeks old rosettes after completely removing the vegetative shoot and root organs. These rosettes were then dried in the hot air oven for more than 12 hrs at 60 °C to measure the dry weight (in g). Shoot length (in cm) was measured by scaling the distance between bottom-most part of the vegetative shoot to its top most part when the plant was six weeks old. Thickness (in mm) of the vegetative shoot from about 3 cm above the rosette was measured using vernier caliper in six weeks old plants. Number of lateral shoots (secondary shoot) formed was counted in six weeks old plants.

3.3 DNA extraction from plant material

DNA from the plant leaves were extracted using Extract-N-Amp™ Plant Kits (Sigma-Aldrich, Taufkirchen, Germany) according to the instructions given in the manufacturer's manual. DNA was extracted from a small piece of leaf tissue of diameter ~ less than 1 cm. Leaf disk was incubated in 100 μl of Extraction solution for 10 min at 95 °C after brief vortexing. 100 μl of Dilution solution was added and vortexed again. The entire preparation was stored at 4 °C until use. Preparation was used for the analysis using polymerase chain reaction (PCR) according to the instructions given in the manufacturer's manual (Extract-N-Amp™ Plant Kits).

3.4 RNA extraction from plant material

Total RNA was isolated from the leaves using a combination of TRIZOL method and Qiagen RNeasy® Mini Kit protocol. 100 mg of frozen homogenized leaf material was mixed with 1 ml of TRIZOL and incubated for 5 minutes (min) at room temperature (RT). After addition of 200 µl of chloroform to the homogenate, tubes were shaken vigorously using a vortexer for 2 min at RT. Following centrifugation at 18,000 g for 15 min at 4 °C the aqueous phase was further purified using RNeasy® Mini Kit according to the instructions given in the manufacturer's manual. On-column DNA digests using Qiagen's RNase-free® DNase to remove DNA contamination was performed as recommended by the manufacturer. Purified total RNA in RNase/DNase free water were quantified and analyzed for purity using the Nanodrop ND-1000 spectrophotometer. Isolated RNA was stored at -80 °C until use.

3.5 cDNA Synthesis and polymerase chain reaction (PCR)

First-strand cDNA synthesis was performed using Invitrogen's Superscript II Reverse Transcriptase following the supplied protocol (Superscript II Reverse Transcriptase – Invitrogen). Details of the reaction mix and steps involved in the cDNA synthesis have been summarized in Table 3. Newly synthesized cDNA was used to amplify and analyze the expression levels of a gene using polymerase chain reaction (PCR). Primers that specifically bind to the target gene segment were designed with the primer designing tool on NCBI website named 'Primer-BLAST'. NCBI / Primer-BLAST designed the primers using primer3 platform combined with BLAST search. Primers were specifically designed using reference mRNA sequence of the gene of interest. Those primer pairs that compliment the gene sequence that are separated by at least one intron (if present) on the genomic DNA were selected. 100 ng of synthesized cDNA were generally used for downstream PCR reaction to amplify desired cDNA template. Either Taq polymerase (5 U/µl) or Phusion high-fidelity DNA polymerase (2 U/µl) were used for the amplification reaction. Details of the PCR reaction mix and steps involved in PCR using both Taq polymerase and Phusion high-fidelity DNA polymerase have been summarized in Table 4.

Table 3 – Reaction mix and steps involved in cDNA synthesis

Reaction mix for the cDNA synthesis

Components per reaction	**Volume (µl)**
5x First Strand Buffer	4
RiboLock RNase Inhibitor (40 U/µl)	1
100 mM DTT	2
20 mM dNTPs	1
Oligo (dT) (500 µg/ml)	0.5
Volume containing 1 µg RNA	10.5
SuperScript II Reverse Transcriptase (200 U/µl)	1

Steps for cDNA synthesis

Step	**Temperature (°C)**	**Incubation time (min)**
Step 1	42	30
Step 2	50	40
Step 3	95	5
Step 4	4	forever

Table 4 – PCR reaction mix and cycler program

Reaction mix for Phusion polymerase based PCR amplification

Components/reaction	**Volume (µl)**
5x Phusion GC buffer	4
20 mM dNTPs	2
10 µM Forward primer	1
10 µM Reverse primer	1
Phusion high-fidelity DNA polymerase (2 U/µl)	0.2
Template cDNA (100 ng made up to 1 µl)	1
Sterile double distilled water	10.8

PCR Cycler program for Phusion polymerase

Temperature	**Time**	**Cycles**
98 °C	30 sec	1 cycle
95 °C	10 sec	25 - 35 cycles
X °C	30 sec	
72 °C	15 sec/1kb	
72 °C	10 min	1 cycle

Reaction mix for Taq polymerase based PCR amplification

Components/reaction	Volume (µl)
10x Reaction buffer	2
20 mM dNTPs	2
10 µM Forward primer	1
10 µM Reverse primer	1
Taq polymerase (5 U/µl)	0.1
Template cDNA (100 ng made up to 1 µl)	1
Sterile double distilled water	12.9

PCR Cycler program for Taq polymerase

Temperature	Time	Cycles
95 °C	2 min	1 cycle
95 °C	30 seconds	
X °C	30 seconds	30 - 40 cycles
72 °C	1 min/1 kb	
72 °C	10 min	1 cycle

3.6 DNA gel electrophoresis

The separation of amplified DNA fragments after PCR was done in agarose gels using TAE buffer. Samples were mixed with 6x loading dye solution before loading and the gels were run at voltage of 100 volts. For the detection of DNA fragments, 0.05 µg/ml ethidium bromide was added to the liquid agarose. After separation, the fragments were visualized by UV light illumination (302 nm).

3.7 Microarray Analysis

Microarrays were used to profile gene expression patterns in *Arabidopsis thaliana*. Total RNA from the rosettes were isolated using RNeasy Plant Mini kit (Qiagen GmbH, Hilden, Germany) according to the instructions given in the manufacturer's manual. Around 70 to 80 mg of frozen and homogenized plant tissue material per sample was used as the starting material. An on-column DNase (Qiagen GmbH, Hilden, Germany) digests to remove DNA contamination was performed as recommended by the manufacturer.

3.7.1 Estimating the quantity and quality of the total RNA

Purified total RNA in RNase/DNase free water were quantified and analyzed for purity using the Nanodrop ND-1000 spectrophotometer. Quality of the total RNA isolates were further confirmed with Agilent 2100 BioAnalyzer. Quality checking and quantification were carried out using Agilent RNA 6000 Nano kit according to the instructions given in the Agilent RNA 6000 Nano kit Guide. Plant RNA Nano version 1.2 was used as the assay class. RIN (RNA integrity number) was used to assess the quality of the RNA with a lower threshold value of 7.

3.7.2 Agilent One-Color Microarray-Based Gene Expression Analysis

Microarray analysis was carried out on Agilent platform using the technique 'One-Color Microarray-Based Gene Expression Analysis' with 'Low Input Quick Amp Labeling' technology. Microarray analysis was carried out according to the protocol described in the manual provided by Agilent (G4140-90040). mRNA from the samples were reversibly transcribed to synthesize cDNA. Newly synthesized cDNA were used as a template to synthesize cRNA which incorporates Cy3 labeled cytidine nucleotides. Labeled cRNA was hybridized onto a chip probed with numerous spots of short DNA segments, each corresponding to unique gene. Binding of cRNA with these short DNA segments occurs in a concentration dependent manner. More cRNA in the sample implies enhanced binding with DNA segments and hence a significant increase in fluorescence. The scheme for this technique is shown in Figure 6.

3.7.3 Custom 8x60K microarray designing

8 x 60K *Arabidopsis thaliana* microarray chip with design ID 29132 was printed by selecting biological and replicated probe groups already designed by Agilent which represents approximately 43K probes. In addition to this main probe group, a replicated probe-group of selected 477 genes was also included in the array design. The objective of this additional probe group was to use them for multiplicative detrending purposes to eliminate artifacts that might have been introduced during array hybridization.

3.7.4 Use of One-Color RNA Spike Mix

Before microarray analysis, isolated total RNA were mixed with One-Color RNA Spike mix. Each spike mix used ten *in vitro* synthesized, polyadenylated transcripts in predetermined ratios. When they were hybridized onto Agilent microarray control probes, the data needed to track

performance and assure confidence was readily accessible that made microarray workflow linear, sensitive and accurate.

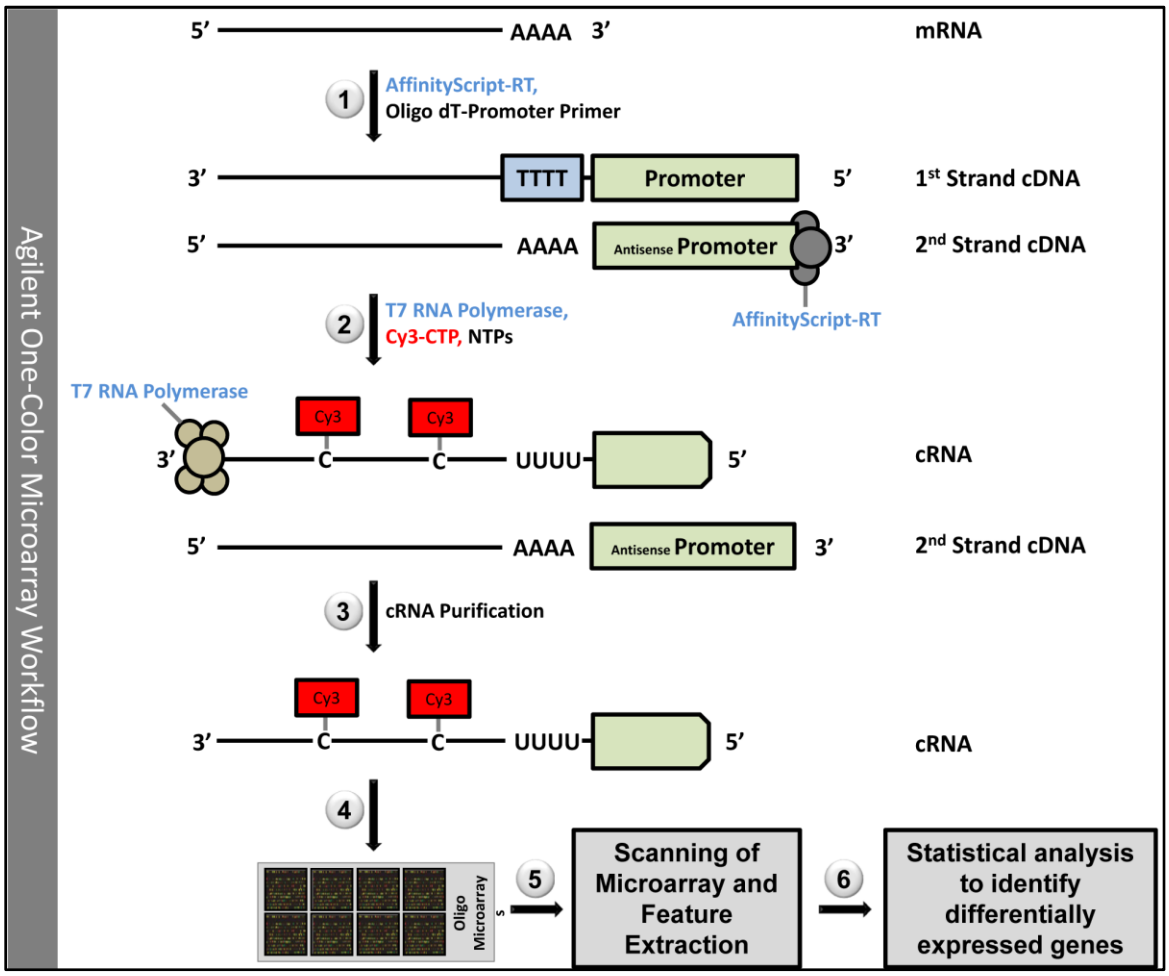

Figure 6 - Schematic of Agilent microarray analysis.
(1) Total RNA was used as template to synthesis cDNA attached with a promoter sequence required to induce cRNA synthesis. (2) cRNA was synthesized using cDNA as a template by the recombinant T7 RNA polymerase which also incorporated Cy3 labeled CTPs into newly synthesized cRNA. (3) cRNA were purified and hybridized (4) to Agilent custom designed 8x60K microarray. (5)After hybridization, the arrays were scanned to yield microarray image files. Agilent's feature extraction software v10.7 with the protocol GE1_107_Sep09, read and processed raw microarray image files in an automated mode. The software was designed to detect the microarray grids, reject outlier pixels, accurately determine feature intensities and ratios, flag outlier pixels, and calculate statistical confidences. (6) The raw data produced after scanning were normalized using Agilent GeneSpring software making it accessible to statistical tools.

3.8 Protein extraction from plant material

After harvesting, *Arabidopsis* rosettes were immediately frozen in liquid nitrogen and stored at -80 °C until they were used. Frozen leaf material was uniformly homogenized using tissue

dismembrator without thawing. 400 mg of frozen homogenized tissue material was vortexed vigorously in protein extraction buffer. After centrifugation at 12,000 g for 20 min at 4 °C, supernatant was filtered through 70 µm nylon membrane. Protein extract was then desalted using PD-10 desalting columns equilibrated with protein extraction buffer according to the manufacture's instruction (GE Healthcare, Munich, Germany). Desalted protein extract was stored in -80 °C until they were used.

3.9 Estimation of protein concentration using Bradford reagent assay

Bradford reagent (Bio-Rad Laboratories, Munich, Germany) was used to photometrically determine the concentration of proteins after extraction (Harlow & Lane, 2006). In order to measure and plot a standard curve of protein concentration versus absorbance at 595 nm, a series of dilutions of bovine serum albumin (BSA) protein standard stock solution was prepared. 1 ml of reaction mixture contained 790 µl of water, 200 µl of Bradford reagent and 10 µl of known concentration of BSA. A standard curve was plotted and used as a reference to quantify protein extracts with unknown concentrations.

3.10 Glycine sodium dodecyl sulfate polyacrylamide gel electrophoresis

Glycine-SDS-PAGE was used to separate proteins according to their molecular weight (Laemmli, 1970). The preparation of buffers and solutions as well as 4% stacking gel and 12% of resolving gels for Glycine-SDS-PAGE was performed. Protein samples were mixed with 6x sample buffer (final conc. 1x) and incubated for 5 minutes at 95 °C for denaturation. Not more than 20 µl of the protein sample was loaded per well. Electrophoresis was carried out by applying a current of 25 mA per gel till Bromophenol blue front reached the bottom of the gel. Afterwards, the gels were stained for at least 1 h in Coomassie R-250 staining solution followed by overnight destaining.

3.11 Silver staining of the SDS gels

Silver staining of SDS-PAGE gels was performed as described by Shevchenko et al. (Shevchenko et al., 1996) after a few modifications. Gels were incubated twice in fixation solution for 30 minutes each. Fixed gels were then washed thrice with 50% ethanol followed by 1 minute sensitization in sensitizing solution. After washing with water for 5 minutes, gels were stained with staining solution for 25 minutes. Stained gels were rinsed with water to remove

excess silver nitrate and were introduced into the developing solution and incubated there with gentle agitation until proteins spots were clearly visible.

3.12 Protein transfer and immunoblotting

Semi-dry blotting method was used for immunochemical detection of proteins on membranes (Western Blot). After glycine-SDS-PAGE, a blotting sandwich was assembled from equilibrated gel and Whatman nitrocellulose membrane (0.45 µm pore size) and blotting paper soaked in blotting buffer according to the transfer unit's manual. Protein transfer was performed by applying a current of 1.5 mA/cm^2 of gel area for 1 hour. After the transfer, free binding sites on the membrane were blocked by incubation in 50 ml blocking buffer for 1 h at RT with gentle shaking. After washing with TBS-T solution for three times, blotted membrane was incubated with 1:3000 diluted anti-GSNOR rabbit polyclonal serum antibody in 25 ml of TBS-T solution for 2 h at RT with gentle agitation. The washing was repeated again as described above and the membrane was incubated in 25 ml of secondary antibody solution, 1:10,000 dilution of Anti-Rabbit IgG (Fc)-AP in TBS-T, for 1 h at RT with gentle agitation. The membrane was washed once again as described above followed by a final wash in TBS buffer for 10 min. After cross-reaction, protein bands were visualized using BCIP and NBT as substrates.

3.13 Two dimensional difference gel electrophoresis (2D-DIGE)

Using 2D clean-up kit (GE Healthcare, Munich, Germany), 50 µg of proteins extracted from the rosettes were cleaned-up according to the instructions given in the manufacture's manual. Purified proteins were dissolved in 15 µl of labeling buffer and the pH was adjusted to 8.5 using 1M NaOH.

3.13.1 Fluorescent labeling of proteins

2D-DIGE was carried out using Ettan DIGE system. Labeling proteins with fluorescence emitting dyes (CyDye DIGE Fluor minimal dyes) combined with sample multiplexing (Typhoon Variable Mode Imager) and image analysis (DeCyder 2D software) makes Ettan DIGE system beneficial over the classical second dimension SDS PAGE. The use of CyDye DIGE Fluor minimal dyes enables multiplexing of three separate protein mixtures, each labeled with separate dyes (Cy2, Cy3 and Cy5) on the same second dimension SDS PAGE gel (Figure 7). The NHS ester reactive group of CyDye DIGE Fluor minimal dyes binds covalently with the epsilon amino

group of lysine residues forming an amide linkage. The dye was added to the protein such that the amount of dye was limiting within the labeling reaction. The lysine amino acid in proteins carries an intrinsic +1 charge at neutral or acidic pH. CyDye DIGE Fluor minimal dyes also carry a +1 charge which, when coupled to the lysine, replaces the lysine's +1 charge with its own, therefore the pI of the protein does not alter significantly. A second dimension SDS PAGE gel contains one internal standard protein labeled with Cy2 and two treatment protein samples labeled with Cy3 and Cy5

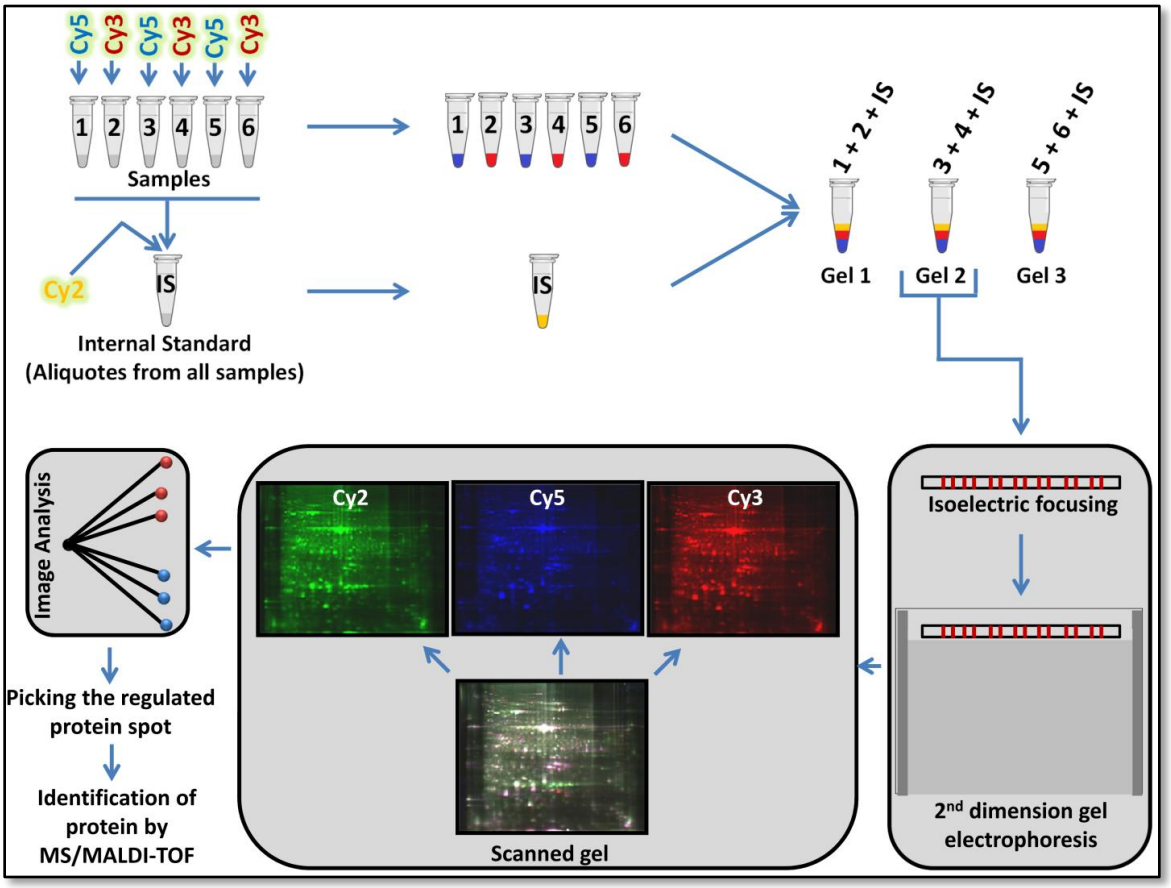

Figure 7 - Schematic representation of 2D-DIGE analysis.
Protein extracts from the treated samples were labeled with Cy3 and Cy5 dyes. An internal standard (aliquots from all the samples used in the analysis) was labeled with Cy2. One 2D-DIGE gel contains two treated sample labeled with Cy3 and Cy5 and one Cy3, which is same across all the gels. One dimensional isoelectric focusing and second dimension SDS gel electrophoresis separated the proteins according to their pI and molecular weight respectively. Each gel was scanned at three different wavelengths belonging to each dye. Acquired images were analyzed by Ettan 2D DeCyder software to identify regulated protein spots. These spots were analyzed using MS/MALDI-TOF to identify regulated proteins.

Internal standard (IS) was created by pooling an aliquot of all the biological samples in the experiment. This implied that every protein from all the samples could be represented in the IS. 50 µg of the proteins from this grand mix was run on every gel along with 50 µg of proteins from two treatment samples (Figure 7). The incorporation of the same IS on every gel eliminates gel-to-gel variation, thereby significantly increasing accuracy and reproducibility of the system. Lyophilized 5 nmol CyDye DIGE Fluor minimal dyes (Cy2, Cy3 and Cy5) were dissolved in 5 µl of dimethylformamide (DMF) each to prepare dye stocks of 1000 pmol/µl. Working stock was prepared immediately before use by diluting 1 part of dye stock with 1.5 parts of DMF to get 400 pmol/µl, immediately before use. For each gel, IS and the two treatment protein samples were added with 1 µl (400 pmol) each of Cy2, Cy5 and Cy3 respectively. The mixtures were incubated in the ice for half an hour in dark. The reaction was stopped by adding 1µl of 10% lysine (w/v) to each of the tubes followed by 15 minutes of incubation in dark at 4 °C. Each of the three samples labeled with CyDyes was transferred into a single tube (Figure 7) and diluted with an equal volume of 2x lysis buffer.

3.13.2 One dimensional isoelectric focusing

Isoelectric focusing of the labeled proteins was done using 24 cm long Immobiline DryStrips (pH 4-7) and Ettan IPGphor 3 apparatus supported by Ettan IPGphor 3 control software. Immobiline DryStrips were rehydrated on Immobiline DryStrip reswelling tray soaked in rehydration buffer for at least 18 hours before isoelectric focusing. Rehydrated Immobiline DryStrips were then placed in the Manifold inside Ettan IPGphor 3 apparatus. Water-soaked paper electrodes were placed on both the acidic and basic ends of the Immobiline DryStrips. It served as a contact for the electrodes that connects the Immobiline DryStrips to the electric circuit. Sample loading cup was clipped above the Immobiline DryStrips near to the acidic end. 100 ml of DryStrip Cover Fluid was slowly poured into the manifold. 100 µl of labeled protein samples were loaded onto the Loading Cup. 25 µl of DryStrip coverfluid was then added above the sample to avoid evaporation of the sample buffer. Ettan IPGphor 3 control software was used to set isoelectric focusing parameters as summarized in Table 5.

3.13.3 Second dimension SDS PAGE

Isoelectrically separated proteins were further separated by SDS PAGE using Ettan DALTsix of Ettan DALT electrophoresis systems. Ettan DALTsix can hold up to six large second dimension

SDS PAGE gels that are stacked in gel cassettes made of low fluorescent glass plates separated with 1mm spacers. The gel cassettes were casted on Ettan DALT gel caster. Pre-cooled degassed homogenous monomer solution was uniformly poured into the gel caster after adding 2 ml of 10% APS (w/v). Water saturated 2-butanol was uniformly added over the gel cassettes and kept for solidifying for more than 10 hrs.

Table 5 - Voltage and running parameters for first dimension isoelectric focusing

Isoelectric focusing parameters			
Temperature			20°C
Current per strip			75 µA
Strip length			24 cm
pH gradient			4 to 7
Step 1	step & hold	150 V	3 hrs
Step 2	step & hold	300 V	3 hrs
Step 3	gradient	1000 V	6 hrs
Step 4	gradient	10000 V	1 h
Step 5	step & hold	10000 V	5 hrs
	Total time		**18 hours**

Isoelectrically focused Immobiline DryStrips were equilibrated first with equilibration buffer containing 0.5% (w/v) DTT for 15 min followed by equilibration buffer containing 2.5% (w/v) iodoacetamide. Equilibrated Immobiline DryStrips were carefully placed in between the glass plates on the top of the SDS PAGE gel. Immobiline DryStrips were then sealed with 0.5% agarose sealing solution. Ettan DALTsix of Ettan DALT electrophoresis system contains two chambers, lower and upper chamber. Lower chamber was filled with 1x SDS running buffer up to the filling mark. After the cassette holder with gel cassettes was placed in the lower chamber, the upper chamber was assembled on the top of it. Both the lower chamber and the upper chamber were filled with 1x and 2x SDS running buffer respectively up to the filling mark on the tank. After closing Ettan DALT electrophoresis system, it was connected to power supply unit EPS 601. Second dimension electrophoresis was carried out in two steps (Table 6) to separate proteins according to their size.

Table 6 – Voltage and running parameters for second dimension electrophoresis

Running conditions for second dimension electrophoresis			
	Current	**Voltage**	**Time**
Step 1	10 mA per gel	0.3 W per gel	1.5 hrs
Step 2	15 mA per gel	Maximum	16 - 17 hrs

3.13.4 Image acquisition using Typhoon trio 9100

2D DIGE gel cassettes were removed from Ettan DALT electrophoresis system after completing the 2D protein separation. Gel cassettes were carefully cleaned and proceeded to scan using Typhoon Trio 9100 which was optimized to image the CyDye DIGE Fluor dyes characteristics. Clean gel cassettes were placed in the scanning slot in the scanner using grippers. Image acquisition was carried out using Typhoon Scanner Control v5.0 software. With the image acquisition mode set to fluorescence, emission filters and laser combinations for all the three CyDyes were defined using the software (Table 7). A prescan with 1000 μm pixel resolution was performed with PMT voltage set to 520 for all three dyes. The corresponding low resolution scanned images from each dye were analyzed with ImageQuant TL software to identify suitable PMT voltage required for each dye. This was achieved by analyzing the intensity of 3-5 most intense signal spots on all the gels using straight line feature in the object tool of ImageQuant TL. With the PMT voltages set, high resolution scanning of the gels was carried out at 100 μm pixel resolution for each Dye. Higher resolution scans were used to collect quantitative data through subsequent data analysis using DeCyder 2D software.

Table 7 – Typhoon scanning parameters for 2D-DIGE gels

Typhoon emission filters and laser combinations			
	CyDye	**Emission filter (nm)**	**Laser**
Scan 1	Cy2	520 BP 40	Blue2 (488)
Scan 2	Cy3	580 BP 30	Green (532)
Scan 3	Cy5	670 BP 30	Red (633)

3.13.5 Image Analysis

After scanning, the created gel images were cropped using ImageQuant TL to remove unwanted edges of the gel cassette. Cropped images were further analyzed using DeCyder 2D software version 6.5. It is fully automated image analysis software that enables the detection, quantification, positional matching and differential protein abundance analysis. DeCyder 2D software works in different modules; each carrying its own characteristic feature. Scanned and cropped gel images were imported into the database of the software using the module 'Image Loader' thereby making it accessible to all other modules for the analysis. Protein spots were detected on individual gels under the module 'DIA (Differential In-gel Analysis)' with the upper limit set to 8500 spots per gel. All the gels with protein spots detected in DIA were further analyzed in BVA (Biological Variation Analysis). In BVA, gels were grouped based on NO treatment conditions. Then, same spots across all the gels were matched with the help of Cy2 labeled internal standard, which was found to be the same in all the gels used in the analysis. Protein spots were randomly selected from different areas of the gel to confirm the spot matching. Subsequent statistical analysis was done to compare the average ratio and variation within each group to the average ratio and variation in the other groups to check whether there were any significant changes between the groups. One-way ANOVA (p value set to 0.01) analysis across four experimental groups were carried out. From the spots filtered through ANOVA analysis, regulated spots were identified as those having a significant change in their average ratio by two fold.

3.13.6 Mass-spectrometric analysis

250 µg of protein was first isoelectrically focused on an Immobiline DryStrip gel without CyDye labeling and then separated by second dimension electrophoresis. The gel was then subjected to silver staining according to the protocol mentioned in the section 3.11. The silver stained spots were visually matched with the protein spots that were regulated in the image analysis and the corresponding spots were picked from the silver stained gels using pipette tip into a 96 well plate. Picked gel pieces were rinsed thrice with water and were subjected to mass spectroscopic analysis for the identification of proteins.

Further analysis was conducted at the 'Core facility proteomics –PROT' of the Helmholtz Center Munich. Gel pieces were de-stained with de-staining solution until silver stain disappeared

completely. After brief washing with water the gel pieces were treated with trypsin working solution for protein digestion and incubated overnight. 0.5% of TFA is added and incubated on a shaker for 15 min to stop trypsin activity. 1 µl of the sample suspension was mixed with 80 fmol/µl GluFib peptide as an internal standard. GluFib helps in tuning and calibration of electrospray ionization and MALDI-TOF/TOF mass spectrometers. Samples were then mixed with matrix solution and spotted directly on the MALDI plate. The 1:5 diluted peptide standard in matrix solution was then spotted on to each of the six calibration points on the plate and was placed in the cassette and loaded into the autoloader of Applied Biosciences MALDI 4700 Protein Analyzer. MALDI-TOF was performed using reflector mode to obtain monoisotopic peptide masses followed by MS/MS from selected peptides to get fragment information. For each MS and MS/MS spectrum, 3000 shots were accumulated. For each sample, the eight most intense peptides were selected for additional MS/MS analysis. Mass calibration was performed by using fibrinopeptide autolysis products as internal standards. All MS/MS spectra were analyzed using Mascot (www.MatrixScience.com/) and the proteins were identified using TAIR database (www.Arabidopsis.org) assuming the digestion enzyme trypsin and with a fragment ion mass tolerance of 1Da and a parent ion tolerance of 65 ppm. One miscleavage was allowed. Iodoacetamide derivative of cysteine as stable modification and oxidation of methionine, deamidation of arginine and glutamine as variable modifications were specified in Mascot. UniProtKB/Swiss-Prot database was used to identify the spot contaminations.

3.14 S-nitrosoglutathione reductase (GSNOR) activity assay

Leaf proteins were extracted using GSNOR activity extraction buffer. Extraction and quantification protocols were the same as given in the section 3.8 and section 3.9 respectively. Activity of the GSNOR enzyme was determined according to the protocol explained by Holzmeister et al. (Holzmeister et al., 2011). GSNOR activity is equivalent to the decomposition of NADH that can be photometrically determined at 340 nm at 20 °C. Activity was determined by incubating 50 µg of protein in 1 ml of assay mix containing GSNOR activity buffer and 0.2mM NADH. The reaction was initiated by the addition of S-nitrosoglutathione (GSNO) to a final concentration of 400µM.

3.15 Phenylalanine ammonia lyase (PAL) activity assay

Leaf proteins were extracted using PAL activity extraction buffer. Extraction and quantification protocols were the same as given in the section 3.8 and section 3.9 respectively. Activity of the PAL enzyme was determined according to the protocol explained by Rouhe et al. (Yin et al., 2012). PAL enzyme converts phenylalanine into trans-cinnamic acid and ammonium. Trans-cinnamic acid formed can be photometrically determined at 290 nm at 37 °C. PAL activity is thus equivalent to the amount of cinnamic acid formed from phenylalanine. Activity was determined by incubating 100 µg of total protein in 1 ml of assay mix containing PAL activity buffer (100 mM Tris-HCl, pH – 8.8) and 5 mM L-phenylalanine. After 2 hrs the reaction was terminated by adding 50 µl of 5 M HCl. Mixture was then centrifugated at 14000 g for 15 min. The absorbance was recorded and quantified against that of control samples without L-phenylalanine.

3.16 Biotin switch method to level of protein S-nitrosylation

The entire experiment till Biotin labeling was carried out quickly on ice under light conditions near to darkness. Proteins were extracted from 100 mg of homogenized frozen rosette material by vigorously vortexing them with 200 µl of HENT buffer containing 30 mM N-ethylmaleimide (NEM). Protein extract was then centrifuged at 12,000 g for 10 min at 4 °C. Supernatant was filtered through a 70 µm Nylon membrane and protein concentration was estimated as explained in section 3.9. GSNO (end conc – 2 mM) treated protein extract was used as a positive control. A volume containing 100 µg proteins was pipetted out into a new microcentrifuge tube. Four times volume of HENS buffer containing 30 mM NEM was added. The mixture was incubated at 37 °C for 30 minutes. Excess of NEM was removed by precipitating proteins with acetone. Protein pellets after precipitating with acetone were re-suspended in 50 µl of HENS buffer. Thereafter, 4 µl of 50 mM sinapinic acid (in DMF) and 10 µl of 4 mM Biotin-HPDP (in DMF) were added and incubated at 25 °C for 1 h with gentle agitation. Excess of Biotin and sinapinic acid were removed by precipitating proteins with acetone. This protocol is a modification of the traditional Biotin Switch S-nitrosylation assay (Jaffrey & Snyder, 2001) with reference to Kallakunta et. al. (Kallakunta et al., 2010). Subsequent Glycine-SDS-PAGE and western blot analysis were carried out as explained in sections 3.10 and 3.12 respectively with different antibodies. HRP-linked anti-biotin antibody (Cell Signaling technologies, Germany) was used herein. It was detected by

the chemiluminescent reaction using the SuperSignal® West Pico Chemiluminescent detection kit (Thermo scientific, Bonn, Germany) according to the instructions given in the manufacturer's user manual. The signals were captured and recorded using X-ray photographic film (Amersham Hyperfilm - GE Healthcare, Munich, Germany).

3.17 Total nitrosothiol, nitrate and nitrite content in *Arabidopsis* rosette

Sievers 280i nitric oxide analyzer (NOA) was used to detect total nitrosothiol, nitrite and nitrate content in the *Arabidopsis thaliana* rosettes. NOA equipped with high sensitivity detector measured NO based on a gas-phase chemiluminescent reaction between NO and ozone. NOA was connected to a purging vessel. Purging vessel were filled with desired volume of strong reducing agent (3.5 ml of acidified KI/I_3 solution for NO and nitrite measurement and 3.5 ml of vanadium chloride solution for nitrate measurement). Purging vessel was covered with a heating water jacket to provide optimum temperature. Using a gas-tight micro-syringe samples were injected into the purging vessel through the rubber septa at the top. Pure nitrogen gas was bubbled with steady pressure through the reaction mixture in the vessel that pushed gases evolved from the reaction vessel into NOA machine. NOA machine was protected from Iodine and other vapors coming out of purge vessel by i) cooling vessel that condense vapors and ii) chemical trap filled with 1M NaOH; both were placed between the purging vessel and the machine. In the machine reaction between NO and ozone generated excited NO_2 and O_2. Excited NO_2 releases energy in the form of light to bring itself back into ground state. Emission from electronically excited nitrogen dioxide in the red and near-infrared region of the spectrum, and was detected by a thermoelectrically cooled, red-sensitive photomultiplier tube. The detection limit of the NOA for measurement of NO and its reaction products was ~1 picomole.

3.17.1 Detection of total nitrosothiol (RSNO) content

Leaf proteins were extracted using PBS extraction buffer. The entire procedure until sample injection was carried out quickly in ice under light conditions near to darkness. Extraction and quantification protocols were the same as given in the section 3.8 and section 3.9 respectively. 500 µl of leaf extract was treated with 60 µl of 29 mM sulphanilamide (in 1 M HCl) and incubated in ice for 5 min. Sulphanilamide could remove nitrite from the extract that interfered with nitrosothiol quantification. 250 µl of sample was injected using Hamilton gas-tight syringe into the purging vessel containing 3.5 ml of acidified KI/I_3 solution. Temperature of the purging

vessel was set to 30 °C. Recorded mV signals were automatically plotted against a calibration curve. The calibration was carried out earlier using known concentrations of sodium nitrite solution (1:10 serial dilutions of 100 µM sodium nitrite solution). Results were reported in terms of pmol RSNO/mg protein.

3.17.2 Detection of total nitrite content

Leaf proteins were extracted using PBS extraction buffer. Extraction and quantification protocols were the same as given in the section 3.8 and section 3.9 respectively. 100 µl of the leaf protein extract sample was injected using Hamilton gas-tight syringe into the purging vessel contained 3.5 ml of acidified KI/I_3 solution. Temperature of purging vessel was set to 30 °C. Recorded mV signals were automatically plotted against calibration curve. Calibration was carried out earlier using known concentrations of sodium nitrite solution (1:10 serial dilutions of 100 µM sodium nitrite solution). Results were reported in terms of nmol nitrite/mg protein.

3.17.3 Detection of total nitrate content

Leaf proteins were extracted using PBS extraction buffer. Extraction and quantification protocols were the same as given in the section 3.8 and section 3.9 respectively. 60 µl of the leaf protein extract sample was injected using Hamilton gas-tight syringe into the purging vessel containing 3.5 ml of vanadium chloride solution. Appropriate dilution of the leaf extracts were made if the signal exceeds the upper limit of 1000 mV. Temperature of the purging vessel was set to 95 °C. Recorded mV signals were automatically plotted against a calibration curve. The calibration was carried out earlier using known concentrations of sodium nitrate solution (1:10 serial dilutions of 100 µM sodium nitrate solution). Results were reported in terms of nmol nitrate/mg protein.

3.18 Colorimetric determination of ammonia content in the *Arabidopsis* leaf extract

1 g of frozen leaf material was shaken with 5 ml of Milli-Q water for two hours. The mixture was then centrifuged at 8000 g and the supernatant was transferred into a new tube. Determination of soluble ammonia in the supernatant was conducted at the research unit of Analytical Biogeochemistry of Helmholtz Zentrum Munich. Ammonia content was analyzed using Skalar colorimetric segmented continuous flow analyzer. To complex the cations, the samples were mixed (flow rate set to 0.42 ml/min) with Buffer A (117 mM potassium sodium tartrate, 82 mM trisodium citrate dehydrate, 0.1% of 30% Brij 35 (v/v)) (flow rate set to 0.80 ml/min). Ammonia ions react with hypochlorite ions generated by the alkaline hydrolysis of

sodium dichloroisocyanurate (flow rate set to 0.32 ml/min) to form monochloramine which in turn reacted with the salicylate ions of sodium salicylate solution (625 mM sodium hydroxide and 500mM sodium salicylate; flow rate set to 0.32 ml/min) in the presence of sodium nitroprusside (flow rate set to 0.16 ml/min) to form a green colored complex with ammonium ion. The absorbance of this compound was determined photometrically at 660 nm at 40 °C and was related to the ammonia concentration by means of a calibration curve using DiscreteAccess software.

3.19 HPLC analysis to determine flavonol content

3.19.1 Sample preparation for HPLC analysis

100 mg of leaf tissue homogenate was added to 1 ml of methanol and incubated on a shaker for 1 h at RT in the dark. The mixture was then centrifuged at 10,000 g for 5 minutes. 75% of the supernatant was mixed with 25% double distilled water and centrifuged for 5 min at 10,000 g. The clear supernatant was transferred into a HPLC micro-vial.

3.19.2 HPLC analysis

Samples were analyzed using Beckman Gold 7.11 HPLC system at a flow rate of 1 ml/min with sample injection volume of 10 µl. Solvent A (double distilled water and 5% ammonium formate in formic acid; mixed in 98**:**2 ratio respectively) and solvent B (methanol, double distilled water and ammonium formate; mixed in 88.2**:**9.8**:**2 ratio respectively) were used for the separation. The separation was isocratic with 100% solvent A in first 5 min; linear gradient to 100 % solvent B in 40 min; isocratic with 100% solvent B for 5 min; linear gradient to 0% solvent B in 5 min; isocratic with 100% solvent A for 5 min. The separation was completed in 60 min. Flavonols were separated with Bischoff Prontosil Spheribond ODS2 Type NC column (5µm - 250mm x 4.6mm) and pre-columned at 20 °C. Absorbance at 280 nm was recorded using Beckman diode-array detector model 168 and scan mode was set between 250 to 450 nm. The flavonol aglycone and sinapate ester derivatives were identified by the diode array spectra and retention time in comparison with authentic standards.

3.20 HPLC analysis to determine anthocyanin content

3.20.1 Sample preparation for HPLC analysis

100 mg of leaf tissue homogenate was added to 1 ml of methanol and incubated on a shaker for 1 h at RT in the dark. Mixture was then centrifuged at 10,000 g for 5 min. 75 µl of methanol extract was mixed with 1 µl of 32% HCl and 24 µl of ddH_2O and centrifuged at 10,000 g for 5 min. The clear supernatant was transferred into a HPLC micro-vial.

3.20.2 HPLC analysis

Samples were analyzed using Beckman Gold 7.11 HPLC system at a flow rate of 1 ml/min with sample injection volume of 10 µl. Solvent A (10% formic acid in water) and solvent B (10% formic acid in methanol) were used for the separation. The separation was isocratic with 100% solvent A in first 5 min; linear gradient to 75% solvent B in 30 min; linear gradient to 100% solvent B in 2 min; isocratic with 100% solvent B for 5 min; linear gradient to 0% solvent B in 3 min; isocratic with 100% solvent A for 5 min. The separation was completed in 50 min. Anthocyanin was separated with Bischoff Prontosil Spheribond ODS2 Type NC column (5 µm – 250 mm x 4.6 mm) and pre-columned. Absorbance at 535 nm was recorded using Beckman diode-array detector model 168 and scan mode was set between 250 to 550 nm. The anthocyanin derivatives were identified by diode array spectra and retention time upon comparison with authentic standards.

3.21 HPLC analysis to determine pigment composition in *Arabidopsis* leaf extract

3.21.1 Sample preparation

100 mg of homogenized frozen leaf material was suspended in 0.7–1.5 ml of DMF. 1 mg of calcium carbonate was added to each sample to prevent any damage to the pigment by acids. It was further centrifuged at 10,000 g for 10 min at 4 °C. The supernatant was then added with half volume of DMF in 50% methanol making the samples more hydrophilic. Centrifugation step was repeated and the samples were filtered through a 0.45 µm PTFE filter.

3.21.2 HPLC detection of pigments

The HPLC unit for pigment analysis consisted of two Model 515 pumps, a 717 cooled Autosampler, a Model 2996 photo diode array detector, a Model 447 fluorescence detector and the Empower 2 chromatographic software.

The pump flow rate was set to 0.9 ml/min. With the sample injection volume of 50 µl, the pigment separations were performed on Merck LichroCART 125-4 Cartridge (LiChrospher 100 RP-18, 5 µm) that was protected with a LichroCART 4-4 Guard pre-column insert. Separation was carried out at 30 °C. Solvent A (acetonitrile, methanol and 0.2 M tris-buffer of p*H* 8.0, mixed in 74:6:1 ratio respectively) and solvent B (methanol and hexane, mixed in 5:1 ratio respectively) were used for separation. The separation was isocratic with 100% solvent B in first 3.5 min; linear gradient to 100% solvent B in 4 min; isocratic with 100% solvent B for 5.5 min; linear gradient to 0% solvent B in 2 min. The separation was completed in 15 min. The peaks were identified and quantified using calibration standards. (Calibration standards: neoxanthin, violaxanthin, antheraxanthin, lutein, zeaxanthin, α-carotene and β-carotene were purchased from DHI Water & Environment, Hørsholm, Denmark; chlorophyll a and b were purchased from Sigma-Aldrich and α-tocopherol was purchased from Merck KGaA, Darmstadt, Germany). Both the accurate retention time as well as the peak spectra supported the peak identification.

3.22 Analysis for total carbon and nitrogen content in the soil

Analysis was conducted at the research unit of Analytical Biogeochemistry of Helmholtz Zentrum Munich. Soil for the analysis was freeze dried and sieved using sieve of 250 Micron. About 2 mg of the sieved soil was weighed in a tin container and loaded into the autosampler of Carlo-Erba NA 1500 analyzer. The autosampler introduced the sample into a high temperature combustion reactor maintained at 1020 °C. Both the sample and the tin container melted in an oxygen enriched atmosphere; presence of tin and oxygen helped even thermally resistant substances to completely oxidize with a violent flash reaction. Helium was the carrier gas that carried the combustion mixture through an oxidation catalyst of chromium trioxide in the reaction combustion tube. The combustion products like CO_2, N_2, NO_x and water were passed into the reduction reactor with metallic copper maintained at 650 °C. This initiated the removal of excess oxygen and helped in the reduction of nitrogen oxides to elemental nitrogen. Thereafter nitrogen along with CO_2 and water was passed through a tube containing magnesium perchlorate for the removal of water. Subsequently, the dried and reduced products were directed into the chromatographic column using helium as the carrier gas. This process allowed the separation of nitrogen and carbon. Both elements were subsequently monitored by a thermal conductivity detector which generated an electrical signal proportional to the concentrations. Analyzing a

standard of known composition under the same conditions made it possible to calibrate the instrument and quantify the content of nitrogen and carbon in the sample.

3.23 Colorimetric determination of ammonia content in the soil extracts

Analysis was carried out at the research unit of Analytical Biogeochemistry of Helmholtz Zentrum Munich. 20 g of soil was shaken with 50 ml of Milli-Q water for two hours. After centrifugation the supernatant was filtered using black ribbon filter paper. Ammonia content in the soil extract was analyzed using Skalar colorimetric segmented continuous flow analyzer. To complex the cations samples were mixed (flow rate set to 0.42 ml/min) with Buffer A (117 mM potassium sodium tartrate, 82 mM Trisodium citrate dehydrate, 0.1% of 30% Brij 35 (v/v); flow rate set to 0.80 ml/min). Ammonium ions reacted with hypochlorite ions generated by the alkaline hydrolysis of sodium dichloroisocyanurate (flow rate set to 0.32 ml/min) to form monochloramine which in turn reacted with the salicylate ions of sodium salicylate solution (flow rate set to 0.32 ml/min) in the presence of sodium nitroprusside (flow rate set to 0.16 ml/min) to form a green colored complex. The absorbance of this compound was determined photometrically at 660 nm at 40 °C and was related to the ammonia concentration by means of a calibration curve using DiscreteAccess software.

3.24 Ion chromatographic determination of nitrite and nitrate in the soil extracts

A mixture of 20 g of soil sample was shaken with 50 ml of Milli-Q water for two hours. Mixture was then centrifuged and the supernatant was filtered using black ribbon filter paper. 25 µl of the filtered supernatant was analyzed for total nitrite and nitrate content using Dionex ICS 1500 Ion chromatography with a flow rate of 1 ml/min. A mixture of 1.8 mM Na_2CO_3 and 1.7 mM $NaHCO_3$ was used as eluent. Dionex AG 4 anion exchange pre-column and Dionex AG 4 anion exchange column were used for separation of anions. Nitrite and nitrate were determined based on their conductivity with respect to the standard solutions used for calibration of the device.

4 RESULTS

4.1 Phenotype of the *Arabidopsis thaliana* plants grown in nitric oxide enriched air

To understand the impact of nitric oxide (NO) accumulation in the biological processes of plants and to study the role of S-nitrosoglutathione reductase (GSNOR) in regulating these processes, *Arabidopsis thaliana* plants were fumigated with 0, 200, 400 and 800 ppb of NO gas. Two plant lines from Wassilewskija (Ws) background were used for the study *viz.* wild-type (WT) and knock-out mutants of *AtGSNOR* (*atgsnor-KO*). Climatic plant growth chambers were used to fumigate the plants with NO gas (Figure 5). NO fumigation was restricted to 10 hours daily starting from the 5th day after germination (DAG). The air inside the chambers was continuously monitored for NO concentration (Figure 8). Plants were grown under 14-h-light (20 °C)/10-h-dark (16 °C) cycle with a photon flux density (PFD) of 300 µmol/m^2/s. The strong light intensity of 300 µmol/m^2/s was selected to resemble the natural conditions and has shown to induce high levels of photosynthesis without causing any photodamage in the plants (Russell et al., 1995, Trojan & Gabrys, 1996, Mishra et al., 2012).

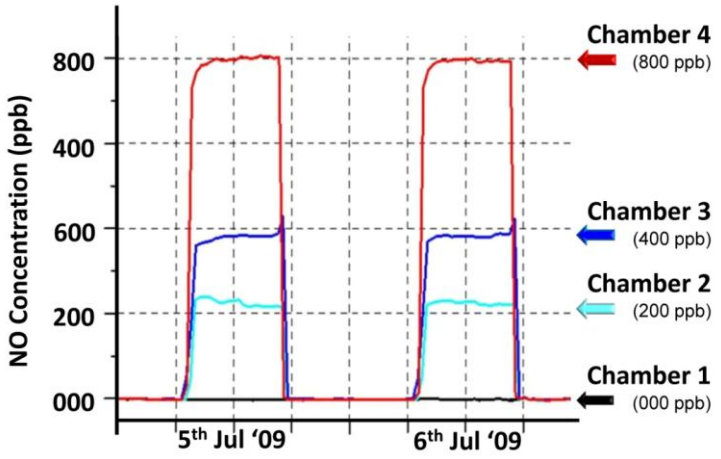

Figure 8 - Measured NO concentrations in the fumigation chambers (Short treatment).
NO concentrations in the four growth chambers used to grow WT and *atgsnor-KO* plant lines with different NO concentrations (legends in the figure) were measured and recorded. The graph demonstrates the detected NO levels (chemiluminescence detection) during the first two days of NO fumigation.

Germination in the *atgsnor-KO* mutants was late as compared to that of WT plants. Vegetative shoot formation and flowering in the *atgsnor-KO* plants were delayed by approximately 7-8 days with respect to that of WT. Due to these significant differences in the plant development, WT plants were compared with 1 week older *atgsnor-KO* lines in almost all the analysis performed in

this study. During fourth week after germination (WAG), plant rosettes from all the treatment groups started exhibiting red senescence (Figure 9). While young leaves remained green, older leaves showed complete red senescence (Figure 9). 5 WAG, WT Ws plants fumigated with 800 ppb showed a slight delay in the development of red senescence as compared to those grown with 0 ppb of NO (Figure 9). A similar phenotype was also visible in *atgsnor-KO* plants during 6th WAG (data not shown). However, no differentially regulated protein spots were detected among the different NO treated samples in the two-dimensional difference gel electrophoresis (2D DIGE) analysis (pH range: 3 – 11).

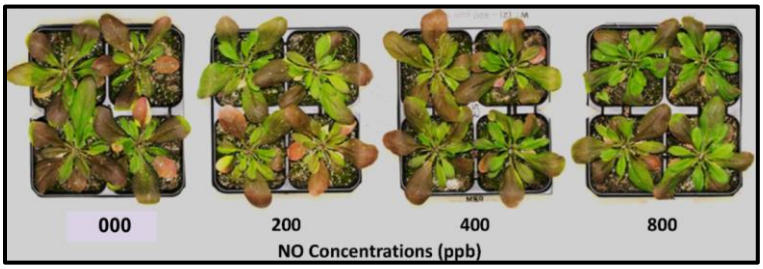

Figure 9 – Phenotype of the plants fumigated with different NO concentrations.
Images of the rosettes from 5-week old WT Ws plants. Similar results were obtained in 4 independent experiments.

Since the plants showed a marginal improvement in their phenotypic response to 800 ppb of NO concentration, but with no significant difference in protein accumulation, we modified our strategy by treating the plants with higher concentrations of NO. Thus, both WT Ws and *atgsnor-KO* Ws plants were grown in chambers fumigated with ambient, 0.8, 1.5 and 3 ppm NO concentrations. The fumigation was continuous starting from 5 DAG till the plants were harvested. Continuous monitoring of NO concentration inside the chambers showed that the NO fumigation was steady in all the four treatment conditions over the entire period of the treatment (Figure 10). NO concentrations in the ambient chambers were ranging between 0 and 0.3 ppm (Figure 10 – readings of chamber 1 ambient, plot in magenta). 0.8, 1.5 and 3 ppm were all above the ambient NO concentrations and were intended to induce NO stress in the plants. Chamber conditions were 14-h-light (20 °C)/10-h-dark (16 °C) cycle with a photon flux density (PFD) of 300 µmol/m^2/s and relative humidity of 80% (Figure 5, Table 2).

Rosettes of both WT (4 WAG) and *atgsnor-KO* (5 WAG) plants showed distinctively different phenotype to NO treatment (Figure 11A). Red senescence in the rosette leaves was delayed in plants which were fumigated with NO. The difference became more prominent with the increase

in NO concentration and the red senescence was completely absent in plants fumigated with 3 ppm of NO (Figure 11A).

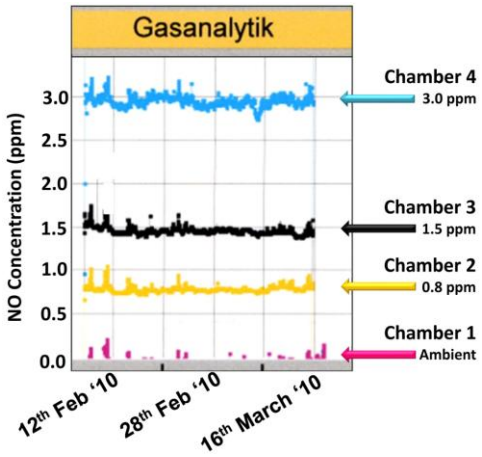

Figure 10 – Measured NO concentrations in the fumigation chambers (Long treatment).
The graph demonstrates the detected NO levels (chemiluminescence detection) in all the growth chamber during the course of one complete experiment.

However, the emerging young rosette leaves remained green in all the NO fumigated plants. Until 3rd WAG in WT and 4th WAG in *atgsnor-KO* plants, differences in the phenotype was not observed between different NO treated plants (Figure 11B). Flowering stage of the plants were not significantly affected by the NO fumigation.

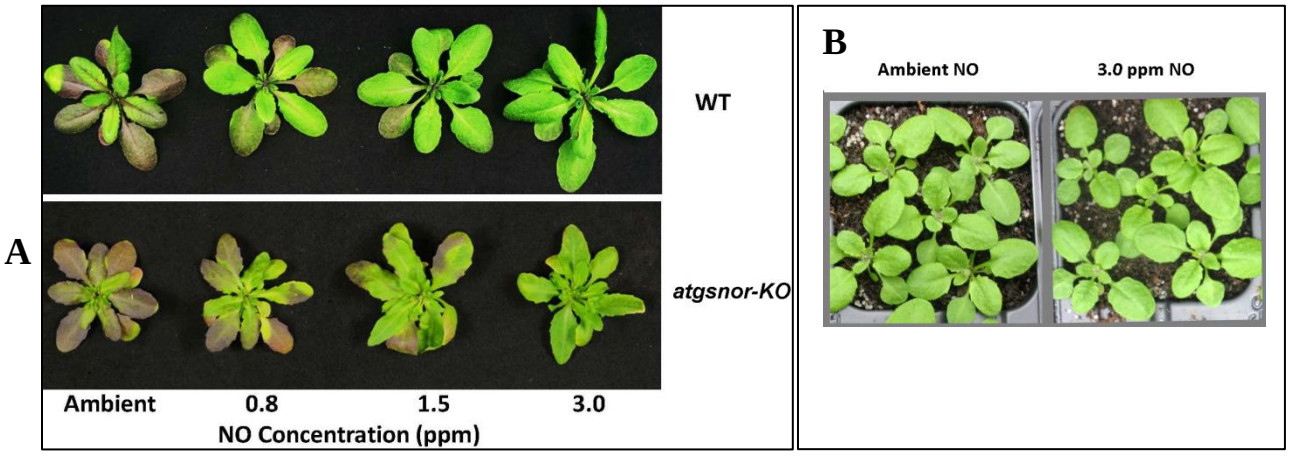

Figure 11 – Rosette phenotype of the plants fumigated with high NO concentration.
A) Images of the rosettes from four-week old WT plants and five-week old *atgsnor-KO* plants grown in different NO gas concentrations (See the legend in the figure). Results were consistent during all the four independent experiments. B) Images of 21 days old WT Ws plants grown in different NO concentrations.

4.2 Effect of NO exposure in the soil fertilization

The effect of NO fumigation on soil nutrient levels and the loss of N-metabolites by growing plants in it were determined. Extracts of the soil with plants (used) and without plants (unused) fumigated with ambient and 3 ppm NO was analyzed for total nitrate, nitrite and ammonia levels. Of the three, nitrate was the highest concentration in the soil containing nitrogen fertilizers. It was up to 337 mg/Kg in the unused soil. Ammonia levels were almost around $1/10^{th}$ (up to 41.4 mg/Kg) of the nitrate content. However, plants used up more than 90% of ammonia, nitrate and nitrite of the soil in 4 WAG (Figure 12). While almost 99% of nitrate and nitrite was consumed by the plants, loss of ammonia from the soil was around 90%. Analysis was performed on the soil collected from the top layer of 3 to 4 cm of the total soil bed of 5.5 cm deep. Each pot had a total of 5 plants growing in it. However, NO fumigation did not influence the levels of N-metabolites in the soil (Figure 12).

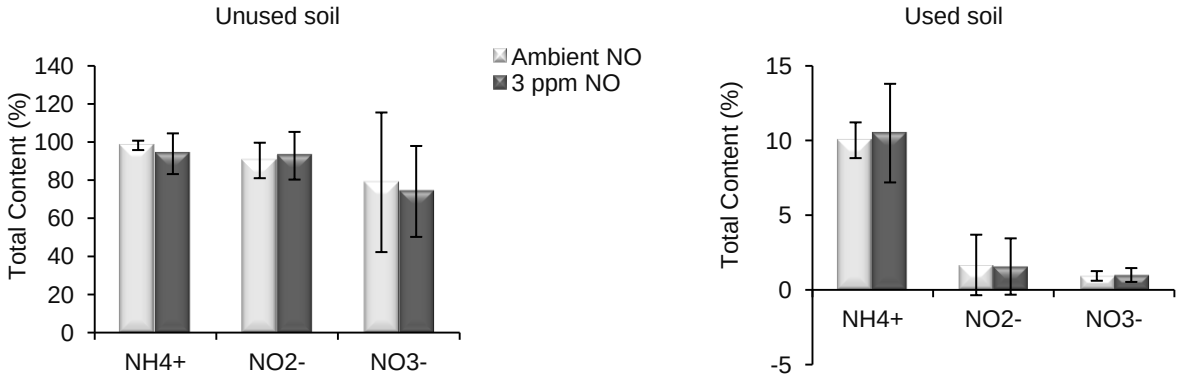

Figure 12 – Nitrate, nitrite and ammonia contents in the soil extracts.
Colorimetric determination of ammonia and chromatographic determination of nitrate and nitrite were used to compare their levels in the used and unused soil. Percentage was calculated relative to the maximum detected quantity across each of the three biological replicates. Maximum detected values were: for nitrate - 337 mg/kg, for nitrite – 194 mg/kg and for ammonia - 41.4 mg/kg.

Total carbon (C) and nitrogen (N) content from the ambient and 3 ppm NO fumigated soil was determined to see the effect of NO fumigation. While C constitutes more than 40% of the total soil elements, N constitutes only about 0.8% of the soil and was thus showing a C to N ratio of 50:1. However, this ratio remained unchanged even after the NO fumigation showing that NO fumigation does not have an effect on the soil N content (Figure 13).

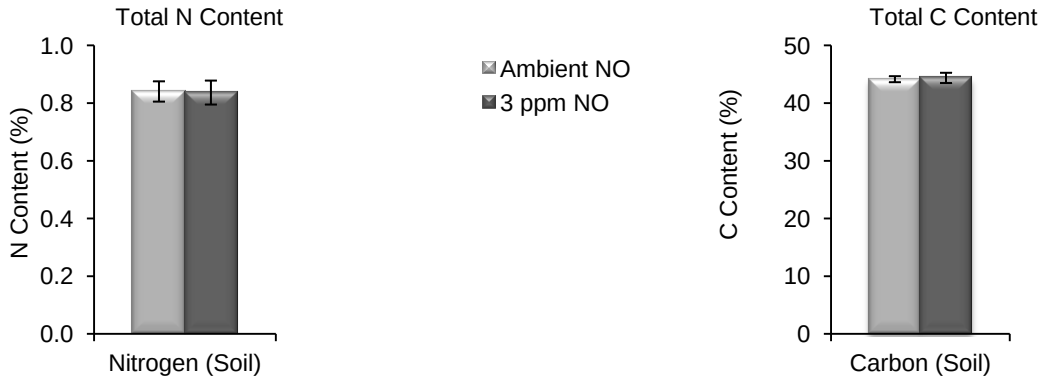

Figure 13 – Estimation of total nitrogen (N) and carbon (C) content in the soil
Total C and N content in the soil were estimated after their chromatographic separation. Four-week old soil exposed to NO was compared. Percentage values represent proportion of the element to the total element pool in the soil.

4.3 Quantification of anthocyanin in NO fumigated plants

Age-related red senescence is often associated with an increase in the anthocyanin accumulation, which imparts the red coloration to the leaves (Diaz et al., 2006). To compare anthocyanin accumulation in NO fumigated plants, total anthocyanin content in the rosette leaves was determined using HPLC. Age-dependent increase in the total anthocyanin content was evident in both WT and *atgsnor-KO* plants grown under all the NO treatment conditions (Figure 14). In 3 week old WT plants, anthocyanin accumulation was negligible in all the treatment groups. Obviously plants did not show red senescence at this age (Figure 11B). Four WAG, there was a sharp increase in the accumulation of anthocyanin content in the ambient NO treated plants (6 μmol/gFW) and a further increase was observed during five WAG (10 μmol/gFW) (Figure 14). These observations were in line with the red senescence phenotype observed during aging in the plants from ambient NO treatment group (Figure 11A). A similar tendency was also observed in the *atgsnor-KO* plants. However, NO fumigation significantly affected the age-dependent anthocyanin accumulation. In 4 week-old WT plants rosettes for instance, the age dependent increase of anthocyanin accumulation was reduced with NO fumigation; reduction level was inversely proportional to NO fumigation concentration (Figure 14). In 3 ppm NO plants anthocyanin accumulation was completely reduced to levels that corresponded to week 3 plants (Figure 14). This was evident in the phenotype of 4 week-old 3 ppm NO fumigated WT plants that did not show any symptoms of red senescence (Figure 11A).

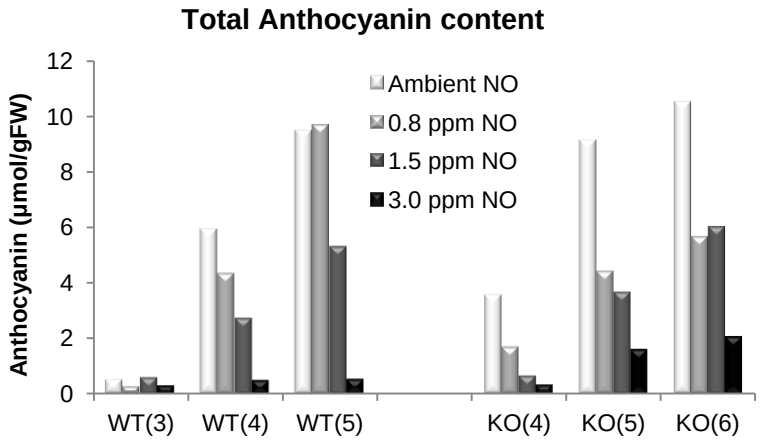

Figure 14 – Total anthocyanin content in the leaf rosette extracts.
Total anthocyanin content was quantified using reverse-phase HPLC after acid hydrolysis of the methanol extracts from leaves. WT – wild type and KO – *atgsnor-KO*. 3,4,5 and 6 – WAG.

4.4 Effect of NO treatment N-metabolite levels in plant rosette

In order to investigate whether the NO fumigation influenced the inorganic N-metabolite (nitrate, ammonia and nitrite) accumulation in both WT and *atgsnor-KO* plants, their levels in the leaf rosettes were estimated. Nitrate content in the *atgsnor-KO* plants were higher than that of WT Ws plants grown under ambient conditions - a difference of almost 100% (Figure 15). Fumigation with 3 ppm NO increased nitrate levels in both the plant lines almost 5 times (Figure 15). Total nitrite content in the five-week old WT plants from ambient NO treatment group was around 1 pmol/gFW of the rosette leaves. Plants from 3 ppm NO group had around 2 pmol/gFW of nitrite in the rosette leaves (Figure 15). A similar difference was also observed in six-week old *atgsnor-KO* plants (Figure 15). Increase in the nitrite levels was directly proportional to NO fumigation. Accumulation of nitrite was higher in *atgsnor-KO* plants (~1.3 nmol/gFW) than that of WT plants (~1 nmol/gFW) grown under ambient conditions (Figure 15). Ammonia levels too increased significantly with NO fumigation in both WT and *atgsnor*-KO (Figure 15). However, the difference in the levels of ammonia between ambient and NO treated plants were not as significant as in the case of nitrate content (Figure 15).

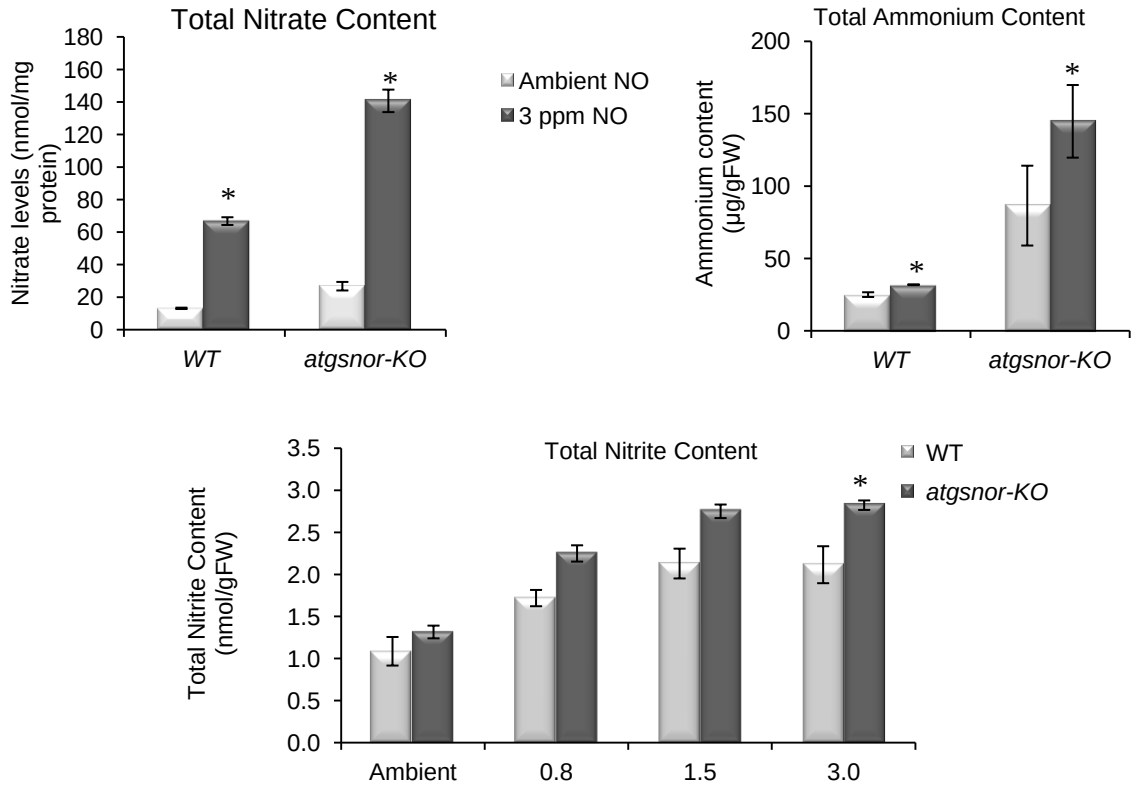

Figure 15 - Total nitrate, nitrite and ammonia levels in plant rosettes.
Nitrate content of the four-week old plant leaves of both WT and *atgsnor-KO* were estimated using chemiluminescence detection method. Ammonia content of the four-week old plant leaves of both WT and *atgsnor-KO* were estimated calorimetrically. Nitrite content in the four-week old WT and five-week old *atgsnor-KO* were determined using Apollo 4000 free radical analyzer. * indicates the significant difference between ambient and 3 ppm NO treatment ($p<0.01$). ±SD was determined from four independent experiments.

4.5 Uptake of fumigated NO by plant rosette leaves

Increase in the RSNO levels in plants can be considered either as an increase in the NO accumulation or as a decrease in the RSNO metabolism in the plants. RSNO levels and activity and accumulation of GSNOR were determined in the plants fumigated with NO. Rosette leaves from 4 week-old plants were harvested and analyzed for total RSNO levels. RSNO levels in the *atgsnor-KO* plants (~15 pmol/ mg protein) were 50% higher than that of WT plants (~10 pmol/ mg protein) grown under ambient conditions (Figure 16A). However, NO fumigation resulted in an increase of the RSNO levels by 150% in both the plant lines regardless of the presence or absence of functional GSNOR enzyme (Figure 16A). Biotin switch assay was performed to see the effect of increased RSNO accumulation (by NO fumigation) on the protein S-nitrosylation.

This assay however, did not show a major increase in the S-nitrosylation levels of proteins in WT plants (Figure 16B).

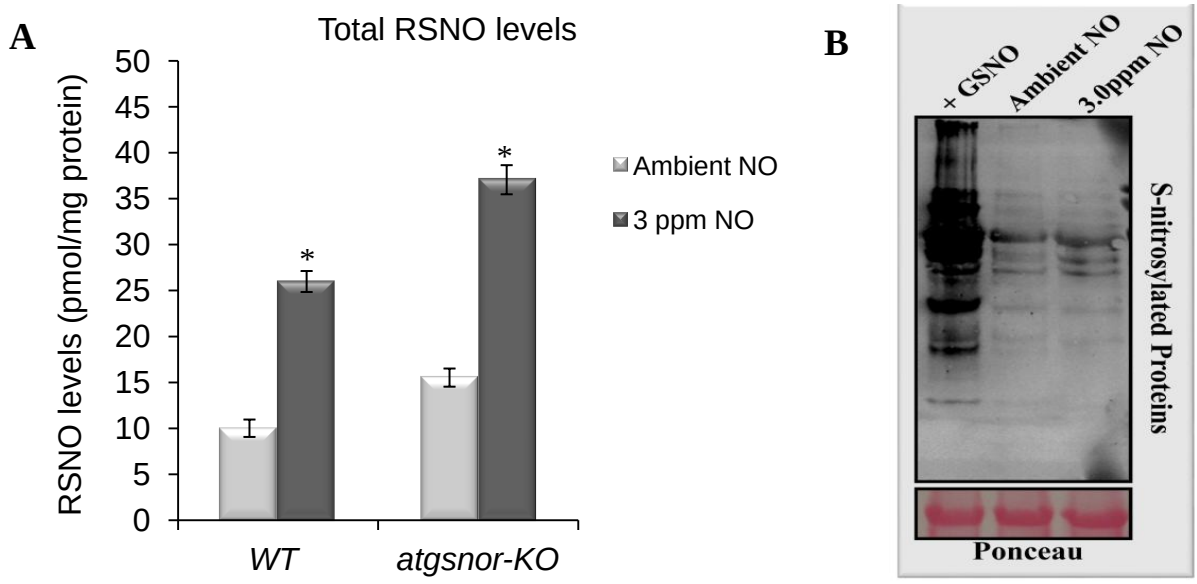

Figure 16 - Detection of RSNO levels and protein S-nitrosylation levels in plant leaves.
A) RSNO levels of the four-week old plant leaves of both WT and *atgsnor-KO* were estimated using chemiluminescence detection method. *shows the significant difference ($p<0.01$) in the RSNO level due to 3 ppm NO fumigation. B) Four-week old WT plant leaves were used to study the protein S-nitrosylation using biotin-switch method. GSNO treated protein sample from ambient conditions were used as a positive control. Ponceau stain showed uniform protein loading in all the three samples. Similar tendency was observed in all the four independent experiments.

Western blot analysis and GSNOR activity assay were further carried out to see whether the RSNO accumulation in plants was due to the inhibition of GSNOR protein accumulation or its activity respectively. Total RSNO levels were determined by chemiluminescent detection method. Though there was an increase in the accumulation of GSNOR proteins with age, no noticeable differences were observed in its accumulation due to NO fumigation at any point of time (Figure 17A). As expected, GSNOR proteins were not detectable in the *atgsnor-KO* plants in the immunoblotting analysis using the polyclonal antibody raised against functional GSNOR proteins (Figure 17A). Activity of GSNOR spectrophotometrically is equivalent to consumed NADH which it uses as an electron acceptor for each molecule of GSNO metabolized in the reaction vial. GSNOR activities from both ambient NO and 3 ppm NO treated rosette leaves were measured as 0.386 and 0.389 μkat/mg of protein (Figure 17B) showing no significant differences between the two treatment groups.

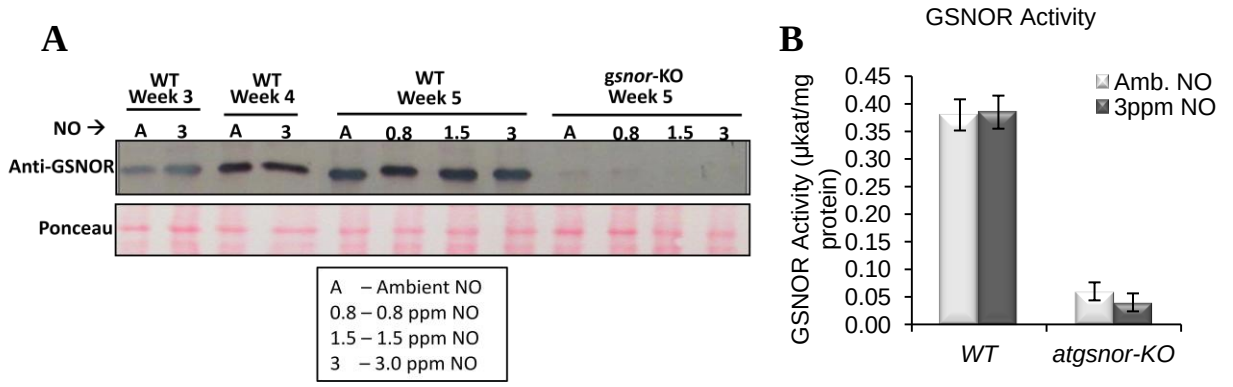

Figure 17 – Response of GSNOR to NO fumigation

A) Accumulation of GSNOR proteins were analyzed using western blot in WT and *atgsnor-KO* plants. Ponceau staining of the blotted membrane showed that same amount of proteins were loaded in all the samples. Similar results were obtained in all the four biological repeats. B) GSNOR activity was determined by spectrophotometric analysis. ±SD was determined from four independent experiments.

4.6 Alteration of gene expression profiles in response to NO fumigation

An expression profiling of more than 27,000 *Arabidopsis thaliana* nuclear transcripts of both ambient and 3 ppm NO fumigated plants from WT and *atgsnor-KO* was carried out using microarray technique (based on Agilent One Color Microarray-based Gene Expression Analysis platform). Total RNA from the rosette leaves was isolated and their quality was assured using Agilent RNA 6000 Nano kit on Agilent 2100 BioAnalyzer. All the RNA isolates showed a RNA integrity number (RIN) value much above the threshold minimum of 7. Two slides carrying eight 60K microarray chips were used to analyze four biological replicates from four treatment groups (WT Ambient, WT 3 ppm NO, *atgsnor*-KO Ambient and *atgsnor*-KO 3 ppm). Following cRNA synthesis, chip hybridization, scanning and feature extraction, raw expression data of the genes was analyzed using GeneSpring GX software tool. One of the four biological replicates failed to pass quality control and hence the final analysis was restricted to three biological replicates from each group. Statistical analysis were carried out to identify the differentially expressed genes ($p<0.05$) between the treatments in both the lines using One Way ANOVA analysis with the Benjamini-Hochberg multiple test correction (FDR) and SNP Post-hoc test. From the gene list, those that are differentially regulated at least by two fold difference were filtered for downstream analysis.

A total of 1534 genes were differentially regulated in the WT plants after NO fumigation. Out of 1534, 1097 genes were upregulated in plants fumigated with 3 ppm NO compared to ambient

plants and 437 genes were upregulated in plants grown under ambient conditions compared to 3 ppm NO fumigated plants(Figure 18A). In *atgsnor-KO* plants, 1862 genes were differentially expresses in plants grown in grown in different NO conditions. 1262 genes were upregulated in 3 ppm NO fumigated plants and 600 genes upregulated in the plants grown under ambient conditions (Figure 18A). WT and *atgsnor-KO* were then compared to identify gene candidates that were differentially affected by NO (Figure 18B). While 6 genes (AT5G37970, AT4G14080, AT5G51950, AT3G42960, AT4G28790 and AT1G72110) were upregulated in 3 ppm NO fumigated *atgsnor-KO* plants, the same genes showed upregulation in the ambient NO grown plants of WT. On the other hand, only one gene (AT5G28237) that showed upregulation in ambient grown *atgsnor-KO* was observed to be upregulated in 3 ppm NO fumigated plants of WT. However, WT and *atgsnor*-KO plants showed similar upregulation of 626 genes in 3 ppm NO fumigated plants and upregulation of 236 genes in ambient grown plants. More than 50% of the genes remained either regulated in WT or *atgsnor*-KO alone (Figure 18B). However these genes were showing similar tendencies in the both lines but they failed to reach the threshold of 2 fold difference in their expression between the two treatment groups. This might be due to the differences in the age of WT and *atgsnor-KO* plants used for the analysis.

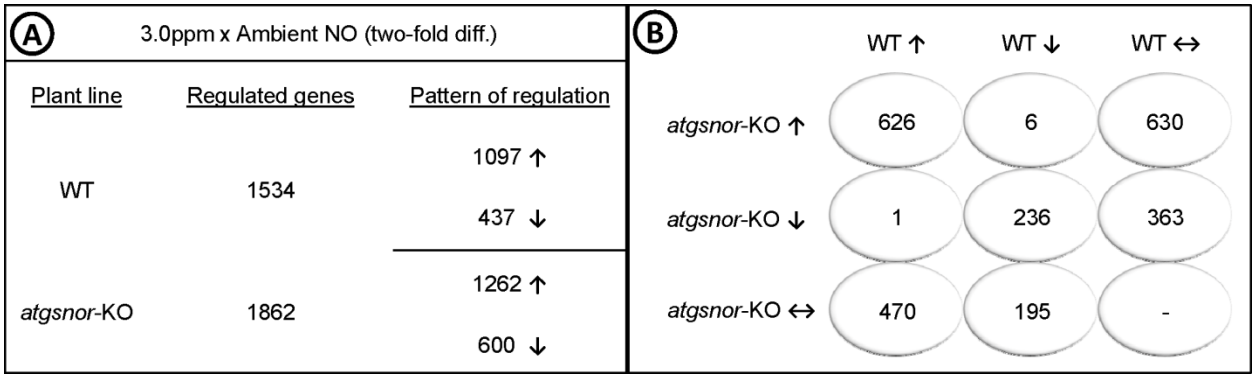

Figure 18 - Differential gene expression in NO fumigated plants
A) Figure highlights the total number of genes that showed a difference in expression by 2 fold in WT and *atgsnor-KO* plant lines after microarray analysis. Their direction of regulation (up or down) is also given. B) A comparative analysis between NO-regulated genes of WT and *atgsnor-KO* plants. '↑' denotes the up-regulated genes; '↓' denotes the down-regulated genes; and '↔' denotes no differential regulation.

4.6.1 Gene ontology enrichment analysis of differentially regulated genes

Gene ontology (GO) enrichment analysis was carried out using the regulated set of genes from both the lines to identify the major biological processes influenced by NO fumigation treatment.

TAIR's GO annotations platform was used for the analysis (Berardini et al., 2004). GO analysis showed similar percentage of distribution of genes among the biological processes in both WT and *atgsnor-KO* plants.

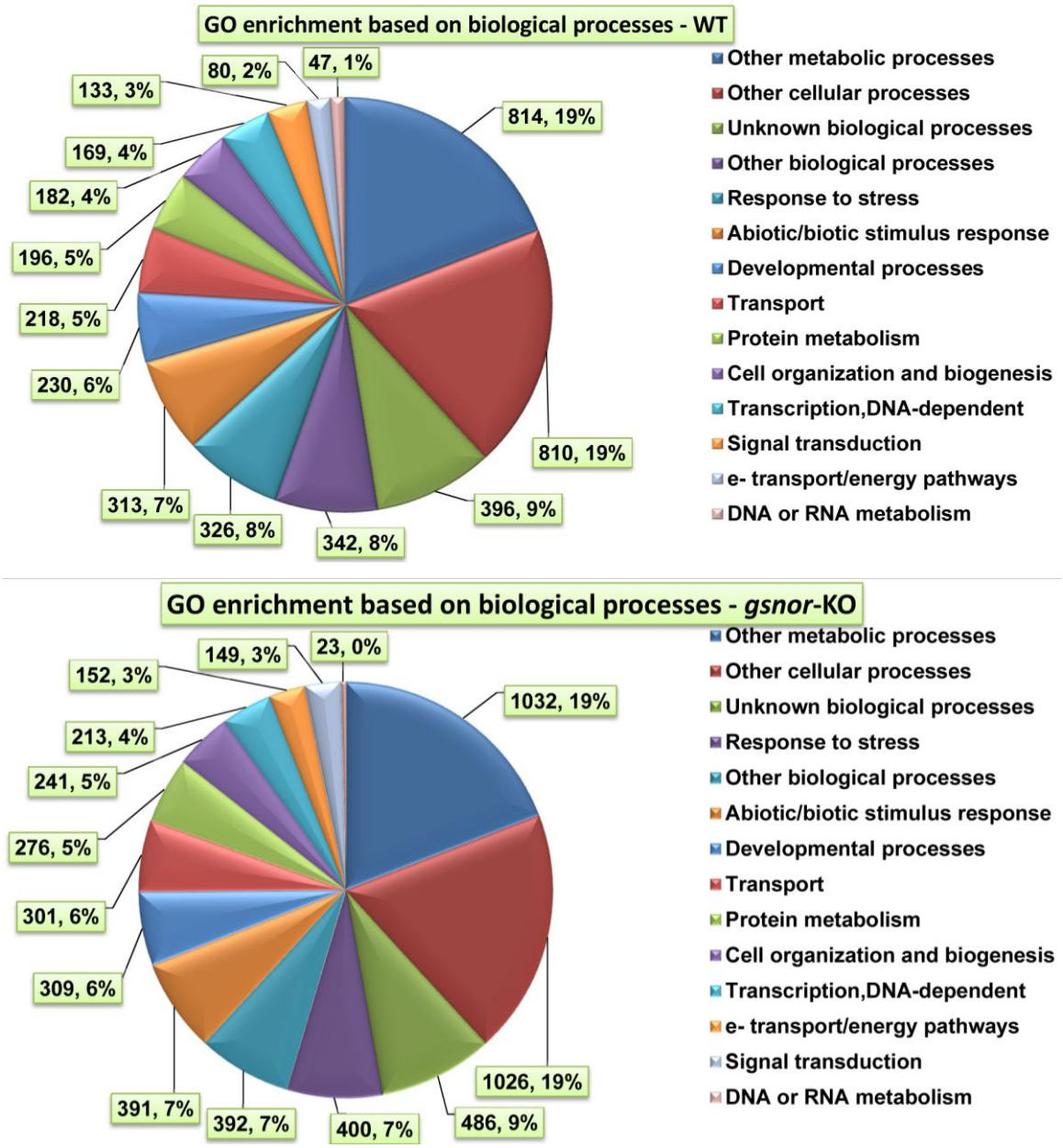

Figure 19 - Pie chart - GO enriched 2-fold regulated genes.
Information in the box contains number of genes and percentage of the genes in that group.

1624 genes from WT (about 40%) and 2058 genes from *atgsnor-KO* (about 40%) plants were those having a significant role in the normal cellular/metabolic processes (Figure 19). This provided a clear indication that NO accumulation could significantly alter the cellular metabolic

processes in plants. About 10% of the differentially regulated genes from both WT and *atgsnor-KO* were those not having a specific function assigned to them (unknown function). Another interesting group of differentially regulated genes in the both plants was of those having function in stress related processes. They constitute about 9% of the regulated genes in both plant lines (Figure 19). NO is known to be an important regulator and mediator of stress related responses in *Arabidopsis thaliana*. GO analysis revealed that though there is a big difference in the number of genes regulated in WT and *atgsnor-KO* due to NO fumigation (Figure 18), percentage of genes that belongs to each category was always the same in both the plant lines.

4.6.2 Identification of the major pathways influenced by NO treatment.

To identify major pathways influenced by NO fumigation, transcripts from both WT and *atgsnor-KO* plants that were significantly upregulated by 1.5 fold were mapped against the metabolic pathways in *Arabidopsis thaliana* using Mapman Software 3.5.1R2. It has been suggested that the gene with a numerical fold change greater than 1.5 can be considered as differentially expressed genes specifically for pathway analysis (Joung et al., 2009). This allows one to include the major and minor contributors of a significantly affected pathway. The input file for mapping contained gene identifier (locus tag) and $\log_2$ fold change value. Mapman mapped all the genes quantitatively to the predefined pathways. Statistical significance (p-value cut-off 0.05 with Benjamini-Hochberg FDR) was calculated based on the number of elements (individual genes) present in each pathway. List of statistically significant pathways influenced by NO fumigation in WT plants and *atgsnor-KO* plants are given in the Table 8 and Table 9 respectively. Most influenced gene groups in both WT and *atgsnor-KO* plants by NO fumigation were those involved in the pathways associated with photosystem (PS). NO fumigation significantly upregulated most of the genes in this pathway. Secondary metabolism was also significantly affected in both the plants. While the genes involving secondary metabolism of flavonoids and phenylpropanoids were significantly upregulated under ambient NO grown plants, those involved in the synthesis of sulfur-containing glucosinolates were significantly upregulated 3 ppm NO fumigated plants (Table 8 and Table 9). Other significantly affected pathways include amino acid synthesis and protein synthesis. Auxin and jasmonic acid (JA) responsive genes were also significantly upregulated during 3 ppm NO fumigation.

Table 8 - List of pathways influenced by NO treatment in WT plants

[a)]Bin	[b)]Name	[c)]no	[d)]p-value
1	PS	83	0.00000
1.1	PS.lightreaction	65	0.00000
35.1.5	not assigned.no ontology.pentatricopeptide repeat-containing protein	47	0.00000
1.1.1	PS.lightreaction.photosystem II	36	0.00001
16.5.1	secondary metabolism.sulfur-containing.glucosinolates	37	0.00002
17.2.3	hormone metabolism.auxin.induced-regulated-responsive-activated	40	0.00008
1.1.1.1	PS.lightreaction.photosystem II.LHC-II	13	0.00009
29.2	protein.synthesis	57	0.00013
16.5	secondary metabolism.sulfur-containing	40	0.00019
17.2	hormone metabolism.auxin	48	0.00036
16.5.1.1	secondary metabolism.sulfur-containing.glucosinolates.synthesis	22	0.00038
27.1	RNA.processing	25	0.00075
1.1.2	PS.lightreaction.photosystem I	19	0.00106
29	protein	321	0.00173
26.16	misc.myrosinases-lectin-jacalin	19	0.00274
20.1.7.12	stress.biotic.PR-proteins.plant defensins	10	0.00274
20	stress	176	0.00287
17	hormone metabolism	111	0.00720
29.2.1	protein.synthesis.ribosomal protein	41	0.00787
1.1.2.2	PS.lightreaction.photosystem I.PSI polypeptide subunits	12	0.01132
26	misc	334	0.01180
29.5.9	protein.degradation.AAA type	11	0.01212
16.5.1.1.1	secondary metabol.S-containing.glucosinolates.synthesis.aliphatic	16	0.01380
20.1.7.6.1	stress.biotic.PR-proteins.proteinase inhibitors.trypsin inhibitor	5	0.01419
29.2.1.2	protein.synthesis.ribosomal protein.eukaryotic	19	0.01580
20.1	stress.biotic	84	0.01884
27.2	RNA.transcription	12	0.01995
9	mitochondrial electron transport / ATP synthesis	6	0.02165
16.8	secondary metabolism.flavonoids	37	0.02713
27	RNA	363	0.02801
1.1.1.2	PS.lightreaction.photosystem II.PSII polypeptide subunits	23	0.03055
20.1.7	stress.biotic.PR-proteins	39	0.04471

The table highlights the significantly affected metabolic pathways in WT Arabidopsis thaliana plants by the exposure to 3.0ppm NO. The analysis was carried out using Mapman software 3.5.1.R2 using the differentially regulated gene data obtained from comparitive microarray analysis of WT plants exposed to ambient and 3.0ppm NO. Locus tag along with the fold change values (≥ 1.5) obtained from the microarray analysis were the input data given to Mapman. Mapman compare this data with the mapping file Ath_AGI_TAIR9_Jan2010 from agilent and produces a score that depends on the number of elements (genes) found in a specific pathway and their fold change.

a) Number assigned to pathways by the mapping file in Mapman software b) Title of the pathway c) Number of elements (genes) found in each pathway d) Probability is measured using number elements identified (genes) involved in a specific pathway against the total number of elements present in the pathway, hierarchical order of the elements in the pathway and the fold change.

NO fumigation treatment also induced defense related proteins. In general, accumulation of NO induced many pathways related to plant metabolic processes and also those associated with NO signaling processes. Genes that encode proteins involved in mitochondrial electron transport chain were upregulated in ambient grown plants suggesting a metabolic shift from photosynthesis to respiration in these plants.

Table 9 - List of pathways influenced by NO treatment in *atgsnor-KO* plants

[a)]Bin	[b)]Name	[c)]no	[d)]p-value
1.1	PS.lightreaction	79	0.00000
1	PS	118	0.00000
1.1.1	PS.lightreaction.photosystem II	41	0.00000
1.1.2	PS.lightreaction.photosystem I	19	0.00000
1.1.1.2	PS.lightreaction.photosystem II.PSII polypeptide subunits	28	0.00000
1.1.1.1	PS.lightreaction.photosystem II.LHC-II	13	0.00000
17.2.3	hormone metabolism.auxin.induced-regulated-responsive-activated	38	0.00001
1.1.2.2	PS.lightreaction.photosystem I.PSI polypeptide subunits	13	0.00002
1.3	PS.calvin cyle	27	0.00005
17.2	hormone metabolism.auxin	45	0.00011
29.2.1.1	protein.synthesis.ribosomal protein.prokaryotic	37	0.00149
29.2.1.1.1	protein.synthesis.ribosomal protein.prokaryotic.chloroplast	32	0.00368
16.8	secondary metabolism.flavonoids	44	0.00698
19	tetrapyrrole synthesis	24	0.00977
1.1.2.1	PS.lightreaction.photosystem I.LHC-I	6	0.01325
29.2.1	protein.synthesis.ribosomal protein	43	0.01548
17	hormone metabolism	122	0.03157
16.5.1	secondary metabolism.sulfur-containing.glucosinolates	36	0.03346
29.2.1.1.1.2	protein.synthesis.ribosomal protein.prokaryotic.chloroplast.50S	23	0.03841
13.1.3	amino acid metabolism.synthesis.aspartate family	11	0.03841
20.1.7.12	stress.biotic.PR-proteins.plant defensins	13	0.04079
26.13	misc.acid and other phosphatases	20	0.04079
34.16	transport.ABC transporters and multidrug resistance systems	21	0.04454
1.1.5	PS.lightreaction.other electron carrier (ox/red)	7	0.04717
30.1	signalling.in sugar and nutrient physiology	5	0.04717
30.1.1	signalling.in sugar and nutrient physiology	5	0.04717

The table highlights the significantly affected metabolic pathways in *atgsnor*-KO Arabidopsis thaliana plants by the exposure to 3.0ppm NO. The analysis was carried out using Mapman software 3.5.1.R2 using the differentially regulated gene data obtained from comparitive microarray analysis of *atgsnor* KO plants exposed to ambient and 3.0ppm NO. Locus tag along with the fold change values (≥ 1.5) obtained from the microarray analysis were the input data given to Mapman. Mapman compare this data with the mapping file Ath_AGI_TAIR9_Jan2010 from agilent and produces a score that depends on the number of elements (genes) found in a specific pathway and their fold change.

a) Number assigned to pathways by the mapping file in Mapman software b) Title of the pathway c) Number of elements (genes) found in each pathway d) Probability is measured using number elements identified (genes) involved in a specific pathway against the total number of elements present in the pathway, hierarchical order of the elements in the pathway and the fold change.

4.7 Proteomic analysis to identify differentially accumulated proteins

Differences in the accumulation of proteins were investigated in order to understand the important changes in the protein level induced by NO fumigation. Protein extracts from the rosettes of WT Ws and *atgsnor-KO* Ws plants were analyzed using two dimensional difference gel electrophoresis (2D-DIGE). 2D-DIGE was carried out on Ettan DIGE platform. Proteins were labeled with fluorescence emitting dyes. It should be noted that the ability to bind with fluorescent dyes depends on the protein accumulation. Higher the protein accumulation due to NO treatment, higher will be its binding to the fluorescent dye. Proteins were then separated

based on their charge and size. After 2D-DIGE separation, images of fluorescent intensities of each sample labeled with dye was acquired and analyzed. We performed one-way ANOVA (*p* value set to 0.01) analysis across four groups with FDR correction (Benjamini Hochberg multiple testing correction) to minimize false-positive hits. From the spots filtered through ANOVA analysis, differentially accumulated protein spots were identified. These were at least two-fold regulated in all the three biological replications used. List of protein extracts from NO exposed leaves of plants and the dyes used to label them for 2D DIGE analysis are given in the Supplementary Table 1.

From the image analysis, 57 protein spots each from WT and *atgsnor-KO* gels were identified to be differential accumulated due to NO fumigation. These spots were numbered (Figure 20) and proteins in each spot were identified using Matrix-assisted laser desorption/ionization time-of-flight mass spectroscopy (MALDI-TOF/TOF MS) analysis. The accumulation pattern of these identified proteins on the gel has been summarized in Table 10. Supplementary Table 2 shows list of these proteins and their regulation pattern after fumigating plants with 3 ppm NO.

Table 10 – Differential regulation pattern of the identified proteins
↑ - enhanced accumulation and ↓ - decreased accumulation of proteins due to NO treatment.

	0.8 ppm NO		1.5 ppm NO		3 ppm NO	
WT	04	03 ↑	27	23 ↑	87	75 ↑
		01 ↓		04 ↓		12 ↓
atgsnor-KO	04	04 ↑	41	36 ↑	87	76 ↑
		00 ↓		05 ↓		11 ↓

A total of 93 proteins were identified using MALDI-TOF/TOF analysis from 57 protein 2D-DIGE gel spots. Out of 93, 71 proteins showed higher accumulation in 3 ppm NO fumigated plants and 10 showed higher accumulation under ambient grown plants in a similar fashion in both WT and *atgsnor*-KO plants (Figure 21). While 4 and 2 proteins respectively were accumulated alone in the 3 ppm NO fumigated plants of WT and *atgsnor-KO*, 2 and 1 proteins respectively were accumulated alone in the ambient grown plants of WT and *atgsnor-KO* (Figure 21). However these unique proteins showed similar accumulation pattern in both the plant lines but failed to reach the threshold of two-fold difference (Supplementary Table 2).

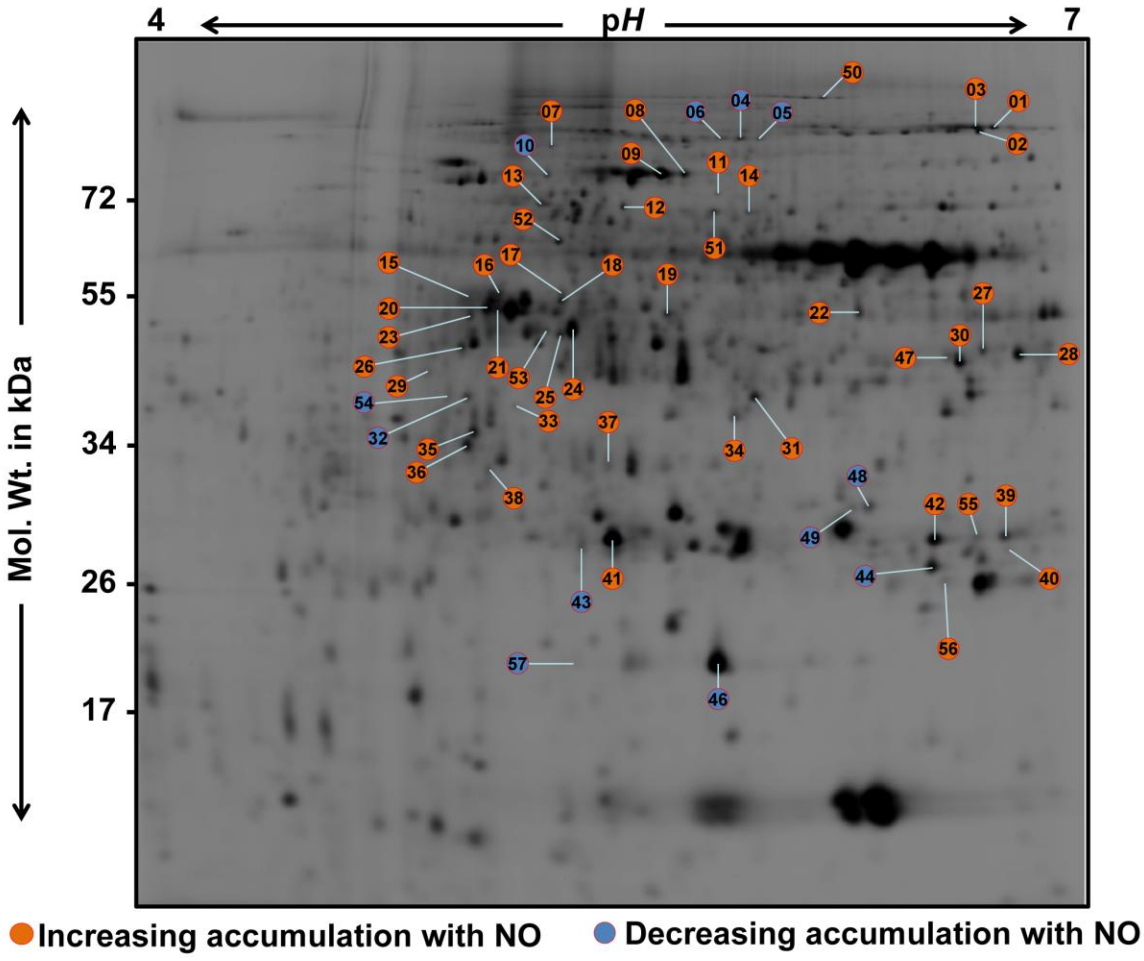

Figure 20 – Numbering of the differentially regulated protein spots in 2D-DIGE gel.
Saffron circles: ≥ 2-fold accumulation; Blue circles: ≤ -2-fold accumulation.

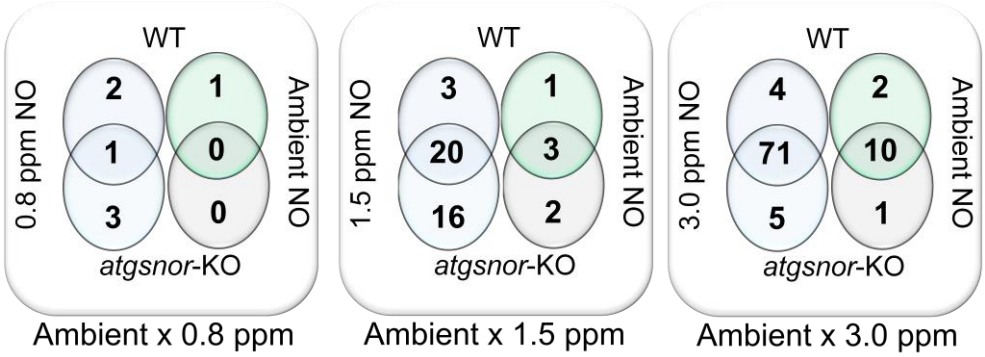

Figure 21 – Three experiment groups showing 2-way distribution of accumulated proteins.
1st way – Left to right: Each of three Venn diagram represents number of accumulated proteins in the corresponding NO treated group (left) and those accumulated under Ambient NO group (right). 2nd way – Top to bottom: Plant line-wise comparison of the differentially accumulated proteins in each of the three combinations analyzed in 1st way.

4.7.1 GO enrichment analysis of the identified proteins

Differentially expressed proteins in Ws WT plants were screened for the GO enrichment analysis to classify them based on the cellular compartments wherein they function (Figure 22) and the biological processes in which they participate (Figure 23). Analysis was carried out to identify the main class of proteins that are influenced by different NO conditions. TAIR's GO annotations platform was used for the analysis (Berardini et al., 2004).

4.7.2 GO Enrichment of the identified proteins from WT plants

GO enrichment analysis based on cellular compartments (Figure 22) reveals that about a quarter of the total identified proteins (25%) are those that are functioning in plastids and chloroplasts. Chloroplast is the main center of photosynthesis and N-assimilation. While 16% of the identified proteins were localized into cytoplasmic components, 6% were plasma membrane proteins. Mitochondrial and nuclear proteins were 4% of the total proteins identified. GO enrichment analysis based on cellular components suggested that proteins localized in the chloroplast are the ones most affected by NO fumigation. Similar results were obtained using microarray data (Figure 19). The above data suggests that chloroplast is the most significantly affected plant component upon NO fumigation treatment.

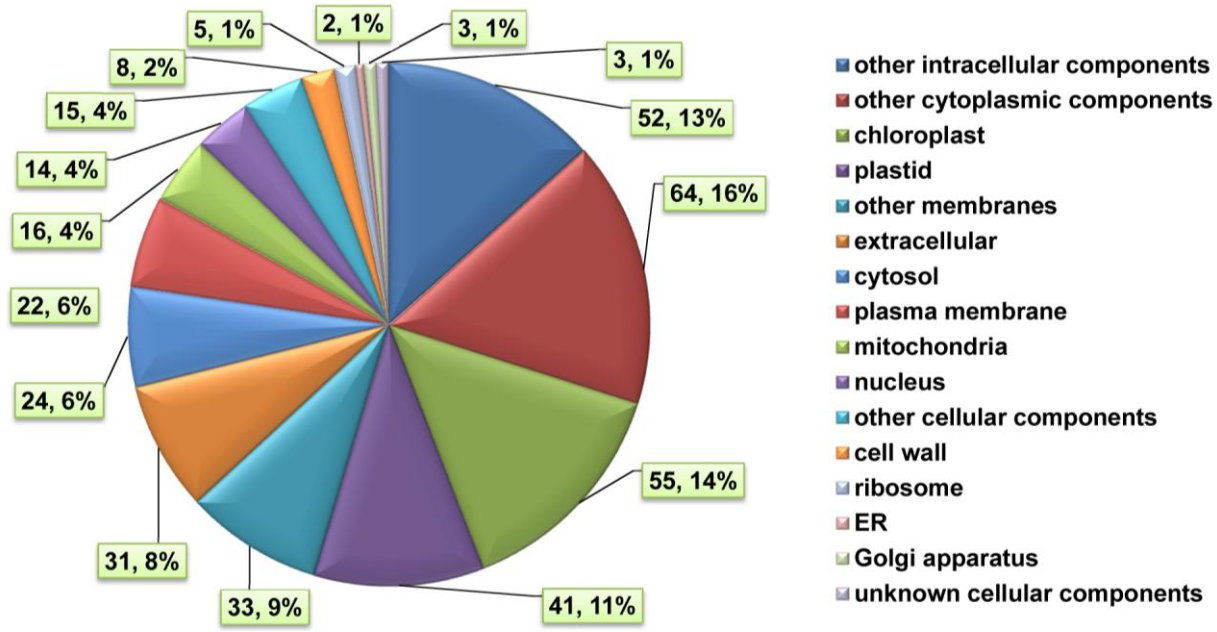

Figure 22 - Pie chart - GO enriched 2-fold regulated proteins (cellular components)
Information in the box contains number of proteins and percentage of proteins in that group.

4.7.3 GO enrichment of the identified proteins from *atgsnor-KO*

GO enrichment analysis based on biological processes (Figure 23) highlights that the proteins involved in metabolic and cellular processes (~30%) are the major class of proteins affected by NO treatment. NO is known to be an important regulator of patho-physiological processes. About 22% of identified proteins have stress related functions. Other major classes of proteins affected by NO exposure were those having functions in cell organization and biogenesis, energy transduction, transport, developmental processes and signal transduction. Again, functional analysis of the proteins was in strong agreement with regulation pattern of transcripts obtained after the microarray analysis (Figure 19).

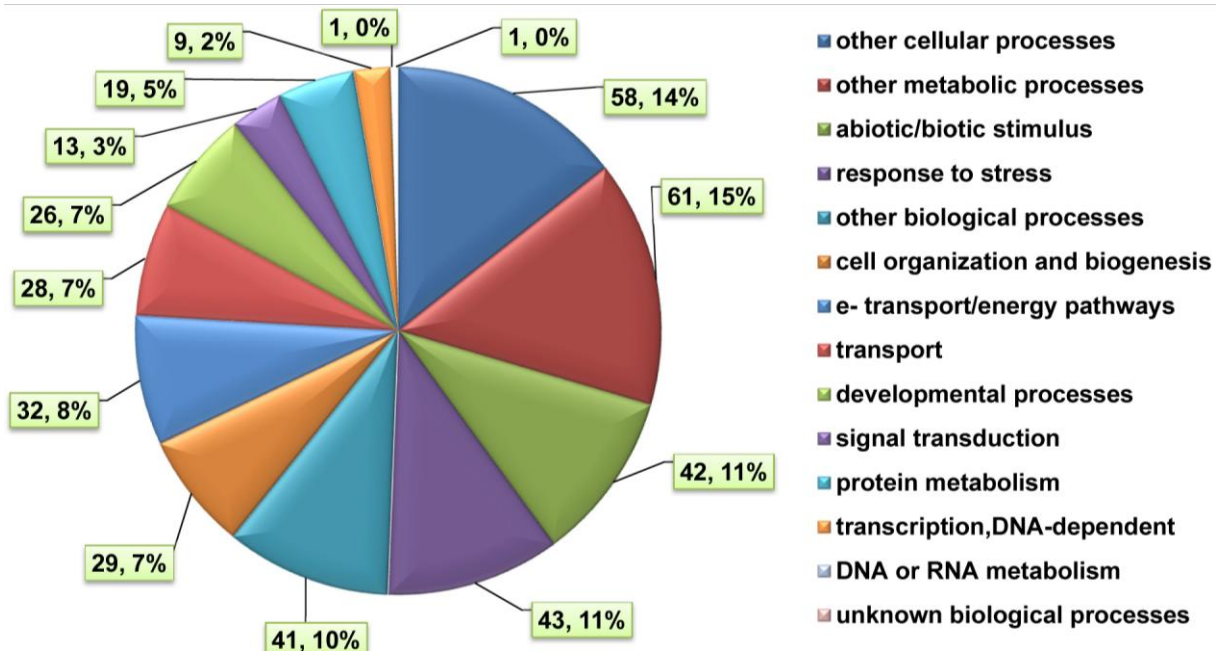

Figure 23 - Pie chart - GO enriched 2-fold regulated proteins (biological processes).
Information in the box contains number of genes and percentage of genes in that group.

In the high through-put transcriptome and proteome analysis, about 50% of the proteins that showed significant difference in their accumulation at the protein level were also regulated at the transcript level (Supplementary Table 3). Of these, the enzymes involved in nitrate assimilation (nitrite reductase 1), light reaction (photosystem II subunit oxygen evolving), cellular metabolism (ferredoxin-NADP(+)-oxidoreductase 2, transketolase and phosphoglycerate kinase) and redox processes (glutathione-S-transferase PHI 2) were the ones that showed significant accumulation in all the treatment groups analyzed using 2D-DIGE and microarray.

4.8 Analysis of the pathway mediated by phenylalanine ammonia lyase

Genes involved in the phenylpropanoid pathway, which leads to the flavonoid synthesis showed significant difference in their regulation between the plants grown in different NO conditions (Table 8 and Table 9). Many genes involved in this pathway showed a reduced expression in the plants fumigated with 3 ppm NO in comparison to the plants grown under ambient conditions. A simplified representation of the phenylpropanoid pathway, important enzymes involved in the pathway and their regulations at transcript level have been summarized in Figure 24.

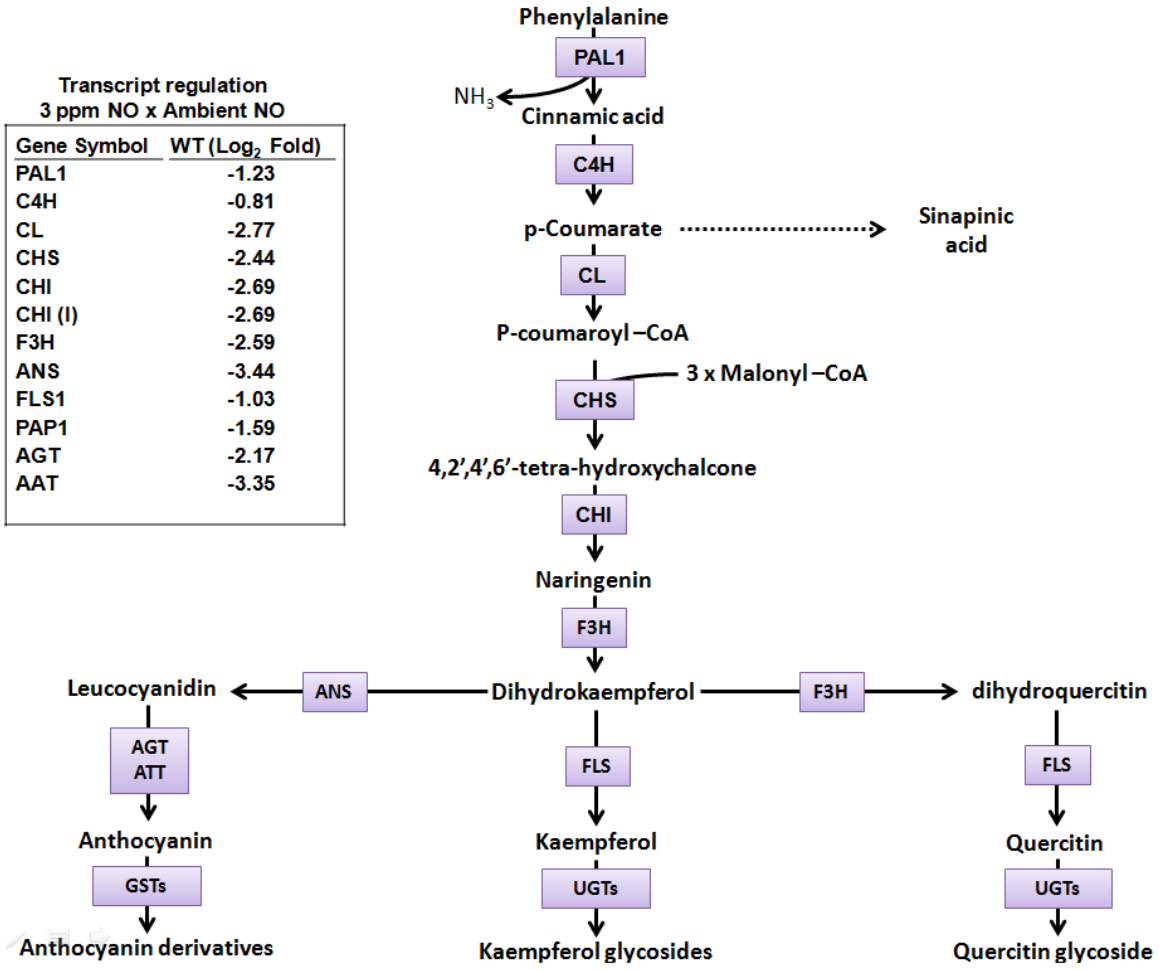

Figure 24 - Phenylpropanoid pathway and regulated genes in the pathway.
Simplified form of the Phenylpropanoid pathway which leads to the biosynthesis of flavonoid (MacKay et al., 1997, Tohge et al., 2005, Rubin et al., 2009, Yin et al., 2012). Inset shows the NO-dependent fold change of each gene involved in the pathway in WT plants. PAL1 – Phenylalanine ammonia lyase 1, C4H – Cinnamate-4-hydroxylase, CL – 4-Coumarate-CoA ligase, CHS – Chalcone synthase, CHI – Chalcone isomerase, F3H – Flavanone-3-hydroxylase, ANS – Anthocyanidin synthase, AGT – Anthocyanin glycosyltransferase, AAT – Anthocyanin acyltransferase, FLS – synthase, GSTs – Glutathione-S-transferases and UGTs - UDP-glycosyltransferase.

Most of the genes that encodes important enzymes in the phenylpropanoid pathway showed reduced expression in the four- week old WT plants (Figure 24 - inset). Similar regulation pattern of the transcripts of these enzymes were also observed in 3 ppm NO treated *atgsnor-KO lines* (data not shown). Differential expression of the important genes in this pathway is shown in the Supplementary Figure 1. The only enzyme that did not show a two-fold regulation at its transcript level was cinnamte-4-hydroxylase (C4H) (Figure 24 - inset). C4H enzyme mediates the conversion of cinnamic acid to *p*-coumarate in the phenylpropanoid pathway. Transcripts of *C4H* however, showed a similar tendency like other genes in the pathway (Supplementary Figure 1). Phenylpropanoid pathway leads to the synthesis of anthocyanin and its derivatives. Their accumulation was observed under ambient grown plants; it resulted in red senescence (Figure 11A). Transcripts of the enzymes mediating quercetin and kaempferol synthesis also showed reduced expression in 3 ppm NO fumigated plants (Figure 24). Sinapinic acid is another important secondary metabolite synthesized in this pathway. Phenylalanine ammonia lyase (PAL) is the first enzyme of the phenylpropanoid pathway (Dixon & Paiva, 1995). PAL is encoded by four genes in *Arabidopsis thaliana* named *PAL1* to *PAL4* (Raes et al., 2003). *PAL1, PAL2* and *PAL4* showed reduced expression in the WT plants fumigated 3 ppm NO (Supplementary Figure 1 and Supplementary Figure 2). However, only *PAL1* showed two-fold change in the level of expression after 3 ppm NO fumigation (Supplementary Figure 1 and Supplementary Figure 2). On the other hand, *PAL3* showed higher induction in the plants fumigated with 3 ppm NO (Supplementary Figure 2).

4.8.1 Transcript analysis and activity detection of PAL

mRNA transcripts of *PAL1* and *PAL2* were amplified using semi-quantitative reverse-transcriptase PCR (semi RT-PCR) (Figure 25A). Reduced expression of *PAL1* genes was clearly visible after 30 cycles of PCR in WT and 27 cycles of PCR in *atgsnor*-KO lines in the plants treated with 3 ppm NO in comparison to those grown under ambient conditions. However, *PAL2* expression did not show significant difference between ambient and 3 ppm NO treated plants. Semi RT-PCR results on *PAL1* and *PAL2* were in line with the microarray results. Moreover, the total PAL activity in both WT and *atgsnor*-KO plants was also compared between ambient and 3 ppm NO treatments (Figure 25B). Interestingly, the PAL activity in the both lines showed a significant down-regulation in NO exposed plants. These results are in agreement with the microarray results.

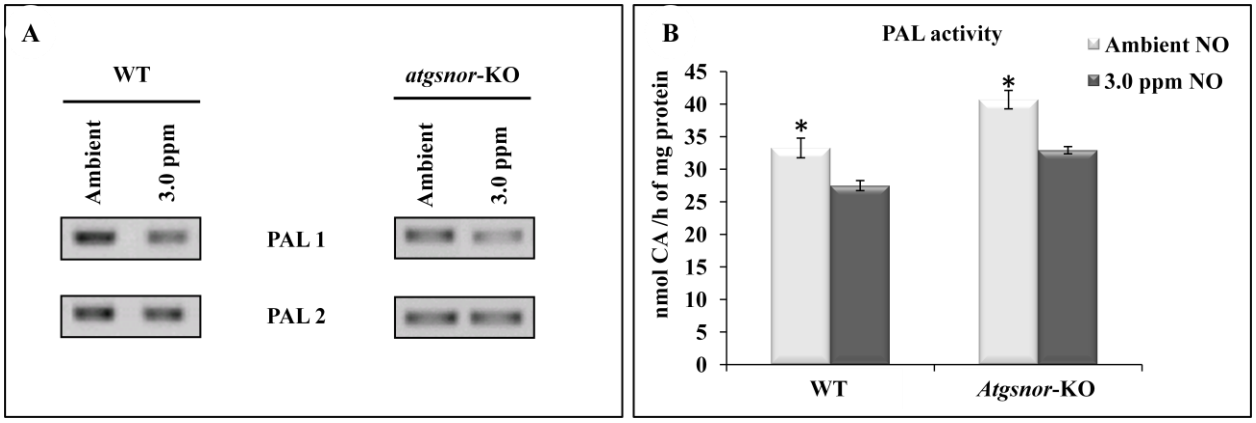

Figure 25 - *PAL* transcript analysis and enzyme activity
A) Transcript analysis was carried out using semi RT-PCR. After 27 cycles for *atgsnor*-KO and 30 cycles for WT, the bands were clearly visible. Similar results were obtained in all the four biological repeats. B) Conversion of phenylalanine to cinnamic acid is mediated by PAL enzyme. Activity was calculated by spectrophotometric determination of cinnamic acid formed in a reaction vessel containing PAL and phenylalanine activity. * denotes the significance level of the difference in PAL activity between Ambient and 3.0 ppm NO groups with $P<0.01$.

4.8.2 Quantification of flavonoid glycosides

Microarray results suggested reduced induction of flavonoid biosynthesis pathways in the plants fumigated with 3 ppm NO compared to plants grown under ambient conditions. Flavonoids generally occur in nature as glycosides. Quercetin and kaempferol belong to a class of flavonoids with 3-hydroxyflavone backbone and hence they are named as flavonol. They have multiple roles during plant development and are considered as antioxidants that can scavenge reactive oxygen species during stress responses (Fini et al., 2011, Winkel-Shirley, 2002). To quantify the flavonol levels in the leaves of NO treated samples, methanol leaf extracts were hydrolyzed to initiate the release of flavonol aglycones which were then analyzed by HPLC. Three major kaempferol glycosides present in leaves of *Arabidopsis thaliana* during non-stressed conditions were kaempferol 3-O-rhamnoside-7-O-rhamnoside, kaempferol 3-O-glucoside-7-O-rhamnoside and kaempferol-3-O-[rhamnosyl(1/2glucoside)]-7-O-rhamnoside (Bloor & Abrahams, 2002). Quercetin derivatives of all these glycosides were also known. 3 Kaempferol glycosides and 2 Quercetin glycosides were present in the detectable range in almost all the samples analyzed.

There was no significant difference in the levels of total kaempferol and quercetin contents in week 3 WT and week 4 *atgsnor*-KO NO treated plants. Plants did not show a phenotypic difference at this stage with respect to NO treatment. However, during 4th WAG differences in the phenotype were associated with differences in the kaempferol and quercetin content in the

plants. Compared to ambient NO treated plants, kaempferol accumulation was reduced by about 20% in four week-old WT plants and five week-old *atgsnor-KO* plants treated with 3 ppm NO (Figure 26). Differences between these two treatment groups were more prominent in the case of quercetin accumulation. There was about 60 – 70% reduction in its level after NO treatment. Their accumulation was directly proportional to the age of the plants and inversely proportional to the NO treatment concentration at each growth stage analyzed (Figure 26).

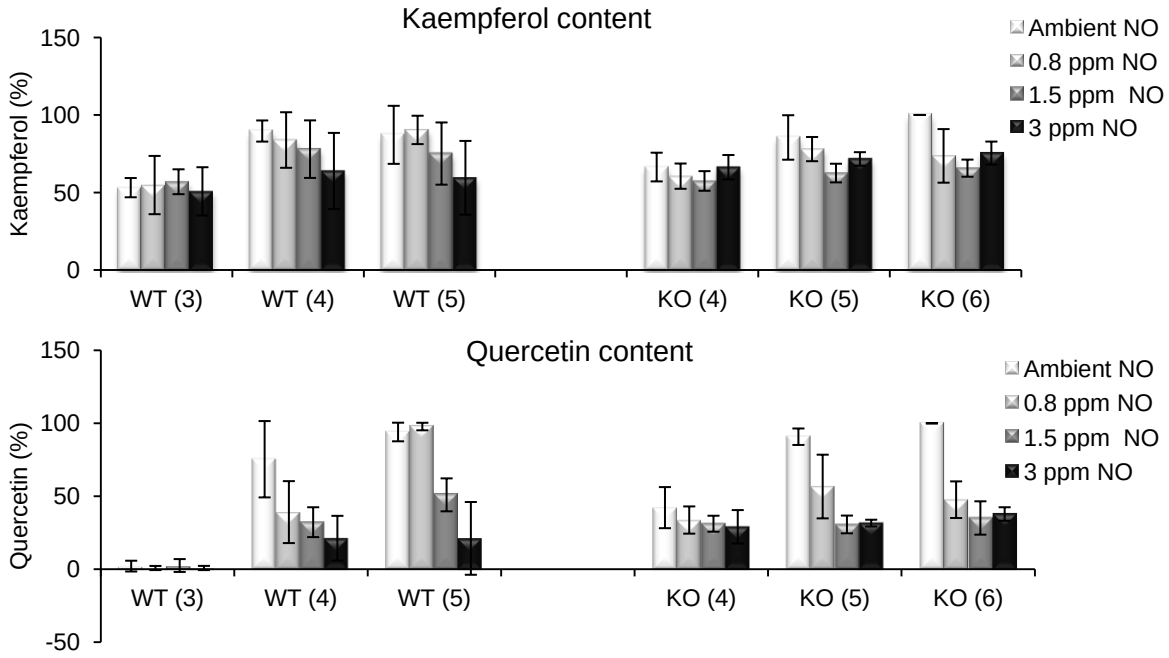

Figure 26 – Quantification of total kaempferol and quercetin content in rosette leaves.
Total kaempferol and quercetin aglycone were quantified after acid hydrolysis of the methanol extracts from leaves using HPLC. Maximum kaempferol content detected in WT was 2540 nmol/gFW and that in KO (*atgsnor-KO*) plants was 2672 nmol/gFW. Maximum quercetin content detected in WT was 451.9 nmol/gFW and that in KO (*atgsnor-KO*) plants was 773.67 nmol/gFW. WT – Wild type, KO- *atgsnor-KO*. 3, 4, 5 and 6 – Week after germination.

4.8.3 Quantification of sinapinic acid

Sinapinic acid is an aromatic secondary metabolite found in *Arabidopsis thaliana* that is synthesized via phenylpropanoid pathway. Though not strictly phenylpropanoid, they generally occur in conjugation with carbohydrates and organic acids and play a significant role in plant development and stress related responses (Dixon & Paiva, 1995). Sinapoylmalate, sinapoylglucose, and sinapoylcholine are the three major sinapate esters accumulated in *Arabidopsis* leaves (Landry et al., 1995, Lorenzen et al., 1996, Shirley et al., 2001, Bloor &

Abrahams, 2002, Fraser et al., 2007). All the three were present in the detectable range in almost all the samples analyzed.

Accumulation of sinapinic acid content was directly proportional to the aging of WT and *atgsnor-KO* plants. In both the plants accumulation was increased by almost 30 – 40% in two weeks (Figure 27). NO treatment, however, reduced the age-dependent accumulation of sinapinic acid in both plants. During 4th WAG in WT and 5th WAG in *atgsnor-KO*, plants showed a significant reduction in the accumulation of sinapinic acid after 3 ppm NO fumigation (Figure 27). The difference in concentration of sinapinic acid between ambient treated NO plants and 3 ppm NO plants increased at later stages. Similar to kaempferol and quercetin, sinapinic acid accumulation was directly proportional to the age of the plants and inversely proportional to the NO fumigation concentration (Figure 27).

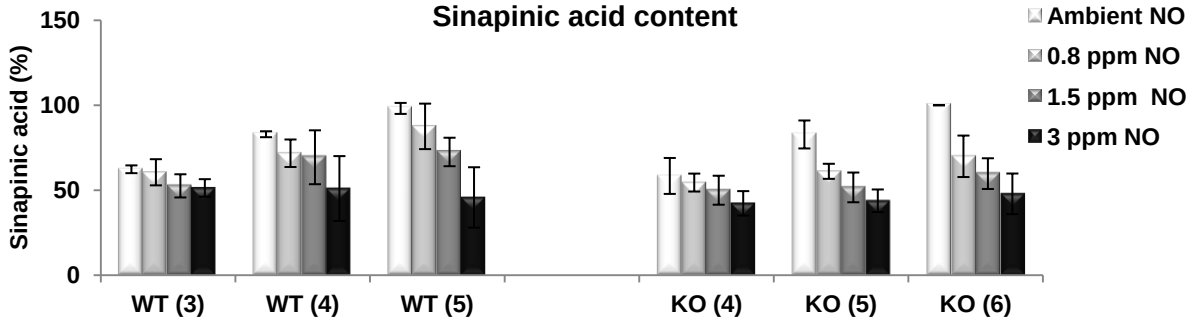

Figure 27 – Quantification of sinapinic acid.
Sinapinic acid quantification after acid hydrolysis of the methanolic extracts from leaves using HPLC. In WT maximum value detected was 1354 nmol/gFW and in KO (*gsnor*-KO) plants it was 1732 nmol/gFW. WT – Wild type, KO- *atgsnor-KO*. 3, 4, 5 and 6 – Week after germination.

4.9 NO exposure and senescence in *Arabidopsis thaliana*

Phenotype and secondary metabolite levels have provided evidences for delayed senescence in the *Arabidopsis thaliana* upon increasing NO fumigation treatment. In plant development, senescence is the final stage that marks the beginning of leaf death. During senescence total RNA, protein levels and chlorophyll levels decline rapidly (Lohman et al., 1994). RNA concentration reduced rapidly with the aging in plants (Figure 28). RNA content in the 5 week-old plants was reduced by 8 times as compared to that of 3 week-old plants. Plants fumigated with 3 ppm NO too showed reduction in the RNA content with age. However, the RNA content in each time point was much higher than those in the ambient NO fumigated plants (Figure 28).

Furthermore, delay in the RNA degradation was proportional to NO treatment concentration in the 5 week-old plants (Figure 28).

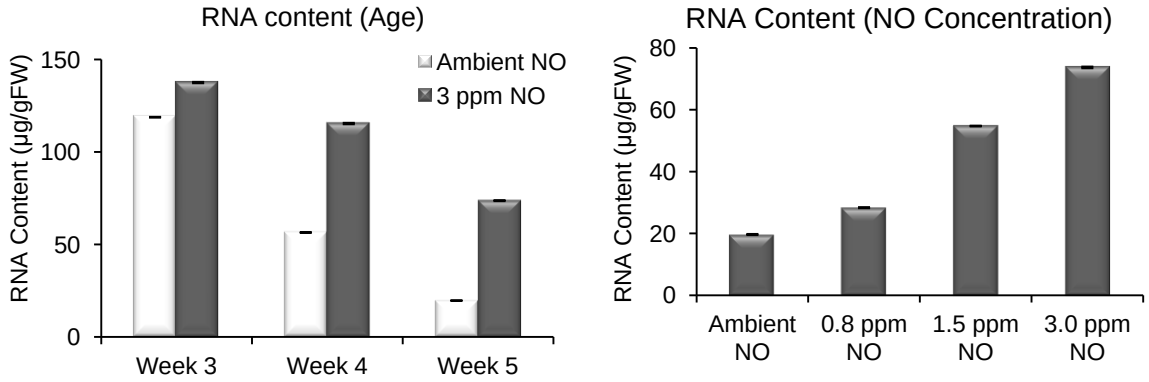

Figure 28 – RNA content in the plants treated with NO.
Total RNA from all the samples was extracted using a combination of Trizol and Qiagen® RNeasy Mini kit (see Section 3.4) and quantified using NanoDrop®1000. Analyzing the 'RNA content (age)' was carried out in WT *Arabidopsis thaliana* from Ws background. 'RNA content (NO Concentration)' was analyzed in the same plant line on 5th week after germination.

While majority of the genes expression were down regulated during senescence, certain genes are up-regulated and have crucial role in carrying out the senescence processes (Lohman et al., 1994). Senescence-associated genes (SAGs) are an important class of genes among them and are known to be induced during senescence. Figure 29 shows a list of some of the identified senescence-associated (SAG) and senescence-related (SRG) genes that are differentially regulated in the NO fumigated plants. Significant reduction in the transcript levels of *SAG12*, *SAG13*, *SAG29* and senescence related gene 1 (*SRG1*) were observed in the plants fumigated with NO in comparison to the plants grown in the ambient conditions (Figure 29). Among senescence associated genes, *SAG12* is the prominent one known in *Arabidopsis thaliana* and is a specific marker for age-related senescence process (Lohman et al., 1994). Delay in the induction of *SAG 12* expression in the 3 ppm NO fumigated plants were further confirmed using semi-RT PCR analysis (Figure 30). Semi-RT PCR could not detect *SAG12* transcripts from the WT plants after 3 WAG (Figure 30). Consequently, these plants did not show red senescence at 3 WAG (Figure 11B). However, *SAG12* was strongly inducted in the four and five-week old WT plants grown under ambient conditions (Figure 30). Accordingly, plants grown under ambient conditions showed red senescence at 4 WAG (Figure 11A). After NO treatment, their induction was significantly delayed. Interestingly, the delay was directly proportional to the fumigated NO

concentration (Figure 30). This was in line with the observed phenotype of the NO fumigated plants (Figure 11B).

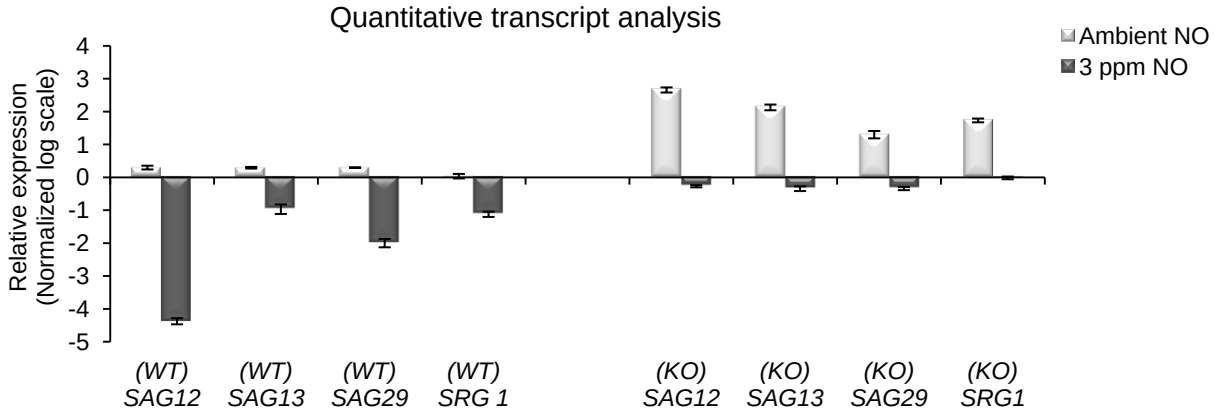

Figure 29 – Regulation of senescence-associated genes (microarray).
Four-week old WT and five week old *atgsnor-KO* (*KO*) lines were analyzed. The real expression values were normalized and baseline transformed (median) and visualized on log-scale. All the candidates (*SAG12*, *SAG13*, *SAG29* and *SRG1*) in both the lines showed at least one-fold expression change in the log scale (two fold change in the numerical scale).

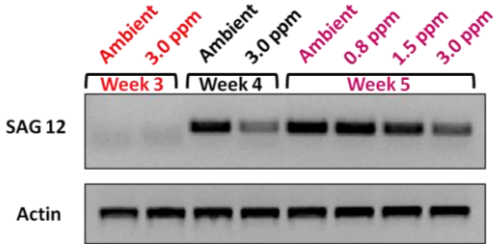

Figure 30 – Semi RT-PCR analysis of *SAG12*.
PCR cycles of 28 were used to amplify transcripts of *SAG12* from all the samples. Results shown are from WT plants. Similar results were obtained in all the four biological repeats of both WT and *atgsnor*-KO lines (27 cycles). Transcripts of actin filaments serve as a positive loading control.

SAG12 codes for a cysteine protease, which along with many other protein degrading enzymes promote total protein degradation in naturally senescing leaves (Lohman et al., 1994). In the plants grown under ambient conditions, there was a significant reduction in the protein content with age (Figure 31). Though, a similar age-dependent drop in the protein content was also observed in NO fumigated plants, their protein content were much high when compared to ambient NO fumigated plants at every time point analyzed (Figure 31). Moreover, increase in the protein content in the five-week old plants was directly proportional to NO concentration used for fumigating the plants (Figure 31).

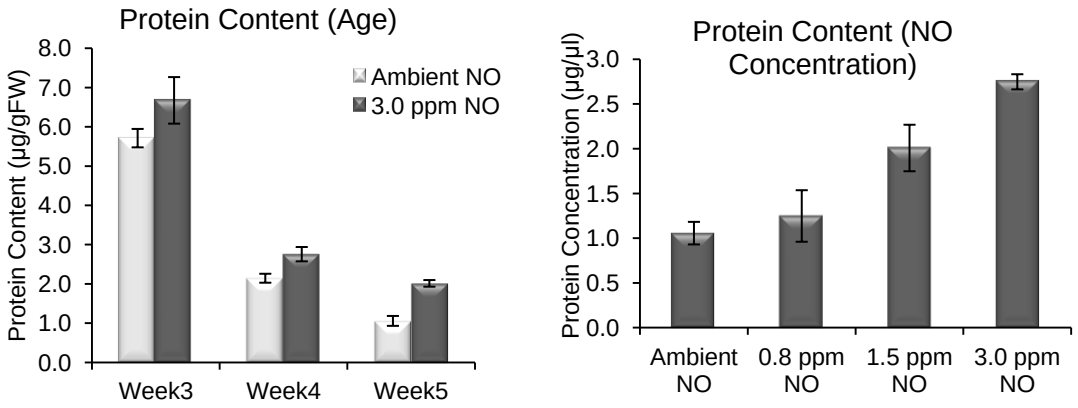

Figure 31 - Protein content in the plants treated with NO.
Proteins from all the samples were extracted using same method. Analyzing the 'Protein content (age)' was carried out in WT *Arabidopsis thaliana* from Ws background. 'Protein content (NO concentration)' was analyzed in the same plant line after 5 WAG. Similar results were obtained for *atgsnor-KO* plants.

Earlier studies have shown that the process of senescence is first initiated in chloroplast (Kaup et al., 2002, Surpin et al., 2002). One of the significant changes in early senescence is the loss of photosynthetic activity along with chlorophyll degradation (Lohman et al., 1994). Rosette leaves fumigated with various NO concentrations from 4 WAG in WT and 5 WAG in *atgsnor-KO* were analyzed using HPLC to quantify chlorophyll a and chlorophyll b pigment levels. WT plants showed higher accumulation of chlorophyll a and b pigments than *atgsnor-KO* plants in all the NO treatment conditions analyzed (Figure 32). Interestingly, accumulation of these pigments was directly proportional to NO treatment concentrations in both the lines (Figure 32). Pigment levels were approximately 25% higher in 3 ppm NO treated plants than those grown under ambient conditions thus showing a significant difference between these two treatments.

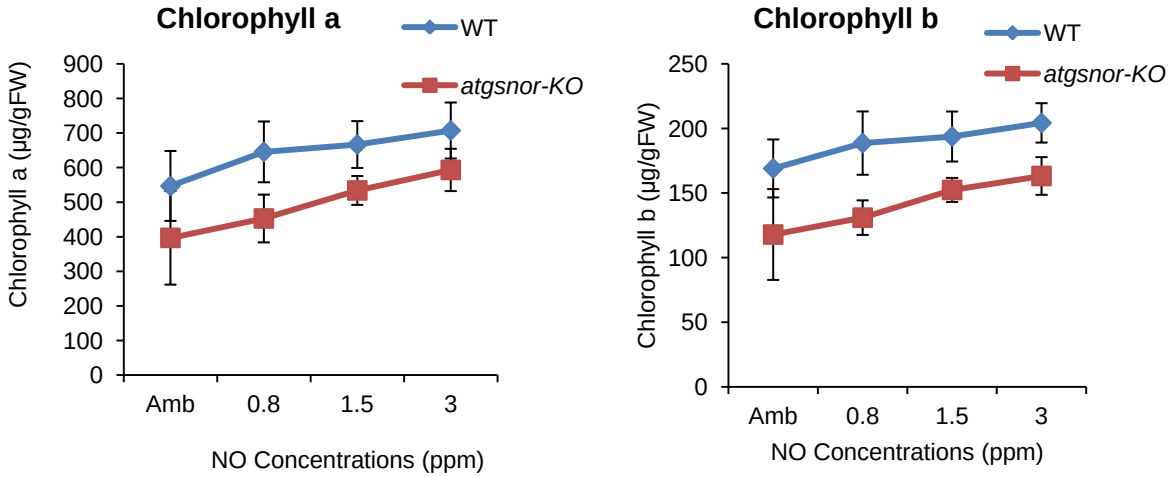

Figure 32 – Quantification of chlorophyll a and b pigments in rosette leaves using HPLC

Carotenoid pigments like carotene (α-carotene and β-carotene) and xanthophylls (lutein, violaxanthin, neoxanthin and antheraxanthin) were also analyzed using HPLC. Carotenoids can either transmit light energy to the photosystem that they absorb from chlorophyll or can function as a membrane-bound antioxidant to protect photosystem from photoinhibition (Telfer et al., 1994, Frank & Cogdell, 1996, Niyogi, 1999, Ruiz-Sola & Rodriguez-Concepcion, 2012). Lutein and neoxanthin were higher in plants fumigated with 3 ppm NO in comparison to plants grown under ambient conditions ($p \leq 0.05$). The increase was proportional to NO concentration. Rest of the carotenoids did not show significant difference (Figure 33).

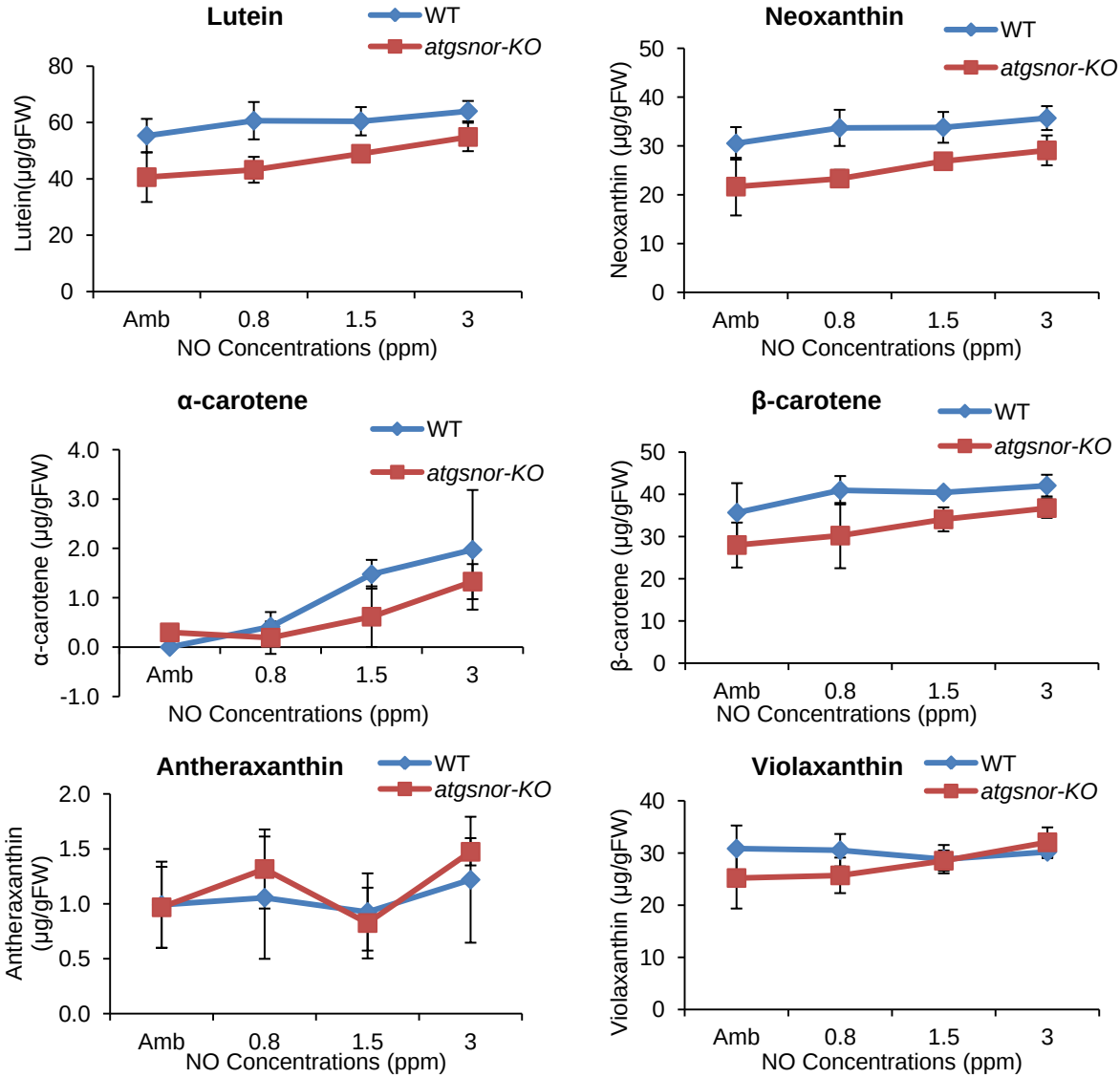

Figure 33 – Quantification of carotenoid pigments using HPLC.

4.10 Regulation of N-metabolism and nitrate metabolism

Accumulation of inorganic N-metabolites increased in the rosette leaves of the plants fumigated with 3 ppm NO (Figure 15). It has been proposed earlier that NO might be converted into nitrite non-enzymatically (Wellburn, 1990). Nitrite is transported into chloroplast and is assimilated in to amino acid synthesis. However, nitrate accumulation is not involved in this pathway. In plants, non-symbiotic hemoglobin can oxidize NO into nitrate during hypoxia stress (Igamberdiev & Hill, 2004, Perazzolli et al., 2004). Hypoxia stress is associated with NO accumulation. Also, non-symbiotic hemoglobin mediated conversion of NO to nitrate has not reported to influence N-assimilation yet. Here, based on our findings we proposed a new pathway connecting NO and N-assimilation cycle mediated by non-symbiotic hemoglobin (Figure 34).

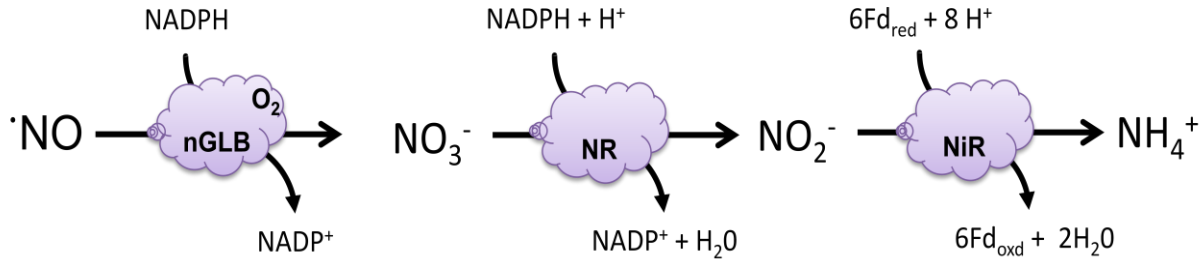

Figure 34 - Proposed pathway for aerial NO fixation.
Non-symbiotic hemoglobin with high oxygen binding affinity can oxidize NO to nitrate. Nitrate formed is reduced to nitrite and further to ammonia by nitrate reductase and nitrite reductase respectively.

Microarray data from the WT and *atgsnor*-KO plants treated with ambient NO and 3 ppm NO gas showed that non-symbiotic hemoglobin 1 (*GLB1*) and the enzymes involved in N-assimilation were induced after NO treatment in the plants. *GLB1*, nitrate reductase (NIA2) and nitrite reductase (*NiR1*) were significantly up regulated showing a two-fold difference (linear scale) in their expression after NO treatment (Figure 35A). Non symbiotic hemoglobin 2 (GLB2), another non-symbiotic hemoglobin, did not show a two-fold up regulation in both lines. However, *GLB2* expression in the NO treated plants was higher than that in the plants grown under ambient conditions (Figure 35A). Microarray results were further confirmed using semi-RT PCR analysis of these candidate genes (Figure 35B). While *GLB1*, *NIA2* and *NiR1* expression was significantly higher in NO treated plants, *GLB2* expression remained unchanged after NO treatment (Figure 35B)

A

3 ppm NO x Ambient NO (log_2 fold change)		
Gene Name	WT	*atgsnor*-KO
GLB1	1.27	1.08
GLB2	0.19	0.90
NIA2	2.03	1.72
NiR1	1.38	1.80

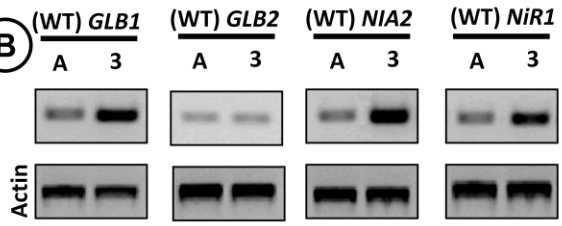

Figure 35 – Transcript analysis of the *GLB1*, *GLB2*, *NIA2* and *NiR1* genes.
A) Microarray analysis of candidate genes of four-week old WT and five-week old *atgsnor*-KO lines were analyzed. All the candidates (*GLB1, NIA2* and *NiR1*) except *GLB2* showed at least one-fold expression change in the log scale (two fold change in the linear scale). B) semi-RT PCR analysis of four-week old WT plants. Similar results were obtained in all biological replicates from both WT and *gsnor*-KO lines.

4.11 Phenotypic analysis of transgenic non-symbiotic hemoglobin lines

Plants with altered *GLB* expression were fumigated with ambient and 3 ppm concentrations of NO gas. Class 1 *GLB* over-expressing lines (*GLB1-Ox*), class 2 *GLB* over-expressing lines (*GLB2-Ox*), RNAi silenced class 1 *GLB* lines (*glb1-RNAi*), T-DNA insertion mutant of class 2 *GLB* lines (*glb2-KO*), and wild type Columbia-0 (WT Col-0) were generously provided by the scientific group of Asst. Prof. Dr. K. H. Hebelstrup from the Aarhus University, Denmark (Hebelstrup & Jensen, 2008). All the GLB transgenic plant lines were generated from WT (Col-0) and hence WT was used as the control for the fumigation experiments.

Similar phenotype was observed in *GLB1-Ox*, *GLB2-Ox* and WT Col-0 plants grown under ambient NO conditions (Figure 36). However, *glb1-RNAi* and *glb2-KO* plants were slightly smaller in size than that of WT Col-0 plants (Figure 36). Also, the width of the leaf blade of *glb1-RNAi* plants was thinner than that of WT Col-0 plants. Red senescence was developed in all the plant lines grown under ambient NO condition during 4th WAG and was absent in the plants fumigated with 3 ppm NO gas (Figure 36). However, all the plants except *glb2-KO* lines during NO fumigation showed bigger rosette size than their ambient counter-parts; *glb2-KO* responded to 3 ppm NO fumigation with a reduced growth phenotype with respect to its ambient counter-part (Figure 36). Interestingly, during NO fumigation the rosettes of both *GLB1* and *GLB2* overexpression plant lines appeared to be bigger than that of WT Col-0 plants (Figure 36). In the case of *glb1-RNAi* plants, though the 3 ppm NO fumigated plants appeared to have bigger rosette after NO fumigation, they were still showing the thinner leaf blade phenotype. Various growth parameters were measured to quantify and compare their differences between the plant lines and NO fumigated plants.

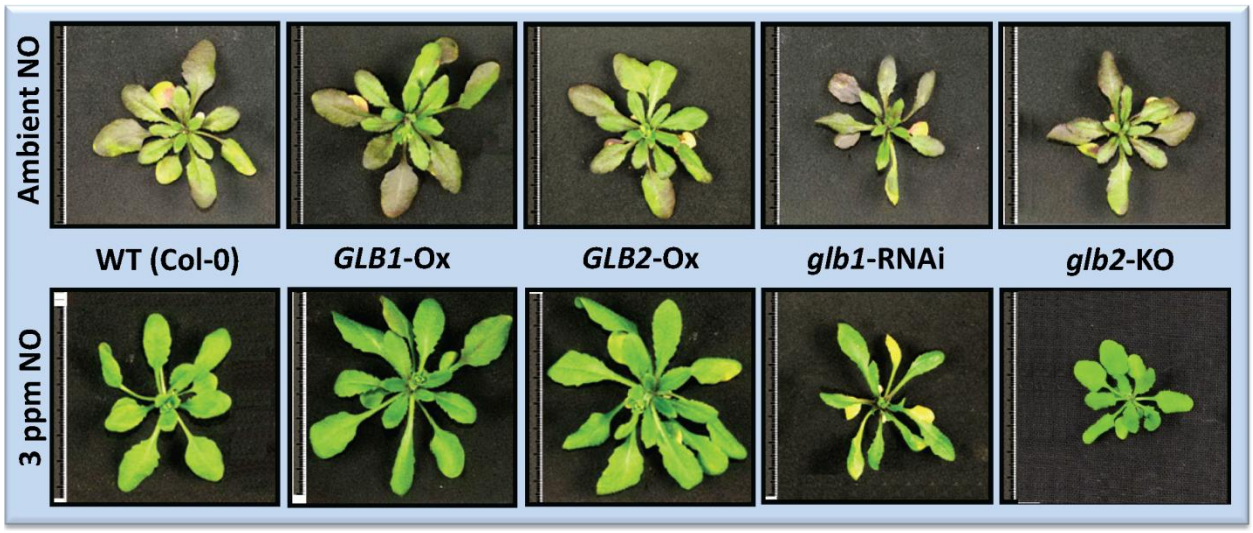

Figure 36 – Phenotype of the plants with altered *GLB* expression fumigated with NO gas.
Four week old plants were photographed.

Growth parameters estimated were rosette size (diameter), rosette fresh weight, rosette dry weight, thickness of the vegetative shoot, length of the vegetative shoot and number of secondary (lateral) shoot. Ratio of difference between 3 ppm NO fumigated plants to that of ambient NO fumigated plants for each parameter was calculated in each plant line (Table 11).

After four weeks of germination, WT, *glb1-RNAi*, *GLB1-Ox* and *GLB2-Ox* plants grown under ambient conditions had almost similar rosette size of about 4.3 cm in diameter. Rosette size of the *glb2-KO* plants (3.9 ± 0.26 cm in diameter) was smaller than that of other plants (Table 11). Response of all the plant lines to 3 ppm NO fumigation were evident four WAG. NO fumigation significantly increased the rosette size of WT, *glb1-RNAi*, *GLB1-Ox* and *GLB2-Ox* plants (Supplementary Figure 3). While the ratio of the increase in WT plants was 1.14, both *GLB1-Ox* and *GLB2-Ox* responded with much higher ratios of 1.37 and 1.44 respectively (Table 11). Ratio of increase in the rosette size of the *glb1-RNAi* plants (1.15) was similar to that of WT plants. However, NO treatment reduced the rosette size of *glb2-KO* plants that showed a ratio of 0.85 (Table 11).

Fresh weight of the rosettes from ambient and 3 ppm NO fumigated plants were measured four WAG. WT, *GLB1-Ox*, *glb2-KO* and *GLB2-Ox* plants grown under ambient conditions had almost similar fresh weight of about 1.05 g. While, the rosette fresh weight of *glb1-RNAi* plants (0.8 ± 0.01 g) was much lower than that of WT Col-0 (1.05 ± 0.01) grown under ambient conditions, other plant lines did not show much of a difference (Table 11). However, response of

these plants to 3 ppm NO fumigation was in line with the observed differences in rosette size. Rosette fresh weight of WT, *glb1-RNAi*, *GLB1-Ox* and *GLB2-Ox* plants were significantly increased during 3 ppm NO fumigation four WAG (Supplementary Figure 4). NO treatment significantly reduced the rosette fresh weight of *glb2-KO* lines with ratio being 0.54. Ratio of both *GLB1-Ox* (1.37) and *GLB2-Ox* (1.53) were much higher than that of WT (1.10) and *glb1-RNAi* (1.11) plants (Table 11). However, rosette dry weight of the WT, *glb1-RNAi* and *glb2-KO* plants reduced after 3 ppm NO fumigation. While the decrease in the rosette dry weight was significant in *glb2-KO* (0.40) plants, the decrease was not significant for both WT (0.88) and *glb1-RNAi* (0.93) plants (Supplementary Figure 5). Interestingly, rosette dry weights of the *GLB1-Ox* and *GLB2-Ox* plants were significantly high after 3 ppm NO fumigation. Their ratios were 1.2 and 1.25 respectively (Table 11).

Table 11 – Growth parameters in the NO treated plants

Growth Parameter	**NO treatment**	**WT Col-0**	***glb1-RNAi***	***GLB1-Ox***	***glb2-KO***	***GLB2-Ox***
Rosette Diameter	Ambient NO [a]	4.28 ± 0.17	4,28 ± 0.13	4.38 ± 0.10	3.90 ± 0.26	4.25 ± 0.21
(cm) / Week 4	3 ppm NO [b]	4.88 ± 0.17	4.93 ± 0.32	5.98 ± 0.39	3.30 ± 0.63	6.13 ± 0.36
(n = 10)	Ratio [b/a]	1.14	1.15	1.37	0.85	1.44
Rosette Fresh Weight	Ambient NO [a]	1.05 ± 0.01	0.80 ± 0.01	1.07 ± 0.01	1.04 ± 0.02	1.07 ± 0.11
(g) / Week 4	3 ppm NO [b]	1.15 ± 0.01	0.89 ± 0.01	1.46 ± 0.07	0.56 ± 0.03	1.64 ± 0.07
(n = 8 / 5 rosettes)	Ratio [b/a]	1.10	1.11	1.37	0.54	1.53
Rosette Dry Weight	Ambient NO [a]	0.15 ± 0.01	0.12 ± 0.02	0.15 ± 0.03	0.13 ± 0.02	0.16 ± 0.03
(g) / Week 4	3 ppm NO [b]	0.13 ± 0.00	0.11 ± 0.01	0.18 ± 0.03	0.05 ± 0.00	0.20 ± 0.03
(n = 8 / 5 rosettes)	Ratio [b/a]	0.88	0.93	1.20	0.40	1.25
Vegetative Shoot thic-	Ambient NO [a]	0.88 ± 0.09	0.85 ± 0.10	0.94 ± 0.11	0.94 ± 0.12	0.91 ± 0.09
kness (mm) / Week 6	3 ppm NO [b]	1.00 ± 0.12	0.97 ± 0.08	1.12 ± 0.11	0.99 ± 0.15	1.30 ± 0.16
(n = 20)	Ratio [b/a]	1.13	1.14	1.20	1.05	1.43
Vegetative shoot len-	Ambient NO [a]	17.38 ± 2.90	10.90 ± 2.52	17.43 ± 3.25	17.93 ± 2.60	16.48 ± 1.78
gth (cm) / Week 6	3 ppm NO [b]	17.33 ± 2.34	10.83 ± 1.82	19.90 ± 2.42	14.40 ± 2.68	17.85 ± 3.06
(n = 20)	Ratio [b/a]	1.00	0.99	1.14	0.80	1.08
Number of secondary	Ambient NO [a]	0.35 ± 0.67	0.55 ± 0.69	0.30 ± 0.57	0.25 ± 0.55	0.15 ± 0.37
shoot / Week 6	3 ppm NO [b]	1.15 ± 0.93	1.35 ± 0.75	2.50 ± 0.83	1.25 ± 0.91	3.80 ± 0.89
(n = 20)	Ratio [b/a]	3.29	2.45	8.33	5.00	25.33
Total Seed Yield	Ambient NO [a]	37.91	25.36	37.74	34.22	32.84
(mg) / Week 9	3 ppm NO [b]	43.17	23.01	51.05	39.27	64.2
	*Ratio [b/a]	1.14	0.91	1.35	1.15	1.95

Another remarkable difference observed among the plant lines after 3 ppm NO fumigation was the thickness of vegetative shoot stem 6 WAG. 3 ppm NO fumigation significantly increased the shoot thickness of *GLB2-Ox* plants (1.43 times). *GLB1-Ox* plants also showed a significant increase in their stem thickness by 1.20 times. While WT (1.13) and *glb1-RNAi* (1.14) plants showed similar increase in their stem thickness, NO fumigation had no influence on the stem thickness of the *glb2-KO* plants (Table 11). In all the plant lines grown under ambient conditions, there were no significant differences in the stem thickness (Table 11) (Supplementary Figure 6).

Six WAG, no significant differences were observed in the vegetative shoot length of the plant lines grown under ambient conditions except *glb1-RNAi* (Table 11). While the shoot length of all the other plant lines were about 17 – 18 cm, shoot length of *glb1-RNAi* line was significantly smaller (10.9 ± 2.52 cm). However, only *GLB1-Ox* plants fumigated with NO were significantly taller than their ambient counterpart (Supplementary Figure 7). All the plant lines fumigated with 3 ppm NO had significantly higher number of secondary shoot growth (Supplementary Figure 8) (Table 11). Six WAG the plants grown under ambient conditions rarely had secondary shoot growth (0 to 1 secondary shoot in all the plant lines). *GLB1-Ox* and *GLB2-Ox* plants fumigated with 3 ppm NO had more number of secondary shoots (3 – 4 secondary shoots) than WT Col-0, *glb1-RNAi* and *glb2-KO* plants grown in the same conditions (1 – 2 secondary shoot) (Table 11). These differences in the number of secondary shoots formed became more apparent eight WAG (Supplementary Figure 12). Also, the seed yield in GLB overexpression lines were significantly in the 3 ppm NO treatment plants compared to their counterparts in WT (Table 11).

4.12 Effect of NO growth conditions on RSNO and inorganic N-metabolites of plants with altered hemoglobin expression

Our initial studies using WT Ws and *atgsnor-KO* plants have confirmed that the total RSNO levels, nitrate content, nitrite content and ammonia content in the plants increased with increasing NO exposure (Figure 16A and Figure 15). 4 WAG, WT Col-0 and the GLB plant lines (*glb1-RNAi, GLB1-Ox, glb2-KO and GLB2-Ox)* were analyzed for total RSNO, nitrate, nitrite and ammonia after fumigating them with 3 ppm NO.

4.12.1 Nitrosothiol levels in the rosettes of plants with altered *GLB* expression

All the plant lines grown under ambient NO conditions had similar RSNO level of 8 - 9 pmol/mg protein (Figure 37). Fumigation of the plants with 3 ppm NO, significantly enhanced the RSNO levels in all the plant lines (Figure 37). In comparison to the ratio of increase of RSNO levels in WT (Col-0) (3.39), ratio of *glb1-RNAi* and *glb2-KO* were higher (5.69 and 3.77 respectively) and ratio of *GLB1-Ox* and *GLB2-Ox* were lower (2.79 and 2.74 respectively) (Figure 37). Thus, plant lines with reduced *GLB* expression levels had higher RSNO accumulation and increased *GLB* expression reduced the RSNO accumulation.

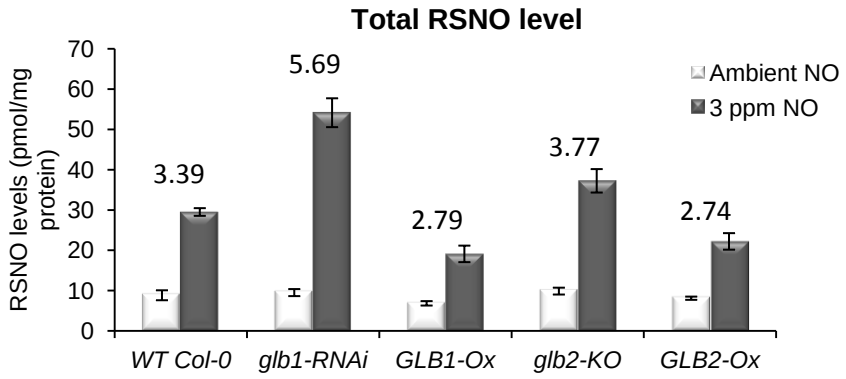

Figure 37 - Detection of RSNO levels in plant leaves with altered *GLB* expression.
RSNO levels of the four weeks old plant leaves were determined using chemiluminescent detection method (Nitric Oxide Analyzer). ±SD was determined from four independent experiments. Number above the measurement bar in each plant line represents the RSNO level ratio of 3 ppm NO plants to ambient NO plants.

4.12.2 Nitrite levels in the rosettes of plants with altered hemoglobin expression

There was no significant difference in the nitrite levels of the WT and GLB plant lines (1-2 nmol/mg protein) grown under ambient conditions (Figure 38). However, NO fumigation significantly increased the nitrite levels in all the plant lines. Among these, the highest increase was observed in *glb1-RNAi* with a ratio of 5.89. *GLB1-Ox*, *GLB2-Ox*, and *glb2-KO* also showed higher accumulation ratio compared to that of WT Col-0. However, the ratios of *GLB1-Ox* (4.8) and *GLB2-Ox* (5.62) were much higher than that of *glb2-KO* (2.67) and WT Col-0 (2.5).

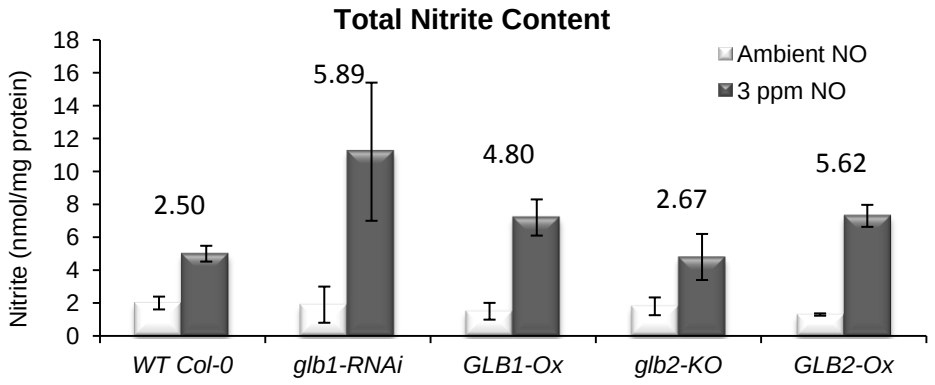

Figure 38 - Detection of nitrite content in plant with altered GLB expression.
Nitrite levels in the four weeks old rosette leaves were determined using Nitric Oxide Analyzer. ±SD was determined from four independent experiments. Number above the measurement bar in each plant line represents the nitrite ratio of 3 ppm NO plants to ambient NO plants.

4.12.3 Nitrate levels in the rosettes of plants with altered *GLB* expression

Under ambient conditions, nitrate levels in *GLB1-Ox* plants (~140 nmol/mg protein) and *GLB2-Ox* plants (~162 nmol/mg protein) were significantly higher than that of WT Col-0 plants (~122 nmol/mg protein). However, nitrate levels in both *glb1-RNAi* (~125 nmol/mg protein) and *glb2-KO* (~113 nmol/mg protein) plants were similar to that of WT Col-0 plants. Plants fumigated with 3 ppm NO showed significantly higher nitrate levels compared to their ambient counterparts. Most significant increase in the nitrate levels were observed in the *GLB1-Ox* lines (8.81 times increase) and in the *GLB2-Ox* lines (8.95 times increase) (Figure 39). Ratio of the increase was almost similar in WT Col-0 (2.55 times increase), *glb1-RNAi* (2.90 times increase) and *glb2-KO* (2.50 times increase) plants (Figure 39).

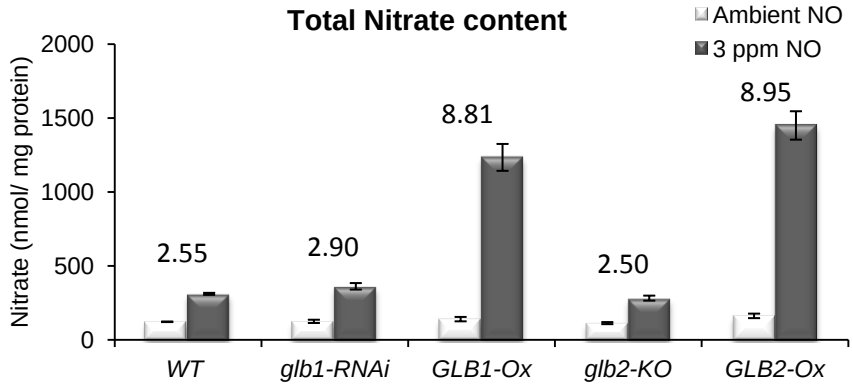

Figure 39 - Detection of nitrate content in plants with altered GLB expression.
Nitrate levels in the four weeks old rosettes were determined using NOA. ±SD determined from four independent experiments. Number above the measurement bar in each plant line represents the nitrate ratio between the plants fumigated with 3 ppm NO to that grown under ambient conditions.

4.12.4 Ammonia levels in the rosettes of plants with altered *GLB* expression

Similar levels of ammonia content were observed in the WT Col-0 and GLB plant lines (~40 – 50 µg/gFW) grown under ambient conditions. Ammonia content increased in the plants after 3 ppm NO fumigation. Compared to WT Col-0 (increase of 1.39 times) higher ammonia levels were observed in both *GLB1-Ox* (increase of 1.83 times) and *GLB2-Ox* (increase of 1.57 times) plants as a result of 3 ppm NO fumigation. On the other hand, increase in the ammonia levels in *glb1-RNAi* (1.27 times increase) and *glb2-KO* (1.28 times increase) plants were lesser than that of WT Col-0 (Figure 40). In the WT (Col-0) and *GLB* over-expression plant lines, the ratio between the plants grown in 3 ppm NO to that grown under ambient NO conditions were compared at different levels starting from nitrate, nitrite and ammonia accumulation to rosette size and weight and shoot stem thickness. These results have been summarized in Table 12.

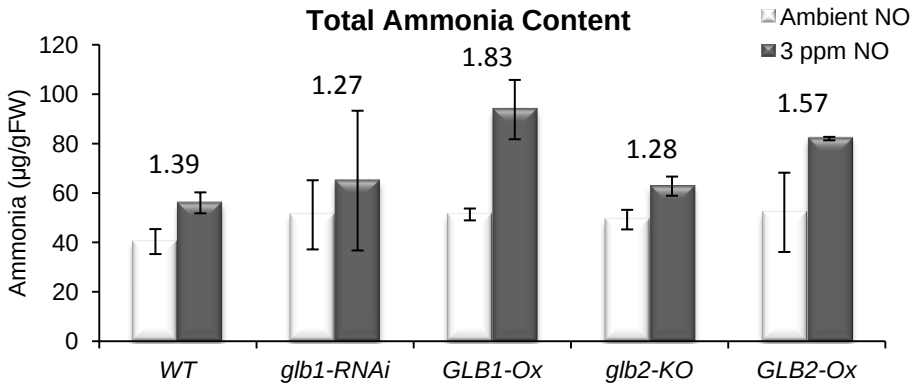

Figure 40 - Detection of ammonia content in plants with altered *GLB* expression.
Ammonia content of the four-week old plant leaves of the WT Col-0 plants and the plants with altered *GLB* expression were determined calorimetrically. Number above the measurement bar in each plant line represents the ammonia ratio between the plants fumigated with 3 ppm NO to that grown under ambient NO conditions.

	Ratio - 3 ppm NO x Ambient NO		
	WT Col-0	*GLB1-Ox*	*GLB2-Ox*
Nitrate content	2.60	8.81	8.95
Nitrite content	2.50	4.80	5.62
Ammonia content	1.39	1.83	1.57
Rosette size	1.14	1.37	1.44
Rosette Fresh weight	1.10	1.37	1.44
Shoot stem thickness	1.13	1.20	1.43

Table 12 – Ratios between 3 ppm and ambient NO fumigated plants.
Ratio of the difference between analyzed components between 3 ppm NO fumigated plants to ambient NO fumigated plants.

4.13 PAL activity and secondary metabolite analysis

Protein extracts from WT Col-0, *GLB1-Ox* and *GLB2-Ox* plants grown under ambient condition showed similar PAL enzyme activity (~50 nmol CA/h/mg of total protein). Fumigation of WT Col-0 plants with 3 ppm NO reduced the enzyme activity of PAL by 0.86 times (Figure 41). Protein extracts from *GLB1-Ox* and *GLB2-Ox* showed even lower enzyme activity after 3 ppm NO fumigation; 0.75 and 0.72 times respectively than their counterparts grown under ambient conditions (Figure 41).

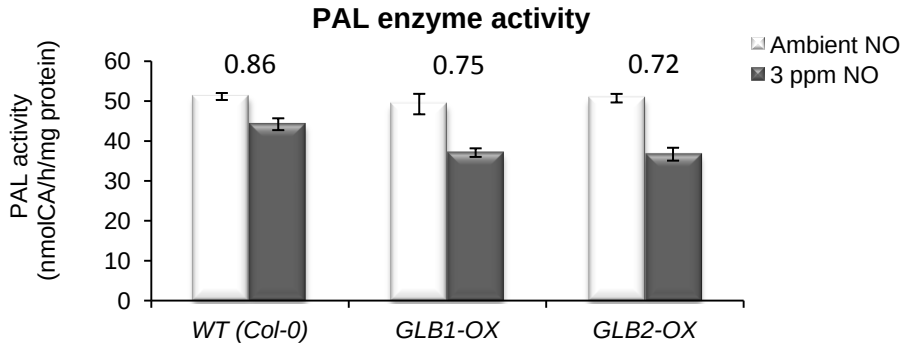

Figure 41 – PAL activity assay in plant rosettes with altered *GLB* expression.
Four-week old rosettes of the plant lines were used for the comparison. ±SD determined from four independent experiments. Number above the measurement bar in each plant line represents the ratio of estimated PAL enzyme activity between the plants fumigated with 3 ppm NO gas to that fumigated with ambient NO.

Secondary metabolites from phenylpropanoid pathway like sinapinic acid and flavonols (quercetin and kaempferol) showed no significant difference in their accumulation levels between WT Col-0, *GLB1-Ox* and *GLB2-Ox* plants under ambient NO conditions (Figure 42). However, plants fumigated with 3 ppm NO showed reduced sinapinic acid content in the WT Col-0 (0.73 times), *GLB1-Ox* (0.60 times) and *GLB2-Ox* (0.54 times) plant lines (Figure 42). Similarly total quercetin and kaempferol content also decreased in the WT Col-0 (0.61 times), *GLB1-Ox* (0.50 times) and *GLB2-Ox* (0.43 times) plant lines fumigated with 3 ppm NO (Figure 42).

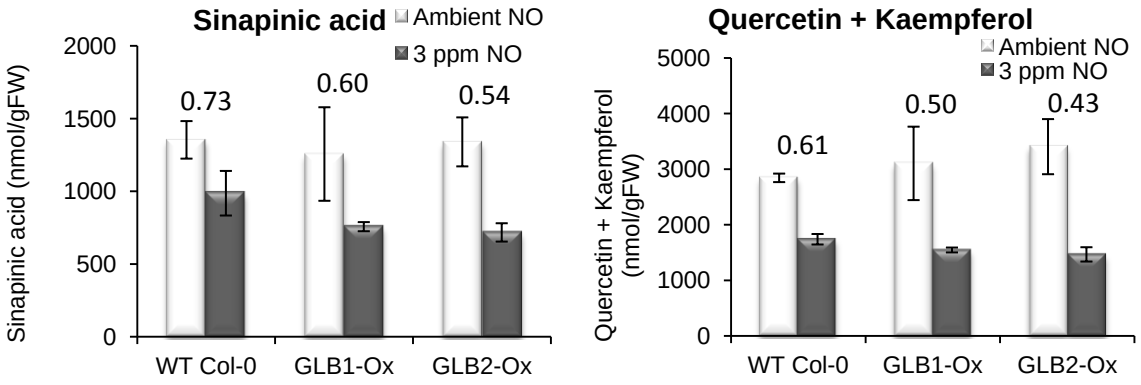

Figure 42 – Secondary metabolite content in plants with altered *GLB* expression

Sinapinic acid and total quercetin and kaempferol content were determined using reverse-phase HPLC. Quercetin and kaempferol were individually analyzed and their combined results were shown. Number above the measurement bar in each plant line represents the ratio of estimated secondary metabolite between the plants fumigated with 3 ppm NO gas to that fumigated with ambient NO.

5 DISCUSSION

Attempts to study the precise role of NO in regulating physiological and pathophysiological processes in plants are hampered due to several reasons: i) Extreme reactivity and unique biochemistry of NO to exist in three reactive forms that are highly sensitive to its environment, ii) unidentified enzymatic source of NO production in plants, iii) lack of a chemical source that specifically produces NO without inducing other side-effects, iv) fast interaction with other known and unknown signaling molecules that are not completely studied, and v) technical limitations to detect NO both *in vivo* and *in vitro*. However, many studies have utilized chemical NO donors to understand the pathways mediated by NO signaling. Also, attempts have been made in the past to fumigate the plants with NO gas and study its impact on plant physiology. Such treatments induced phytotoxic effects and significant growth defects in the plants (Wellburn, 1998). Interestingly, continuous NO gas fumigation induced inhibitory effects to the early stages of growth and development in lettuce cultivars and on the other side beneficially supported its later growth stages (Hufton et al., 1996). Also, plants undergoing stress showed better recovery when exposed to NO gas. Here NO is believed to function as an antioxidant against ROI (Velikova et al., 2008). Furthermore, floral senescence and fruit maturation was delayed in the plants with less NO emission, and application of chemical donors reduced senescence in the flowers and extended the fruit and vegetable post-harvest life (Leshem et al., 1998). Moreover, expression of bacterial NO degrading dioxygenase (NOD) enzyme in *Arabidopsis thaliana* induced early senescence; NOD being the mediator of NO metabolism. However, NO fumigation of these transgenic plants attenuated the early senescence showing the major role of NO in regulating senescence (Mishina et al., 2007).

5.1 Fumigation of *Arabidopsis* plants with NO gas under controlled conditions

Our strategy was to fumigate the plants with NO gas under highly controlled conditions and study its impact on plant physiology and NO signaling using the model plant *Arabidopsis thaliana*. S-nitrosoglutathione reductase (GSNOR) is an enzyme that metabolizes the physiological NO donor S-nitrosoglutathione (GSNO) thereby maintaining the cellular NO homeostasis. In *Arabidopsis thaliana*, GSNOR is encoded by a single copy gene which when knocked-out (*atgsnor-KO*) resulted in the increase of cellular nitrosothiol (RSNO) content in the plants (Feechan et al., 2005, Lee et al., 2008, Holzmeister et al., 2011, Yun et al., 2011). Thus,

we included the *atgsnor-KO* plants to study the effect of NO fumigation in the absence of GSNOR protection to NO. In our initial study we used four different NO concentrations (0, 200, 400 and 800 ppb) to fumigate the plants daily for 10 hours from 5 days after germination (DAG). Maximum NO concentration found in the air (ambient NO) of Helmholtz Zentrum campus was around 300 ppb (Figure 10). Thus 0 and 200 ppb concentrations were considered as ambient NO controls (without and with NO respectively) and 400 and 800 ppb intended to induce NO stress (low and high stress, respectively) in the plants. Rosette leaves of WT and *atgsnor-KO* plants started turning red in color during 4th week after germination (WAG). Red senescence is a programmed cell death associated with aging in the plants (Wingler et al., 2004). Red senescence has already been described in the scientific articles as a cause of anthocyanin accumulation in the upper mesophyll cells of the leaves (Wingler et al., 2004, Diaz et al., 2006, Feild et al., 2001). Fumigation of plants with 800 ppb NO showed slight reduction in the red senescence (Figure 9). This observation prompted us to fumigate plants with even higher concentrations of NO (Ambient, 0.8, 1.5 and 3.0 ppm) for longer periods (continuously around the clock from 5 DAG).

5.1.1 Phenotype of the plants fumigated with high NO concentration (up to 3ppm)

Red senescence started developing during 4th WAG in the plants grown under ambient conditions. Quantification of anthocyanin content showed a significant increase in their levels in the 4th WAG in the rosette leaves of plants grown under ambient conditions (Figure 14). We further examined the reasons for age-dependent red senescence in the early stages of plant growth (4th WAG). Environmental factors like nitrogen (N) deficiency in the growth medium and high light exposure of the rosette leaves have shown to induce anthocyanin accumulation in the plants during early growth stages (Lea et al., 2007, Albert et al., 2009, Morishita et al., 2009). Plants used more than 90% of total inorganic N-metabolites (nitrate, nitrite and ammonia) present in the soil within first four weeks of germination (Figure 12). This fast consumption of the soil might be due the competition of 5 plants sowed in 5.5 x 6 x 5.5 (length x breadth x depth in cm) pot. Also, light conditions used in our experiments (300 µmol photons/m^2/s) were higher than those used in the normal *Arabidopsis* experimental studies (70 µmol photons/m^2/s). 300 µmol photons/m^2/s have earlier shown to generate high levels of photosynthesis without photodamage in the plants that resembles the natural conditions (Russell et al., 1995, Trojan & Gabrys, 1996, Mishra et al., 2012). Higher level of photosynthesis at 300 µmol photons/m^2/s of light might have enhanced uptake of nitrogen from the soil by the plants to compensate for the

higher carbon (C) assimilation through photosynthesis. We have noticed faster growth of the plants in their earlier stages when grown in 300 µmol photons/m^2/s in comparison to that of 70 µmol photons/m^2/s (data not shown). Thus, both light condition and faster depletion of N-content in the soil resulted in the anthocyanin accumulation in the rosette leaves during early growth stages. Anthocyanin is suggested to have a protective role against high light by masking chlorophyll from light (Wingler et al., 2004). Masking effect by anthocyanin helps plants to reduce carbon assimilation to compensate for the low nitrogen availability from the soil. However, the younger leaves in the ambient conditions remained green (Figure 9 and Figure 11), which is common in the age-dependent senescing plants (Diaz et al., 2006). During senescence, accumulation of anthocyanin in the old leaves mobilize the nutrients to younger leaves (Diaz et al., 2006). The red senescence in the older leaves reduced gradually with the increase in NO fumigation concentration. Red senescence disappeared completely in the 4 week-old plants fumigated with 3 ppm NO (Figure 11A). Correspondingly, anthocyanin accumulation was considerably reduced by NO fumigation and the reduction was again proportional to NO fumigation concentration. These results suggested a consistent supply of N for the plants fumigated with 3 ppm NO.

5.1.2 Plants used fumigated NO gas to compensate for reducing soil N-metabolites

We considered two possible ways for the plants to use fumigated NO as a source of N. Firstly, increase of soil N-content after NO fumigation, wherein plants can utilize higher N in the soil and overcome the N-deficiency and delay red senescence. But the uptake of NO into the soil is possible only through biotic means. Abiotic uptake is possible only at very high pH and is unlikely to happen under normal conditions (Ludwig et al., 2001). This was evident in our study where both used (with plants) and unused (without plants) soil did not show a difference in the inorganic N-metabolite levels after NO treatment (Figure 12). Thus, it is apparent that NO fumigation cannot enrich the soil with N-content. We then concluded that the plants might be using NO in the air through its foliar uptake. It is well known that plants can uptake NO through its leaves (Leshem et al., 1998, Wellburn, 1998). However, mechanism of this uptake is not clearly understood. Though, its uptake through stomata has been proposed, under physiological conditions this is suggested to be very low due to internal resistance of plants and due to the lipophilic nature of NO (Stulen et al., 1998). Moreover, NO emission by the plants is also a well known phenomenon. The first physiological function of NO discovered in plants was its

regulation of senescence associated with NO emission from the pea plants (Leshem et al., 1998). Also, NO fumigation induced leaf disc expansion suggesting NO uptake by the pea plants (Leshem et al., 1998). In our study, plants fumigated with 3 ppm NO showed increased nitrosothiol, nitrate and nitrite content than the plants grown under ambient conditions (Figure 16A and Figure 15). This clearly indicated NO accumulation in the NO fumigated plants.

5.2 Role of GSNOR in NO fumigated plants

WT and *atgsnor-KO* plants responded in similar way to high NO fumigation, irrespective of the presence or absence of a functional GSNOR enzyme (Figure 11A). NO fumigation induced accumulation of nitrosothiol content in the both the plant lines (Figure 16A). However, it was surprising that the accumulation and activity of S-nitrosoglutathione reductase (GSNOR) remained unaffected by increasing RSNO levels (Figure 17). These results suggested that GSNOR does not have a regulatory role under these conditions. Studies using *Arabidopsis* plants with altered *GSNOR* expression have shown that GSNOR is required for the pathogen induced defense response (Feechan et al., 2005), herbivore tolerance (Wunsche et al., 2011) and thermotolerance (Lee et al., 2008) in *Arabidopsis thaliana*. However, the regulatory role of GSNOR during stress-induced NO accumulation in the WT *Arabidopsis thaliana* plants is still unclear.

5.3 Influence of enhanced NO-uptake in *Arabidopsis thaliana*

Levels of inorganic N-metabolites like nitrate, nitrite and ammonia also increased in the plants that were fumigated with 3 ppm NO compared to plants grown under ambient conditions (Figure 15). It is therefore clear that NO fumigation helped the plants to enhance N-metabolite levels, which was reduced in the plants grown under ambient condition due to soil N-depletion. Nitrate levels were the most significantly increased among the plant inorganic N-metabolites. In plants, nitrate is an important inorganic biomolecule capable of influencing metabolic processes directly by mediating N-assimilation and indirectly by inducing downstream signaling processes. Plants are extremely sensitive to the changes in the N-content particularly with respect to variations in the nitrate content as it can induce alterations in a wide variety of gene expression within a few minutes (Wang et al., 2000, Wang et al., 2004, Wang et al., 2007). These alterations in gene expression have shown to affect various growth and developmental stages like seed dormancy (Alboresi et al., 2005), leaf development (Alboresi et al., 2005), root architecture (Zhang &

Forde, 1998, Vidal et al., 2010) and flowering (Stitt et al., 2002). Number of microarray studies have shown that changes in N-content can alter the expression of a broad spectrum of physiologically important genes that regulate photosynthesis, carbon metabolism, secondary metabolism, protein synthesis, hormone signaling and transport, and signal transduction (Wang et al., 2000, Wang et al., 2003, Wang et al., 2004, Wang et al., 2007, Gutierrez et al., 2008). All these changes improved the growth and development of the plants. Gene expression profiling showed a similar pattern of changes in the genes in the plants fumigated with 3 ppm NO in comparison to the plants grown under ambient conditions (Table 8 and Table 9). Furthermore, the quantitative proteomic analysis also suggested that NO fumigation improved the plants metabolism. All these results show that NO fumigation induced NO uptake and enhanced N assimilation and plant metabolism.

5.3.1 Effect of NO fumigation on phenylpropanoid pathway

Phenylpropanoid pathway mediates synthesis of a number of secondary metabolites including anthocyanin from the primary metabolite phenylalanine (Figure 24). Compared to the plants grown under ambient conditions, plants fumigated with 3 ppm NO gas showed reduced expression of the genes involved in the flavonoid biosynthesis pathway (Figure 24). One of the key regulators of this pathway is the transcription factor (TF) named ‘production of anthocyanin pigment 1’ (PAP1) (Borevitz et al., 2000). Expression of *PAP1* was reduced by three fold in 3 ppm NO fumigated WT Ws and *atgsnor-KO* plants compared to their ambient counterparts (Supplementary Figure 9). PAP2 is another TF that regulates anthocyanin biosynthesis (Borevitz et al., 2000). However, *PAP2* gene expression was not affected by NO fumigation in both the plant lines. Knock-down lines of *PAP1* showed a significant reduction in the anthocyanin accumulation while knock-down lines of *PAP2* did not (Gonzalez et al., 2008). This might explain why *PAP2* wasn’t affected by NO fumigation. PAP1 is also shown to control the flavonoid biosynthesis through phenylpropanoid pathway starting from phenylalanine ammonia lyase (PAL) (Borevitz et al., 2000). This secondary metabolic pathway has been studied and most of the genes and enzymes involved have been well characterized. PAL serves as a gateway from the primary plant metabolism to the secondary phenylpropanoid metabolism plants. PAL catalyzes the formation of trans-cinnamic acid by removing ammonia from L-phenylalanine. Downstream to cinnamic acid is a wide variety of secondary metabolites that belongs to different classes of phenylpropanoid products like anthocyanins, flavonoids, ultraviolet (UV) protectants,

antimicrobial furanocoumarins, isoflavonoid phytoalexins, lignins and wound phenolic esters (Dixon & Paiva, 1995, Ritter & Schulz, 2004). Thus, PAL can be considered to be the central player and the branching point that induces the biosynthesis of flavonoids.

In *Arabidopsis thaliana*, PAL is encoded by four different genes named *PAL1* to *PAL4* (Raes et al., 2003). While plants fumigated with 3 ppm NO showed reduced *PAL1, PAL2* and *PAL4* expressions compared to plants grown under ambient conditions, *PAL3* showed an increased expression level with NO fumigation (Supplementary Figure 1 and Supplementary Figure 2). While, *PAL1, PAL2* and *PAL4* are highly expressed in shoots, *PAL3* expression is relatively low in the shoot and hence is not having any significant role in PAL enzymatic activity in the shoots (Raes et al., 2003). Among the four *PAL* genes *PAL1* and *PAL2* are the most important stress-responsive family members (Raes et al., 2003). PAL activity is induced during defense response in plants and has shown to be mediated by nitric oxide (Durner et al., 1998). While nitric oxide induced PAL activity, scavenging NO radicals using chemical scavengers blocked its activity (Durner et al., 1998). The mechanism of interaction between NO and PAL activity in this scenario is not known. It can be either a direct influence of NO or an indirect effect in combination with other signaling molecules or mechanisms. However, contrary to this defense related positive association of NO to PAL, NO fumigation experiments showed an inverse relationship between them. After 3 ppm NO fumigation, important stress-related *PAL* transcripts (*PAL1* and *PAL2*) and the PAL activity were reduced (Figure 25). In the context of NO fumigation, where NO accumulation was used by the plants for N-nutrition, the effect of NO on the PAL activity seems to be inhibitory. Reduced N-nutrition in plants is reported to induce PAL activity and downstream secondary metabolism in plants (Kovacik et al., 2007). One of the products of PAL activity is ammonia. Last inorganic biomolecule in the N-assimilation pathway is also ammonia. However, no studies have conducted to show a feedback inhibition of *PAL* expression by ammonia. Hence, it is not clear how the N-depletion is inducing of *PAL* expression in the plants. Furthermore, flavonol glycosides like quercetin glycosides and kaempferol glycosides and sinapate esters are all the secondary metabolite products synthesized by the phenylpropanoid pathway. Along with anthocyanins, the levels of these secondary metabolites too increased in the aging plants (Figure 26 and Figure 27). Fumigation with NO gas reduced the levels of all the secondary metabolites analyzed in our study (Figure 26 and Figure 27). The accumulation of flavonoids in the plants is often a hallmark of plant defense against the

stress response (Winkel-Shirley, 2002). However, the role of flavonoids in stress response is poorly understood. Its antioxidant activity has been argued as beneficial effect during stress and is therefore used as health-promoting additives for animals. Some of its well characterized functions are protecting the plants from harmful radiation and controlling the auxin transport (Winkel-Shirley, 2002). Accumulation of the flavonoids with the aging process is most likely to be associated with its antioxidant role. Aging process is always associated with the oxidative stress in plants (Munne-Bosch & Alegre, 2002). Thus, reduction in the levels of flavonoids in NO fumigated plants must be due to the delay in the aging process.

5.3.2 NO fumigation delayed age-related senescence in *Arabidopsis thaliana*

We further investigated the senescence process at the molecular level. Age-related senescence in the plants is influenced by many external factors. Once induced, senescing processes initiate shifts in the gene expression that leads to the degradation of many cellular macromolecules like chlorophyll, nucleic acids, proteins and lipids (Guo, 2012). Both RNA and protein content in the plants reduced with the age in both ambient grown plants and 3 ppm NO fumigated plants (Figure 28 and Figure 31). To confirm that this degradation is induced by age-related senescence process, we also analyzed expression of senescence marker gene, *SAG12*. *SAG12* encodes for a cysteine protease (Lohman et al., 1994). Senescence in plants can be induced by various means like detachment, pathogenesis, darkness, wounding and also by hormones like abscisic acid and ethylene (Weaver et al., 1998). However, *SAG12* is unique in responding specifically to age-related senescence (Weaver et al., 1998). Increasing expression of SAG12 during general nucleic acid breakdown is a clear indication of natural leaf senescence in *Arabidopsis thaliana* (Weaver et al., 1998). Semi-quantitative reverse transcriptase-polymerase chain reaction (semi RT-PCR) analysis of *SAG12* showed that its expression is strongly induced during fourth WAG in the plants grown under ambient NO conditions. Its expression further increased during fifth WAG suggesting age-dependent increase in the expression levels of *SAG12* (Figure 30). Decrease in the protein content during senescence process is caused by the increase in the proteolytic activity and decrease in the protein synthesis (Quirino et al., 2000). Increase in the *SAG12* expression matched the decrease in protein content with aging (Figure 28, Figure 30 and Figure 31). Thus, it is clear that the plants started senescing during fourth WAG. This very well coincided with the development of red senescence phenotype observed during fourth WAG. NO fumigated plants also showed an age-dependent degradation of RNA and protein - however, their degradation rate

was significantly delayed compared to plants grown under ambient conditions (Figure 28 and Figure 31). This was also evident in the expression of *SAG12*, which showed significantly reduced expression levels in NO fumigated plants compared to ambient grown plants (Figure 30). Furthermore, NO fumigation-dependent delay of *SAG12* expression was completely dependent on the concentration of NO fumigated; higher the NO concentrations lower was the induction of *SAG12* in the plants. Degradation of chlorophyll decreases the total chlorophyll content in the senescing leaves (Matile et al., 1999). Consequently, plants grown under ambient conditions showed higher senescence and reduced chlorophyll content compared to the 3 ppm NO fumigated plants. Increase in the chlorophyll content was directly proportional to the concentration of NO fumigated (Figure 32). Thus, the NO fumigation provided the plants with N-nutrition and delayed the senescence process. Also, enhanced N-assimilation reduced the accumulation of flavonoids in the plants fumigated with 3 ppm of NO gas (Figure 26). Plants suffering from N-deficiency have shown to induce flavonoid pathway (Lea et al., 2007). Accordingly, plants high in N-content after NO fumigation showed reduced flavonoid accumulation compared to the ambient grown plants (Figure 26 and Figure 27)

5.3.3 NO fumigation induced increased carbon assimilation in *Arabidopsis thaliana*

With NO fumigation resulting in higher N-assimilation, a corresponding increase in the C-assimilation must be induced to balance the C-N ratio (Lawlor, 2002). Plants achieve the required C:N ratio through improved carbon-fixation and photosynthesis (Lawlor, 2002). Gene expression profiling of the plants from NO fumigation study showed that the genes involved in photosynthesis and carbon-fixation are the most significantly induced set of genes in 3 ppm NO fumigated plants compared to plants grown under ambient conditions (Table 8 and Table 9). Increased carbon-fixation by Calvin cycle demand enhanced carbon dioxide (CO_2) uptake through stomata. CO_2-binding carbonic anhydrase (CA) proteins catalyze the reversible reaction of $CO_2 + H_2O \leftrightarrow HCO_3^- + H^+$ (Evans & vonCaemmerer, 1996). This reaction increases the CO_2 uptake in plants (Evans & vonCaemmerer, 1996). CA also regulates the controlled gas-exchange between plants and the atmosphere (Hu et al., 2010). NO fumigation significantly up regulated two CA genes - *βCA1* (12 fold) and *βCA2* (4 fold) (Supplementary Figure 10). Localization studies have shown that βCA1 and βCA2 are localized in the chloroplast and cytosol respectively (Fabre et al., 2007). Moreover *βCA1* are highly expressed in mesophyll cells and guard cells (Hu et al., 2010). Based on these facts, our studies showed that NO fumigation supported high CO_2

uptake and its fixation. Furthermore, the high C-N content is evident from the enhanced protein synthesis in the NO fumigated plants (Table 8 and Table 9).

5.4 Hypothesis formation – Non-symbiotic hemoglobin is a mediator of NO-fixation!

Atmospheric NO can be taken up by the plants and fumigation with NO further enhanced its aerial uptake and it was later converted into inorganic N-content. Enhanced NO uptake compensated for the reducing N-supply from the soil. In early 1990's, a mechanism was proposed to show a possible method for assimilating atmospheric NO by the plants (Wellburn, 1990). The mechanism mediates a direct non enzymatic conversion of NO to nitrite in the apoplast of the plants (Wellburn, 1990). Formed nitrite was thought to be transported across the plasma membrane and into the chloroplast where it gets reduced to ammonia. In our study, fumigation with 3 ppm NO increased both the nitrite and ammonia levels in the plants (Figure 15). However, these plants also showed increase in the levels of nitrate after NO fumigation (Figure 15). Nitrate is upstream of nitrite in the N-assimilation pathway. In the mechanism proposed by Wellburn et al., 1990, accumulation of nitrate was not involved (Wellburn, 1990). Moreover, the ratio of increase in the nitrate accumulation (4 fold increase) after 3 ppm NO fumigation was much higher than that of increased nitrite (2 fold) and ammonia levels (1.3 fold) (Figure 15).

Microbial heme protein NO dioxygenase (NOD) catalyze the reaction of O_2 and NO to yield nitrate (Gardner et al., 1998). Its primary function is to maintain proper cellular NO levels. In *Arabidopsis*, expression of bacterial NOD has exhibited regulatory role in controlling age-related senescence programming after NO fumigation (Mishina et al., 2007). In mammals, both hemoglobin and myoglobin exhibit NOD activity (Ouellet et al., 2002). Class 1 Non-symbiotic hemoglobin (GLB1) in plants is also known to mediate enzymatic conversion of accumulated NO into nitrate (Perazzolli et al., 2004).

GLB1 expression was increased two fold after NO fumigation (3 ppm) (Figure 35). In plants, *GLB1* is induced during hypoxia stress accompanied by NO accumulation (Igamberdiev & Hill, 2004). GLB1 used the accumulated NO to generate nitrate (Figure 4A). In this process, heme iron in the GLB1 gets oxidized from Fe^{2+} to Fe^{3+} oxidation state and requires recycling (Figure 4B). Thus, the rate limiting step in this process is the recycling of hemoglobin from Fe^{3+} to Fe^{2+} that is mediated by cytosolic monodehydroascorbate reductase (MDHAR) with ascorbate as a

reducing agent and NADPH or NADH as the electron acceptor (Figure 4B) (Igamberdiev et al., 2006, Hebelstrup et al., 2007). (Refer to section 1.2.3 – page number 11, to understand the mechanism of NO metabolism mediated by GLB1). *MDHAR* transcripts were also significantly upregulated after NO fumigation (Supplementary Figure 11). These evidences suggested that the GLB1 might be metabolizing the accumulated NO induced by NO fumigation. We also observed upregulation of the key genes involved in the N-assimilation pathway: cytoplasmic nitrate reductase (*NIA2*) and chloroplast localized nitrite reductase (*NiR1*) genes were also induced after NO fumigation (Figure 35). Based on these observations, we hypothesized that non-symbiotic hemoglobin can mediate N-assimilation in the *Arabidopsis thaliana* plants (Figure 43).

Some of recently published studies on *Arabidopsis thaliana* plants overexpressing *GLB1* (*GLB1-Ox*) and *GLB2* (*GLB2-Ox*) genes highlights potential role of these genes in NO metabolism (Hebelstrup et al., 2012; Mur et al., 2012).

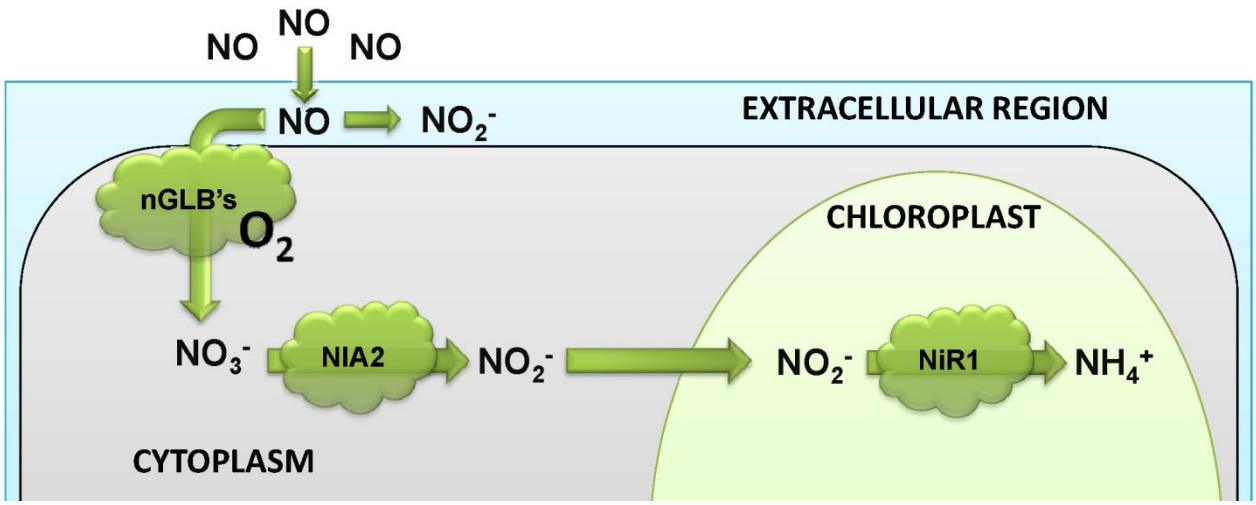

Figure 43 - Hemoglobin mediated incorporation of NO into N-assimilation pathway.
Proposed pathway for NO metabolism to nitrate mediated by hemoglobin. Nitrate formed is further taken into the plant N-assimilation pathway.

When challenged with pathogens both *GLB1-Ox* and *GLB2-Ox* plants showed reduced NO accumulation compared to WT plants (Mur et al., 2012). This suggested that the GLBs are involved in NO metabolism. However, only the *GLB1-Ox* plants showed higher susceptibilty towards, hemibiotrophic and necrotrophic pathogens (Mur et al., 2012). In our studies, GLB1 alone was induced in WT plants after 3 ppm NO fumigation (Figure 35). Also, NO fumigation enhanced the primary metabolism and reduced the secondary metabolism (flavonoid biosynthesis) by increased NO uptake and enhanced N-assimilation. We hypothesized that the

enhanced N-assimilation is mediated by the metabolism of NO by GLB1 (Figure 34). However, plants often reduce the primary metabolism, increase the flavonoid accumulation and NO accumulation in response to the pathogen attack (Reviews by Bolton, 2009, and Treutter, 2005). This help plants to successfully overcome pathogen attack. But plants overexpressing non-symbiotic hemoglobins showed reduced NO accumulation (due to increased NO metabolism), enhanced primary metabolism and reduced secondary metabolism (due to enhanced N-assimilation) after NO fumigation. This suggests that non-symbiotic hemoglobin can negatively regulate plant defense responses altering three crucial defense pathways. Figure 44 demonstrates the hypothetical role of hemoglobin on the responses induced during pathogen defense. Plants however down regulate *GLB1* in resistant WT plants during pathogen defense response to minimize its antagonistic effects (Mur et al., 2012). Interestingly, *GLB2-Ox* plant lines that showed enhanced NO metabolism and enhanced N-assimilation showed the similar resistance to pathogens like WT plants (Mur et al., 2012).

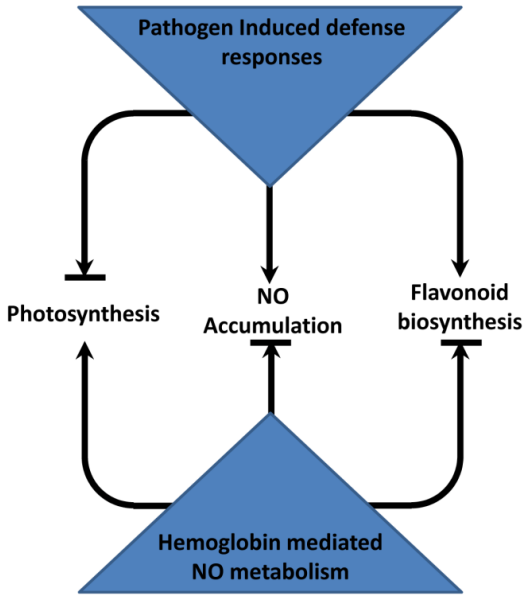

Figure 44 – Antagonist role of hemoglobin during defense response.

All these studies and our results strongly favored GLB mediated nitrate formation from NO accumulation. And we hypothesized that this nitrate is influencing N-assimilation pathway in the plants to improve plant growth.

5.5 Pathway leading to NO fixation

Endogenously produced NO is a very small, nonpolar and hydrophobic molecule capable of diffusing in three dimensions away from a site of synthesis (Lancaster, 1994). The ability of nitric oxide to diffuse freely through aqueous solution might be aiding its entry into the intercellular fluid through the stomatal openings. Such NO diffusion might be proportional to the concentration of the NO gas in the atmosphere. NO is widely accepted as a molecule capable of diffusing freely across the hydrophobic membrane barriers. However, recent studies have contradicted this concept and have shown that the diffusion of NO across membrane is regulated by membrane lipid structures like cholesterol in animals (Miersch et al., 2008). Cellular barrier in plants is more complicated and contains many lipid-derived structures. Hence the free diffusion of NO across these barriers needs more investigation. Moreover, NO molecules might tend to partition from the aqueous milieu into plasma membranes due to its preferentially hydrophobic solubility (Miersch et al., 2008). Also, reaction of NO with hemoglobin within red blood cells in animals is limited by the diffusion of NO into the cell (Liu et al., 1998). With all these evidences, we speculated that most of the NO that entered into the intercellular space might have trapped in hydrophobic plasma membrane lipid bilayer.

Presence of oxygenated hemoglobin in the red blood cells significantly increased NO metabolism into nitrate across the plasma membrane (Liu et al., 1998). We assumed a similar function for non-symbiotic hemoglobin in *Arabidopsis thaliana*. Entry of NO through hydrophobic cavities of GLB might mediate nitrate formation, which is used by the plants for the regular N-assimilation process. RSNO levels in the over expression lines of GLB1 (*GLB1-Ox*) and GLB2 (*GLB2*) were significantly lower than that of wild type Columbia-0 (WT Col-0) plants after 3 ppm NO fumigation (Figure 37). The results indicated a higher NO metabolism by *GLB1-Ox* and *GLB2-Ox* plants lines. Correspondingly, plants with reduced GLB expression (*glb1-RNAi* and *glb2-KO*) failed to oxidize accumulating NO and resulted in significant increase in the RSNO levels in comparison to WT Col-0 plants (Figure 37). However, NO metabolism by *GLB2-Ox* plant lines was surprising because GLB2 is not known for its NO oxidizing function because of its low oxygen affinity (Gupta et al., 2011b). Enhanced NO metabolism mediated by S-nitrosylation of GLB2 cannot be ruled out because a similar mechanism has been suggested to increase the NO metabolism activity in animals (Foster et al., 2003). However, significantly

higher nitrate levels in NO fumigated *GLB*-overexpression lines compared with WT confirmed the role of non-symbiotic hemoglobins in converting NO to nitrate (Figure 39). Increased N-assimilation in these lines is evident from the higher levels of nitrite and ammonia after NO fumigation (Figure 38 and Figure 40). However, the nitrate and ammonia levels of *glb1-RNAi* and *glb2-KO* plant lines were also higher than their ambient counterparts and were not significantly different from WT Col-0 plants (Figure 39 and Figure 40). This can be due to presence of either one of the functional GLB in these mutant lines; GLB2 is functional in *glb1-RNAi* plants and GLB1 is functional in *glb2-KO* plants. Surprisingly, the nitrite content in the *glb1-RNAi* plants fumigated with 3 ppm NO gas was much higher than all the other plants fumigated (Figure 38). A possible reason might be the conversion of accumulated NO into nitrite in the apoplast (Wellburn, 1990) in absence of GLB (Figure 43). NO is known to generate nitrite nonenzymatically in aerobic aqueous solution (Ignarro et al., 1993). However, this high levels of nitrite accumulation was not observed in *glb2-KO* plants after 3 ppm NO fumigation (Figure 38). This shows that the functional GLB1 in *glb2-KO* is more capable than functional GLB2 in *glb1-RNAi* in oxidizing NO. This was also evident in our gene expression profiling where induction of *GLB1* expression was more prominent than that of *GLB2* after 3 ppm NO fumigation (Figure 35).

Increased N-assimilation due to NO fumigation enhanced growth and development phenotypes of the *GLB*-overexpression plants. Both *GLB1-Ox* and *GLB2-Ox* plant lines responded to NO fumigation with bigger rosette size clearly distinguishable from the WT Col-0 controls (Figure 36). However, the rosette size of *glb2-KO* lines significantly reduced after 3 ppm NO treatment (Figure 36). *GLB*-overexpression plant lines also showed enhanced rosette size, rosette fresh weight and rosette dry weight after 3 ppm NO fumigation in comparison to WT Col-0 plants (Table 11). Though not significant, the dry weight of the WT Col-0 plants reduced after 3 ppm NO treatment. This might be attributed due to the enhanced flavonoid biosynthesis in plants grown under ambient conditions (Figure 24). Dry weight of the *Arabidopsis thaliana* flavonoid mutants was significantly lower than that of WT plants (Li et al., 1993). Both *GLB1* and *GLB2* plants showed distinctively different response in the vegetative shoot growth phenotype against NO fumigation. While *GLB2-Ox* showed highly enhanced shoot thickness and lateral (secondary) shoot formation, *Glb1-Ox* showed significantly higher shoot length. *GLB1-Ox* also showed enhanced shoot thickness and secondary shoot formation (Table 11 and Supplementary

Figure 12). The results clearly showed positive regulatory role of hemoglobin on the growth and development of plants during NO accumulation.

Furthermore, the PAL activity and flavonoid biosynthesis were also significantly down-regulated in *GLB* overexpression lines (Figure 41 and Figure 42). However, the exact mechanism of this effect is not clearly understood. One common factor in both N-assimilation pathway is the ammonia (ammonia is in equilibrium with ammonium). PAL activity removes ammonia from phenylalanine to induce downstream phenylpropanoid pathway and flavonoid biosynthesis (Figure 24). Enhanced N-assimilation mediated by hemoglobin increased ammonia levels in the plants (Figure 40). However, the influence of ammonia on the phenylpropanoid pathway needs to be investigated. Moreover, the correlation of the anthocyanin (product of flavonoid pathway) accumulation and soil N-deficiency will make such a study more interesting.

6 CONCLUDING REMARKS

Long term fumigation of *Arabidopsis thaliana* with NO gas has shown that the plants can uptake NO gas and can use it to enhance the N-assimilation through a pathway named as NO-fixation pathway. We also showed that non-symbiotic hemoglobins GLB1 and GLB2 are the important mediators of NO-fixation pathway in *Arabidopsis thaliana*. GLB1 and GLB2 together with NO gas taken up by the *Arabidopsis* plants enhanced its growth and development. As a model organism for agricultural biotechnology, *Arabidopsis* presents the opportunity to provide key insights into the way that these results can affect commercial production of crop plants like barley. Moreover, the identification of plants naturally expressing non-symbiotic hemoglobin in high amounts than that of *Arabidopsis thaliana* would further help to understand the importance of this pathway. Thus, NO-fixation pathway mediated by non-symbiotic hemoglobins might serve as an economically important trait for enhanced biomass production and high yield crop production.

7 REFERENCES

Achkor H, Diaz M, Fernandez MR, Biosca JA, Pares X, Martinez MC, 2003. Enhanced formaldehyde detoxification by overexpression of glutathione-dependent formaldehyde dehydrogenase from *Arabidopsis*. *Plant Physiol* **132**, 2248-55.

Albert NW, Lewis DH, Zhang H, Irving LJ, Jameson PE, Davies KM, 2009. Light-induced vegetative anthocyanin pigmentation in Petunia. *J Exp Bot* **60**, 2191-202.

Alboresi A, Gestin C, Leydecker MT, Bedu M, Meyer C, Truong HN, 2005. Nitrate, a signal relieving seed dormancy in *Arabidopsis*. *Plant Cell and Environment* **28**, 500-12.

Arnelle DR, Stamler JS, 1995. NO^+, NO, and NO^- donation by S-nitrosothiols: implications for regulation of physiological functions by S-nitrosylation and acceleration of disulfide formation. *Archives of biochemistry and biophysics* **318**, 279-85.

Balazy M, Kaminski PM, Mao KY, Tan JZ, Wolin MS, 1998. S-nitroglutathione, a product of the reaction between peroxynitrite and glutathione that generates nitric oxide. *Journal of Biological Chemistry* **273**, 32009-15.

Barroso JB, Corpas FJ, Carreras A, *et al.*, 2006. Localization of S-nitrosoglutathione and expression of S-nitrosoglutathione reductase in pea plants under cadmium stress. *Journal of Experimental Botany* **57**, 1785-93.

Belenghi B, Romero-Puertas MC, Vercammen D, *et al.*, 2007. Metacaspase activity of *Arabidopsis thaliana* is regulated by S-nitrosylation of a critical cysteine residue. *J Biol Chem* **282**, 1352-8.

Benhar M, Forrester MT, Hess DT, Stamler JS, 2008. Regulated protein denitrosylation by cytosolic and mitochondrial thioredoxins. *Science* **320**, 1050-4.

Benhar M, Forrester MT, Stamler JS, 2009. Protein denitrosylation: enzymatic mechanisms and cellular functions. *Nature Reviews Molecular Cell Biology* **10**, 721-32.

Benhar M, Thompson JW, Moseley MA, Stamler JS, 2010. Identification of S-nitrosylated targets of thioredoxin using a quantitative proteomic approach. *Biochemistry* **49**, 6963-9.

Berardini TZ, Mundodi S, Reiser L, *et al.*, 2004. Functional annotation of the *Arabidopsis* genome using controlled vocabularies. *Plant Physiol* **135**, 745-55.

Bethke PC, Badger MR, Jones RL, 2004a. Apoplastic synthesis of nitric oxide by plant tissues. *Plant Cell* **16**, 332-41.

Bethke PC, Gubler F, Jacobsen JV, Jones RL, 2004b. Dormancy of *Arabidopsis* seeds and barley grains can be broken by nitric oxide. *Planta* **219**, 847-55.

Bloor SJ, Abrahams S, 2002. The structure of the major anthocyanin in *Arabidopsis thaliana*. *Phytochemistry* **59**, 343-6.

Bolton MD, 2009. Primary metabolism and plant defense--fuel for the fire. *Mol Plant Microbe Interact* **22**, 487-97.

Borevitz JO, Xia Y, Blount J, Dixon RA, Lamb C, 2000. Activation tagging identifies a conserved MYB regulator of phenylpropanoid biosynthesis. *Plant Cell* **12**, 2383-94.

Chaki M, Valderrama R, Fernandez-Ocana AM, *et al.*, 2011a. High temperature triggers the metabolism of S-nitrosothiols in sunflower mediating a process of nitrosative stress which provokes the inhibition of ferredoxin-NADP reductase by tyrosine nitration. *Plant, cell & environment* **34**, 1803-18.

Chaki M, Valderrama R, Fernandez-Ocana AM, *et al.*, 2011b. Mechanical wounding induces a nitrosative stress by down-regulation of GSNO reductase and an increase in S-nitrosothiols in sunflower (*Helianthus annuus*) seedlings. *Journal of experimental botany* **62**, 1803-13.

Chaki M, Valderrama R, Fernandez-Ocana AM, *et al.*, 2009. Protein targets of tyrosine nitration in sunflower (*Helianthus annuus L.*) hypocotyls. *Journal of experimental botany* **60**, 4221-34.

Chen R, Sun S, Wang C, *et al.*, 2009. The *Arabidopsis PARAQUAT RESISTANT2* gene encodes an S-nitrosoglutathione reductase that is a key regulator of cell death. *Cell Res* **19**, 1377-87.

Coll NS, Vercammen D, Smidler A, *et al.*, 2010. *Arabidopsis* type I metacaspases control cell death. *Science* **330**, 1393-7.

Corpas FJ, Barroso JB, Carreras A, *et al.*, 2004. Cellular and subcellular localization of endogenous nitric oxide in young and senescent pea plants. *Plant Physiol* **136**, 2722-33.

Corpas FJ, Chaki M, Fernandez-Ocana A, *et al.*, 2008. Metabolism of reactive nitrogen species in pea plants under abiotic stress conditions. *Plant Cell Physiol* **49**, 1711-22.

Corpas FJ, Leterrier M, Valderrama R, *et al.*, 2011. Nitric oxide imbalance provokes a nitrosative response in plants under abiotic stress. *Plant science : an international journal of experimental plant biology* **181**, 604-11.

D'angelo P, Lucarelli D, Della Longa S, *et al.*, 2004. Unusual heme iron-lipid acyl chain coordination in Escherichia coli flavohemoglobin. *Biophysical journal* **86**, 3882-92.

Delledonne M, Xia Y, Dixon RA, Lamb C, 1998. Nitric oxide functions as a signal in plant disease resistance. *Nature* **394**, 585-8.

Delledonne M, Zeier J, Marocco A, Lamb C, 2001. Signal interactions between nitric oxide and reactive oxygen intermediates in the plant hypersensitive disease resistance response. *Proc Natl Acad Sci U S A* **98**, 13454-9.

Desikan R, Griffiths R, Hancock J, Neill S, 2002. A new role for an old enzyme: nitrate reductase-mediated nitric oxide generation is required for abscisic acid-induced stomatal closure in *Arabidopsis thaliana*. *Proc Natl Acad Sci U S A* **99**, 16314-8.

Despres C, Chubak C, Rochon A, *et al.*, 2003. The *Arabidopsis* NPR1 disease resistance protein is a novel cofactor that confers redox regulation of DNA binding activity to the basic domain/leucine zipper transcription factor TGA1. *Plant Cell* **15**, 2181-91.

Diaz C, Saliba-Colombani V, Loudet O, *et al.*, 2006. Leaf yellowing and anthocyanin accumulation are two genetically independent strategies in response to nitrogen limitation in *Arabidopsis thaliana*. *Plant Cell Physiol* **47**, 74-83.

Diaz M, Achkor H, Titarenko E, Martinez MC, 2003. The gene encoding glutathione-dependent formaldehyde dehydrogenase/GSNO reductase is responsive to wounding, jasmonic acid and salicylic acid. *FEBS Lett* **543**, 136-9.

Dixon RA, Paiva NL, 1995. Stress-induced phenylpropanoid metabolism. *Plant Cell* **7**, 1085-97.

Durner J, Wendehenne D, Klessig DF, 1998. Defense gene induction in tobacco by nitric oxide, cyclic GMP, and cyclic ADP-ribose. *Proc. Natl. Acad. Sci. USA* **95**, 10328-33.

Espunya MC, De Michele R, Gomez-Cadenas A, Martinez MC, 2012. S-Nitrosoglutathione is a component of wound- and salicylic acid-induced systemic responses in *Arabidopsis thaliana*. *Journal of experimental botany* **63**, 3219-27.

Evans JR, Voncaemmerer S, 1996. Carbon dioxide diffusion inside leaves. *Plant Physiology* **110**, 339-46.

Fabre N, Reiter IM, Becuwe-Linka N, Genty B, Rumeau D, 2007. Characterization and expression analysis of genes encoding alpha and beta carbonic anhydrases in *Arabidopsis*. *Plant Cell Environ* **30**, 617-29.

Feechan A, Kwon E, Yun BW, Wang Y, Pallas JA, Loake GJ, 2005. A central role for S-nitrosothiols in plant disease resistance. *Proc Natl Acad Sci U S A* **102**, 8054-9.

Feild TS, Lee DW, Holbrook NM, 2001. Why leaves turn red in autumn. The role of anthocyanins in senescing leaves of red-osier dogwood. *Plant Physiol* **127**, 566-74.

Fini A, Brunetti C, Di Ferdinando M, Ferrini F, Tattini M, 2011. Stress-induced flavonoid biosynthesis and the antioxidant machinery of plants. *Plant Signal Behav* **6**, 709-11.

Foster MW, Mcmahon TJ, Stamler JS, 2003. S-nitrosylation in health and disease. *Trends Mol Med* **9**, 160-8.

Frank HA, Cogdell RJ, 1996. Carotenoids in photosynthesis. *Photochem Photobiol* **63**, 257-64.

Fraser CM, Thompson MG, Shirley AM, *et al.*, 2007. Related *Arabidopsis* serine carboxypeptidase-like sinapoylglucose acyltransferases display distinct but overlapping substrate specificities. *Plant Physiol* **144**, 1986-99.

Garcia-Mata C, Gay R, Sokolovski S, Hills A, Lamattina L, Blatt MR, 2003. Nitric oxide regulates K^+ and Cl^- channels in guard cells through a subset of abscisic acid-evoked signaling pathways. *Proceedings of the National Academy of Sciences of the United States of America* **100**, 11116-21.

Gardner PR, Gardner AM, Martin LA, Salzman AL, 1998. Nitric oxide dioxygenase: an enzymic function for flavohemoglobin. *Proc Natl Acad Sci U S A* **95**, 10378-83.

Gaupels F, Kuruthukulangarakoola GT, Durner J, 2011. Upstream and downstream signals of nitric oxide in pathogen defence. *Current opinion in plant biology* **14**, 707-14.

Goldstein S, Czapski G, 1996. Mechanism of the nitrosation of thiols and amines by oxygenated $^{\cdot}NO$ solutions: the nature of the nitrosating intermediates. *Journal of the American Chemical Society* **118**, 6806-.

Goldstein S, Squadrito GL, Pryor WA, Czapski G, 1996. Direct and indirect oxidations by peroxynitrite, neither involving the hydroxyl radical. *Free Radic Biol Med* **21**, 965-74.

Gonzalez A, Zhao M, Leavitt JM, Lloyd AM, 2008. Regulation of the anthocyanin biosynthetic pathway by the TTG1/bHLH/Myb transcriptional complex in Arabidopsis seedlings. *Plant J* **53**, 814-27.

Gow AJ, Buerk DG, Ischiropoulos H, 1997. A novel reaction mechanism for the formation of S-nitrosothiol in vivo. *J Biol Chem* **272**, 2841-5.

Guikema B, Lu Q, Jourd'heuil D, 2005. Chemical considerations and biological selectivity of protein nitrosation: implications for NO-mediated signal transduction. *Antioxidants & Redox Signaling* **7**, 593-606.

Guo FQ, Crawford NM, 2005. *Arabidopsis* nitric oxide synthase1 is targeted to mitochondria and protects against oxidative damage and dark-induced senescence. *Plant Cell* **17**, 3436-50.

Guo Y, 2012. Towards systems biological understanding of leaf senescence. *Plant Mol Biol*.

Gupta KJ, Fernie AR, Kaiser WM, Van Dongen JT, 2011a. On the origins of nitric oxide. *Trends in Plant Science* **16**, 160-8.

Gupta KJ, Hebelstrup KH, Mur LA, Igamberdiev AU, 2011b. Plant hemoglobins: important players at the crossroads between oxygen and nitric oxide. *FEBS Lett* **585**, 3843-9.

Gutierrez RA, Stokes TL, Thum K, *et al.*, 2008. Systems approach identifies an organic nitrogen-responsive gene network that is regulated by the master clock control gene CCA1. *Proc Natl Acad Sci U S A* **105**, 4939-44.

Harlow E, Lane D, 2006. Bradford assay. *CSH Protoc* **2006**.

He Y, Tang RH, Hao Y, *et al.*, 2004. Nitric oxide represses the *Arabidopsis* floral transition. *Science* **305**, 1968-71.

Hebelstrup KH, Igamberdiev AU, Hill RD, 2007. Metabolic effects of hemoglobin gene expression in plants. *Gene* **398**, 86-93.

Hebelstrup KH, Jensen EO, 2008. Expression of NO scavenging hemoglobin is involved in the timing of bolting in *Arabidopsis thaliana*. *Planta* **227**, 917-27.

Hebelstrup KH, Van Zanten M, Mandon J, *et al.*, 2012. Haemoglobin modulates NO emission and hyponasty under hypoxia-related stress in *Arabidopsis thaliana*. *J Exp Bot* **63**, 5581-91.

Holzmeister C, Frohlich A, Sarioglu H, Bauer N, Durner J, Lindermayr C, 2011. Proteomic analysis of defense response of wildtype *Arabidopsis thaliana* and plants with impaired NO-homeostasis. *Proteomics* **11**, 1664-83.

Hu H, Boisson-Dernier A, Israelsson-Nordstrom M, *et al.*, 2010. Carbonic anhydrases are upstream regulators of CO_2-controlled stomatal movements in guard cells. *Nature cell biology* **12**, 87-93; sup pp 1-18.

Huang X, Stettmaier K, Michel C, Hutzler P, Mueller MJ, Durner J, 2004. Nitric oxide is induced by wounding and influences jasmonic acid signaling in *Arabidopsis thaliana*. *Planta* **218**, 938-46.

Hufton CA, Besford RT, Wellburn AR, 1996. Effects of NO ($+NO_2$) pollution on growth, nitrate reductase activities and associated protein contents in glasshouse lettuce grown hydroponically in winter with CO_2 enrichment. *New Phytologist* **133**, 495-501.

Igamberdiev AU, Bykova NV, Hill RD, 2006. Nitric oxide scavenging by barley hemoglobin is facilitated by a monodehydroascorbate reductase-mediated ascorbate reduction of methemoglobin. *Planta* **223**, 1033-40.

Igamberdiev AU, Bykova NV, Hill RD, 2011. Structural and functional properties of class 1 plant hemoglobins. *IUBMB Life* **63**, 146-52.

Igamberdiev AU, Hill RD, 2004. Nitrate, NO and haemoglobin in plant adaptation to hypoxia: an alternative to classic fermentation pathways. *J Exp Bot* **55**, 2473-82.

Ignarro LJ, Buga GM, Wood KS, Byrns RE, Chaudhuri G, 1987a. Endothelium-derived relaxing factor produced and released from artery and vein is nitric oxide. *Proceedings of the National Academy of Sciences of the United States of America* **84**, 9265-9.

Ignarro LJ, Byrns RE, Buga GM, Wood KS, 1987b. Endothelium-derived relaxing factor from pulmonary artery and vein possesses pharmacologic and chemical properties identical to those of nitric oxide radical. *Circ Res* **61**, 866-79.

Ignarro LJ, Fukuto JM, Griscavage JM, Rogers NE, Byrns RE, 1993. Oxidation of nitric oxide in aqueous solution to nitrite but not nitrate: comparison with enzymatically formed nitric oxide from L-arginine. *Proc Natl Acad Sci U S A* **90**, 8103-7.

Jaffrey SR, Snyder SH, 2001. The biotin switch method for the detection of S-nitrosylated proteins. *Sci STKE* **2001**, pl1.

Joung JG, Corbett AM, Fellman SM, *et al.*, 2009. Plant MetGenMAP: an integrative analysis system for plant systems biology. *Plant Physiol* **151**, 1758-68.

Kallakunta VM, Staruch A, Mutus B, 2010. Sinapinic acid can replace ascorbate in the biotin switch assay. *Biochim Biophys Acta* **1800**, 23-30.

Kaup MT, Froese CD, Thompson JE, 2002. A role for diacylglycerol acyltransferase during leaf senescence. *Plant Physiol* **129**, 1616-26.

Keszler A, Zhang YH, Hogg N, 2010. Reaction between nitric oxide, glutathione, and oxygen in the presence and absence of protein: How are S-nitrosothiols formed? *Free Radical Biology and Medicine* **48**, 55-64.

Kim YM, Chung HT, Simmons RL, Billiar TR, 2000. Cellular non-heme iron content is a determinant of nitric oxide-mediated apoptosis, necrosis, and caspase inhibition. *Journal of Biological Chemistry* **275**, 10954-61.

Kovacik J, Klejdus B, Backor M, Repcak M, 2007. Phenylalanine ammonia-lyase activity and phenolic compounds accumulation in nitrogen-deficient *Matricaria chamomilla* leaf rosettes. *Plant Science* **172**, 393-9.

Laemmli UK, 1970. Cleavage of structural proteins during the assembly of the head of bacteriophage T4. *Nature* **227**, 680-5.

Lancaster JR, Jr., 1994. Simulation of the diffusion and reaction of endogenously produced nitric oxide. *Proc Natl Acad Sci U S A* **91**, 8137-41.

Landry LG, Chapple CCS, Last RL, 1995. *Arabidopsis* mutants lacking phenolic sunscreens exhibit enhanced ultraviolet-B injury and oxidative damage. *Plant Physiol* **109**, 1159-66.

Lawlor DW, 2002. Carbon and nitrogen assimilation in relation to yield: mechanisms are the key to understanding production systems. *J Exp Bot* **53**, 773-87.

Lea US, Slimestad R, Smedvig P, Lillo C, 2007. Nitrogen deficiency enhances expression of specific MYB and bHLH transcription factors and accumulation of end products in the flavonoid pathway. *Planta* **225**, 1245-53.

Lee U, Wie C, Fernandez BO, Feelisch M, Vierling E, 2008. Modulation of nitrosative stress by S-nitrosoglutathione reductase is critical for thermotolerance and plant growth in *Arabidopsis*. *Plant Cell* **20**, 786-802.

Leshem Y, Haramaty E, 1996. The characterization and contrasting effects of the nitric oxide free radical in vegetative stress and senescence of *Pisum sativum Linn*. foliage. *Journal of Plant Physiology* **148**, 258-63.

Leshem YY, Wills RBH, Ku VV, 1998. Evidence for the function of the free reduced gas – nitric oxide (˙NO) as an endogenous maturation and senescence regulating factor in higher plants. *Plant Physiol. Biochem.* **36**, 825-6.

Li J, Ou Lee TM, Raba R, Amundson RG, Last RL, 1993. *Arabidopsis* flavonoid mutants are hypersensitive to UV-B irradiation. *Plant Cell* **5**, 171-9.

Lillig CH, Holmgren A, 2007. Thioredoxin and related molecules - from biology to health and disease. *Antioxidants & Redox Signaling* **9**, 25-47.

Lindermayr C, Saalbach G, Bahnweg G, Durner J, 2006. Differential inhibition of *Arabidopsis* methionine adenosyltransferases by protein S-nitrosylation. *J Biol Chem* **281**, 4285-91.

Lindermayr C, Saalbach G, Durner J, 2005. Proteomic identification of S-nitrosylated proteins in *Arabidopsis*. *Plant Physiol* **137**, 921-30.

Lindermayr C, Sell S, Muller B, Leister D, Durner J, 2010. Redox regulation of the NPR1-TGA1 system of *Arabidopsis thaliana* by nitric oxide. *The Plant cell* **22**, 2894-907.

Lipton SA, Choi YB, Sucher NJ, Chen HS, 1998. Neuroprotective versus neurodestructive effects of NO-related species. *Biofactors* **8**, 33-40.

Liu L, Hausladen A, Zeng M, Que L, Heitman J, Stamler JS, 2001. A metabolic enzyme for S-nitrosothiol conserved from bacteria to humans. *Nature* **410**, 490-4.

Liu LM, Yan Y, Zeng M, *et al.*, 2004. Essential roles of S-nitrosothiols in vascular homeostasis and endotoxic shock. *Nitric Oxide-Biology and Chemistry* **11**, 39-.

Liu X, Miller MJ, Joshi MS, Sadowska-Krowicka H, Clark DA, Lancaster JR, Jr., 1998. Diffusion-limited reaction of free nitric oxide with erythrocytes. *J Biol Chem* **273**, 18709-13.

Lohman KN, Gan S, M.C. J, R.M. A, 1994. Molecular analysis of natural leaf senescence in *Arabidopsis thaliana*. *Physiologia Plantarum* **92**, 322-8.

Lopez-Sanchez LM, Corrales FJ, Lopez-Pedrera C, Aranda E, Rodriguez-Ariza A, 2010. Pharmacological impairment of S-nitrosoglutathione or thioredoxin reductases augments protein S-nitrosation in human hepatocarcinoma cells. *Anticancer Research* **30**, 415-21.

Lorenzen M, Racicot V, Strack D, Chapple C, 1996. Sinapic acid ester metabolism in wild type and a sinapoylglucose-accumulating mutant of *Arabidopsis*. *Plant Physiol* **112**, 1625-30.

Ludwig J, Meixner FX, Vogel B, Forstner J, 2001. Soil-air exchange of nitric oxide: An overview of processes, dnvironmental vactors, and modeling studies. *Biogeochemistry* **52**, 225-57.

Ma W, Berkowitz GA, 2011. Ca^{2+} conduction by plant cyclic nucleotide gated channels and associated signaling components in pathogen defense signal transduction cascades. *New Phytologist* **190**, 566-72.

Mackay JJ, O'malley DM, Presnell T, *et al.*, 1997. Inheritance, gene expression, and lignin characterization in a mutant pine deficient in cinnamyl alcohol dehydrogenase. *Proc Natl Acad Sci U S A* **94**, 8255-60.

Maldonado-Alconada AM, Echevarria-Zomeno S, Lindermayr C, Redondo-Lopez I, Durner J, Jorrin-Novo JV, 2011. Proteomic analysis of *Arabidopsis* protein S-nitrosylation in response to inoculation with *Pseudomonas syringae*. *Acta Physiologiae Plantarum* **33**, 1493-514.

Martinez MC, Achkor H, Persson B, *et al.*, 1996. *Arabidopsis* formaldehyde dehydrogenase. Molecular properties of plant class III alcohol dehydrogenase provide further insights into the origins, structure and function of plant class p and liver class I alcohol dehydrogenases. *Eur J Biochem* **241**, 849-57.

Matile P, Hortensteiner S, Thomas H, 1999. Chlorophyll Degradation. *Annu Rev Plant Physiol Plant Mol Biol* **50**, 67-95.

Miersch S, Espey MG, Chaube R, *et al.*, 2008. Plasma membrane cholesterol content affects nitric oxide diffusion dynamics and signaling. *J Biol Chem* **283**, 18513-21.

Mishina TE, Lamb C, Zeier J, 2007. Expression of a nitric oxide degrading enzyme induces a senescence programme in *Arabidopsis*. *Plant Cell Environ* **30**, 39-52.

Mishra Y, Jankanpaa HJ, Kiss AZ, Funk C, Schroder WP, Jansson S, 2012. *Arabidopsis* plants grown in the field and climate chambers significantly differ in leaf morphology and photosystem components. *BMC Plant Biol* **12**, 6.

Morishita T, Kojima Y, Maruta T, Nishizawa-Yokoi A, Yabuta Y, Shigeoka S, 2009. *Arabidopsis* NAC transcription factor, ANAC078, regulates flavonoid biosynthesis under high-light. *Plant Cell Physiol* **50**, 2210-22.

Mou Z, Fan W, Dong X, 2003. Inducers of plant systemic acquired resistance regulate NPR1 function through redox changes. *Cell* **113**, 935-44.

Munne-Bosch S, Alegre L, 2002. Plant aging increases oxidative stress in chloroplasts. *Planta* **214**, 608-15.

Mur LA, Sivakumaran A, Mandon J, Cristescu SM, Harren FJ, Hebelstrup KH, 2012. Haemoglobin modulates salicylate and jasmonate/ethylene-mediated resistance mechanisms against pathogens. *J Exp Bot* **63**, 4375-87.

Neighbour EA, Pearson M, Paul ND, *et al.*, 1990. A small-scale controlled environment chamber for the investigation of the effects of pollutant gases on plants growing at cool or sub-zero temperature. *Environmental pollution* **64**, 155-68.

Neill SJ, Desikan R, Clarke A, Hancock JT, 2002. Nitric oxide is a novel component of abscisic Acid signaling in stomatal guard cells. *Plant Physiol.* **128**, 13-6.

Niyogi KK, 1999. PHOTOPROTECTION REVISITED: Genetic and Molecular Approaches. *Annu Rev Plant Physiol Plant Mol Biol* **50**, 333-59.

Ouellet H, Ouellet Y, Richard C, *et al.*, 2002. Truncated hemoglobin HbN protects Mycobacterium bovis from nitric oxide. *Proc Natl Acad Sci U S A* **99**, 5902-7.

Palmer RM, Ferrige AG, Moncada S, 1987. Nitric oxide release accounts for the biological activity of endothelium-derived relaxing factor. *Nature* **327**, 524-6.

Palmieri MC, Lindermayr C, Bauwe H, Steinhauser C, Durner J, 2010. Regulation of plant glycine decarboxylase by S-nitrosylation and glutathionylation. *Plant Physiology* **152**, 1514-28.

Perazzolli M, Dominici P, Romero-Puertas MC, *et al.*, 2004. *Arabidopsis* nonsymbiotic hemoglobin AHb1 modulates nitric oxide bioactivity. *Plant Cell* **16**, 2785-94.

Pieterse CM, Van Loon LC, 2004. NPR1: the spider in the web of induced resistance signaling pathways. *Curr Opin Plant Biol* **7**, 456-64.

Quirino BF, Noh YS, Himelblau E, Amasino RM, 2000. Molecular aspects of leaf senescence. *Trends in Plant Science* **5**, 278-82.

Raes J, Rohde A, Christensen JH, Van De Peer Y, Boerjan W, 2003. Genome-wide characterization of the lignification toolbox in *Arabidopsis*. *Plant Physiol* **133**, 1051-71.

Ritter H, Schulz GE, 2004. Structural basis for the entrance into the phenylpropanoid metabolism catalyzed by phenylalanine ammonia-lyase. *Plant Cell* **16**, 3426-36.

Rodriguez-Serrano M, Romero-Puertas MC, Zabalza A, *et al.*, 2006. Cadmium effect on oxidative metabolism of pea (*Pisum sativum L.*) roots. Imaging of reactive oxygen species and nitric oxide accumulation in vivo. *Plant, cell & environment* **29**, 1532-44.

Romero-Puertas MC, Campostrini N, Matte A, *et al.*, 2008. Proteomic analysis of S-nitrosylated proteins in *Arabidopsis thaliana* undergoing hypersensitive response. *Proteomics* **8**, 1459-69.

Romero-Puertas MC, Laxa M, Matte A, *et al.*, 2007. S-nitrosylation of peroxiredoxin II E promotes peroxynitrite-mediated tyrosine nitration. *Plant Cell* **19**, 4120-30.

Rubin G, Tohge T, Matsuda F, Saito K, Scheible WR, 2009. Members of the LBD family of transcription factors repress anthocyanin synthesis and affect additional nitrogen responses in *Arabidopsis*. *Plant Cell* **21**, 3567-84.

Ruiz-Sola MA, Rodriguez-Concepcion M, 2012. Carotenoid biosynthesis in *Arabidopsis*: a colorful pathway. *The Arabidopsis book / American Society of Plant Biologists* **10**, e0158.

Russell AW, Critchley C, Robinson SA, *et al.*, 1995. Photosystem II Regulation and Dynamics of the Chloroplast D1 Protein in *Arabidopsis* Leaves during Photosynthesis and Photoinhibition. *Plant Physiol* **107**, 943-52.

Rusterucci C, Espunya MC, Diaz M, Chabannes M, Martinez MC, 2007. S-nitrosoglutathione reductase affords protection against pathogens in *Arabidopsis*, both locally and systemically. *Plant Physiol* **143**, 1282-92.

Saito S, Yamamoto-Katou A, Yoshioka H, Doke N, Kawakita K, 2006. Peroxynitrite generation and tyrosine nitration in defense responses in tobacco BY-2 cells. *Plant & cell physiology* **47**, 689-97.

Sakamoto A, Ueda M, Morikawa H, 2002. *Arabidopsis* glutathione-dependent formaldehyde dehydrogenase is an S- nitrosoglutathione reductase. *FEBS Lett* **515**, 20-4.

Schmidt HHHW, Hofmann H, Schindler U, Shutenko ZS, Cunningham DD, Feelisch M, 1996. No ˙NO from NO synthase. *Proceedings of the National Academy of Sciences of the United States of America* **93**, 14492-7.

Sen N, Hara MR, Kornberg MD, *et al.*, 2008. Nitric oxide-induced nuclear GAPDH activates p300/CBP and mediates apoptosis. *Nature cell biology* **10**, 866-73.

Seth D, Stamler JS, 2011. The SNO-proteome: causation and classifications. *Current Opinion in Chemical Biology* **15**, 129-36.

Shevchenko A, Wilm M, Vorm O, Mann M, 1996. Mass spectrometric sequencing of proteins silver-stained polyacrylamide gels. *Anal Chem* **68**, 850-8.

Shirley AM, Mcmichael CM, Chapple C, 2001. The *sng2* mutant of *Arabidopsis* is defective in the gene encoding the serine carboxypeptidase-like protein sinapoylglucose:choline sinapoyltransferase. *Plant J* **28**, 83-94.

Simontacchi M, Buet A, Lamattina L, Puntarulo S, 2012. Exposure to nitric oxide increases the nitrosyl-iron complexes content in sorghum embryonic axes. *Plant science : an international journal of experimental plant biology* **183**, 159-66.

Spoel SH, Loake GJ, 2011. Redox-based protein modifications: the missing link in plant immune signalling. *Current opinion in plant biology* **14**, 358-64.

Stitt M, Muller C, Matt P, *et al.*, 2002. Steps towards an integrated view of nitrogen metabolism. *J Exp Bot* **53**, 959-70.

Stoimenova M, Igamberdiev AU, Gupta KJ, Hill RD, 2007. Nitrite-driven anaerobic ATP synthesis in barley and rice root mitochondria. *Planta* **226**, 465-74.

Stulen I, Perez-Soba M, De Kok LJ, Van Der Eerden L, 1998. Impact of gaseous nitrogen deposition on plant functioning. *New Phytologist* **139**, 61-70.

Sueldo DJ, Foresi NP, Casalongue CA, Lamattina L, Laxalt AM, 2010. Phosphatidic acid formation is required for extracellular ATP-mediated nitric oxide production in suspension-cultured tomato cells. *New Phytologist* **185**, 909-16.

Surpin M, Larkin RM, Chory J, 2002. Signal transduction between the chloroplast and the nucleus. *Plant Cell* **14 Suppl**, S327-38.

Tada Y, Spoel SH, Pajerowska-Mukhtar K, *et al.*, 2008. Plant immunity requires conformational charges of NPR1 via S-nitrosylation and thioredoxins. *Science* **321**, 952-6.

Telfer A, Dhami S, Bishop SM, Phillips D, Barber J, 1994. beta-Carotene quenches singlet oxygen formed by isolated photosystem II reaction centers. *Biochemistry* **33**, 14469-74.

Tohge T, Nishiyama Y, Hirai MY, *et al.*, 2005. Functional genomics by integrated analysis of metabolome and transcriptome of *Arabidopsis* plants over-expressing an MYB transcription factor. *Plant J* **42**, 218-35.

Torres MA, Dangl JL, Jones JD, 2002. *Arabidopsis* gp91phox homologues AtrbohD and AtrbohF are required for accumulation of reactive oxygen intermediates in the plant defense response. *Proc Natl Acad Sci U S A* **99**, 517-22.

Treutter D, 2005. Significance of flavonoids in plant resistance and enhancement of their biosynthesis. *Plant Biol (Stuttg)* **7**, 581-91.

Trojan A, Gabrys H, 1996. Chloroplast distribution in *Arabidopsis thaliana* (L.) depends on light conditions during growth. *Plant Physiol* **111**, 419-25.

Uotila L, Koivusalo M, 1979. Purification of formaldehyde and formate dehydrogenases from pea seeds by affinity chromatography and S-formylglutathione as the intermediate of formaldehyde metabolism. *Archives of biochemistry and biophysics* **196**, 33-45.

Van Der Vliet A, Hoen PA, Wong PS, Bast A, Cross CE, 1998. Formation of S-nitrosothiols via direct nucleophilic nitrosation of thiols by peroxynitrite with elimination of hydrogen peroxide. *J Biol Chem* **273**, 30255-62.

Velikova V, Fares S, Loreto F, 2008. Isoprene and nitric oxide reduce damages in leaves exposed to oxidative stress. *Plant Cell Environ* **31**, 1882-94.

Vidal EA, Araus V, Lu C, *et al.*, 2010. Nitrate-responsive miR393/AFB3 regulatory module controls root system architecture in *Arabidopsis thaliana*. *Proc Natl Acad Sci U S A* **107**, 4477-82.

Von Saint Paul V, Zhang W, Kanawati B, *et al.*, 2011. The *Arabidopsis* glucosyltransferase UGT76B1 conjugates isoleucic acid and modulates plant defense and senescence. *Plant Cell* **23**, 4124-45.

Wang R, Guegler K, Labrie ST, Crawford NM, 2000. Genomic analysis of a nutrient response in *Arabidopsis* reveals diverse expression patterns and novel metabolic and potential regulatory genes induced by nitrate. *Plant Cell* **12**, 1491-509.

Wang R, Okamoto M, Xing X, Crawford NM, 2003. Microarray analysis of the nitrate response in *Arabidopsis* roots and shoots reveals over 1,000 rapidly responding genes and new linkages to glucose, trehalose-6-phosphate, iron, and sulfate metabolism. *Plant Physiol* **132**, 556-67.

Wang RC, Tischner R, Gutierrez RA, *et al.*, 2004. Genomic analysis of the nitrate response using a nitrate reductase-null mutant of *Arabidopsis*. *Plant Physiology* **136**, 2512-22.

Wang RC, Xing XJ, Crawford N, 2007. Nitrite acts as a transcriptome signal at micromolar concentrations in *Arabidopsis* roots. *Plant Physiology* **145**, 1735-45.

Wang YQ, Feechan A, Yun BW, *et al.*, 2009. S-nitrosylation of AtSABP3 antagonizes the expression of plant immunity. *J Biol Chem* **284**, 2131-7.

Weaver LM, Gan SS, Quirino B, Amasino RM, 1998. A comparison of the expression patterns of several senescence-associated genes in response to stress and hormone treatment. *Plant Molecular Biology* **37**, 455-69.

Wellburn AR, 1990. Why are atmospheric oxides of nitrogen usually phytotoxic and not alternative fertilizers? *New Phytol.* **115**, 395-429.

Wellburn AR, 1998. Atmospheric nitrogenous compounds and ozone - is NOx fixation by plants a possible solution? *New Phytologist* **139**, 5-9.

Wilson ID, Neill SJ, Hancock JT, 2008. Nitric oxide synthesis and signalling in plants. *Plant, cell & environment* **31**, 622-31.

Wingler A, Mares M, Pourtau N, 2004. Spatial patterns and metabolic regulation of photosynthetic parameters during leaf senescence. *New Phytologist* **161**, 781-9.

Wink DA, Nims RW, Darbyshire JF, *et al.*, 1994. Reaction kinetics for nitrosation of cysteine and glutathione in aerobic nitric oxide solutions at neutral pH. Insights into the fate and physiological effects of intermediates generated in the NO/O_2 reaction. *Chemical research in toxicology* **7**, 519-25.

Winkel-Shirley B, 2002. Biosynthesis of flavonoids and effects of stress. *Curr Opin Plant Biol* **5**, 218-23.

Wunsche H, Baldwin IT, Wu JQ, 2011. S-Nitrosoglutathione reductase (GSNOR) mediates the biosynthesis of jasmonic acid and ethylene induced by feeding of the insect herbivore Manduca sexta and is important for jasmonate-elicited responses in *Nicotiana attenuata*. *Journal of Experimental Botany* **62**, 4605-16.

Yin R, Messner B, Faus-Kessler T, *et al.*, 2012. Feedback inhibition of the general phenylpropanoid and flavonol biosynthetic pathways upon a compromised flavonol-3-O-glycosylation. *J Exp Bot* **63**, 2465-78.

Yu Q, Tang C, Kuo J, 2000. A critical review on methods to measure apoplastic pH in plants. *Plant and Soil* **219**, 29-40.

Yun BW, Feechan A, Yin M, *et al.*, 2011. S-nitrosylation of NADPH oxidase regulates cell death in plant immunity. *Nature* **478**, 264-8.

Zeidler D, Zahringer U, Gerber I, *et al.*, 2004. Innate immunity in *Arabidopsis thaliana*: lipopolysaccharides activate nitric oxide synthase (NOS) and induce defense genes. *Proc Natl Acad Sci U S A* **101**, 15811-6.

Zhang HM, Forde BG, 1998. An *Arabidopsis* MADS box gene that controls nutrient-induced changes in root architecture. *Science* **279**, 407-9.

8 SUPPLEMENTS

Supplementary Table 1 - List of DIGE gels with dyes assigned to each samples

No.	Cy2	Cy3	Cy5
1	IS	WT_Week3_Ambient NO*	WT_Week3_3.0 ppm NO*
2	IS	WT_Week3_Ambient NO**	WT_Week3_3.0 ppm NO**
3	IS	WT_Week3_3.0 ppm NO***	WT_Week3_Ambient NO***
4	IS	WT_Week4_Ambient NO*	WT_Week4_3.0 ppm NO*
5	IS	WT_Week4_Ambient NO**	WT_Week4_3.0 ppm NO**
6	IS	WT_Week4_3.0 ppm NO***	WT_Week4_Ambient NO***
7	IS	WT_Week5_Ambient NO*	WT_Week5_3.0 ppm NO*
8	IS	WT_Week5_Ambient NO**	WT_Week5_3.0 ppm NO**
9	IS	WT_Week5_3.0 ppm NO***	WT_Week5_Ambient NO***
10	IS	WT_Week5_0.8 ppm NO*	WT_Week5_1.5 ppm NO*
11	IS	WT_Week5_0.8 ppm NO**	WT_Week5_1.5 ppm NO**
12	IS	WT_Week5_1.5 ppm NO***	WT_Week5_0.8 ppm NO***
13	IS	gsnor-KO_Week4_Ambient NO*	gsnor-KO_Week4_3.0 ppm NO*
14	IS	gsnor-KO_Week4_Ambient NO**	gsnor-KO_Week4_3.0 ppm NO**
15	IS	gsnor-KO_Week4_3.0 ppm NO***	gsnor-KO_Week4_Ambient NO***
16	IS	gsnor-KO_Week5_Ambient NO*	gsnor-KO_Week5_3.0 ppm NO*
17	IS	gsnor-KO_Week5_Ambient NO**	gsnor-KO_Week5_3.0 ppm NO**
18	IS	gsnor-KO_Week5_3.0 ppm NO***	gsnor-KO_Week5_Ambient NO***
19	IS	gsnor-KO_Week6_Ambient NO*	gsnor-KO_Week6_3.0 ppm NO*
20	IS	gsnor-KO_Week6_Ambient NO**	gsnor-KO_Week6_3.0 ppm NO**
21	IS	gsnor-KO_Week6_3.0 ppm NO***	gsnor-KO_Week6_Ambient NO***
22	IS	gsnor-KO_Week6_0.8 ppm NO*	gsnor-KO_Week6_1.5 ppm NO*
23	IS	gsnor-KO_Week6_0.8 ppm NO**	gsnor-KO_Week6_1.5 ppm NO**
24	IS	gsnor-KO_Week6_1.5 ppm NO***	gsnor-KO_Week6_0.8 ppm NO***

IS - Internal standard

* First biological replicate

** Second biological replicate

*** Third biological replicate

Supplementary Table 2 - List of regulated proteins (2D-DIGE)

a) Protein Name	b) Spot No.	c) Accession Number	d) Mass/p/	e) Mascot Score			f) Avg ratio (WT)			g) Avg ratio (*gsnor*)		
				Unique Peptide	Seq. Cover	Protein Score	0.8 ppm	1.5 ppm	3 ppm	0.8 ppm	1.5 ppm	3 ppm
Glycine decarboxylase P-protein 1	1	AT4G33010	114/6.51	29	28	315	1.74	1.79	2.14	1.89	1.89	2.12
Glycine decarboxylase P-protein 2	1	AT2G26080	115/6.18	17	18	178	1.74	1.79	2.14	1.89	1.89	2.12
Phragmoplast orienting kinesin 2	1	AT3G19050	318/5.13	32	10	60	1.74	1.79	2.14	1.89	1.89	2.12
Low exp of osmotically responsive genes 1	2	AT1G56070	95/5.89	32	30	305	1.31	1.86	2.16	1.35	1.60	2.34
GTP binding / GTPase	2	AT3G12915	92/5.78	19	19	84	1.31	1.36	2.16	1.65	1.60	2.34
Glycine decarboxylase P-protein 1	3	AT4G33010	114/6.51	27	24	275	1.42	1.78	2.79	1.96	2.08	2.21
Glycine decarboxylase P-protein 2	3	AT2G26080	115/6.18	17	15	172	1.42	1.78	2.79	1.96	2.08	2.21
Phragmoplast orienting kinesin 2	3	AT3G19050	318/5.13	32	11	65	1.42	1.78	2.79	1.96	2.08	2.21
QWRF domain containing 8	3	AT4G30710	70/10.69	15	18	61	1.42	1.78	2.79	1.96	2.08	2.21
Disproportionating enzyme 2	4	AT2G40840	111/5.54	24	24	117	-1.63	-1.85	-2.04	-1.58	-1.89	-2.52
Disproportionating enzyme 2	5	AT2G40840	111/5.54	31	28	174	-1.57	-2.51	-2.01	-1.69	-2.89	-2.01
Phospholipase D Alpha 1	5	AT3G15730	92/5.53	20	26	113	-1.57	-2.51	-2.01	-1.69	-2.89	-2.01
Disproportionating enzyme 2	6	AT2G40840	111/5.54	32	25	182	-1.63	-1.77	-2.66	-1.56	-1.77	-2.40
Snowy cotyledon 1	7	AT1G62750	86/5.43	36	45	532	1.44	1.87	2.13	1.06	2.30	2.63
Transketolase	8	AT3G60750	80/5.94	27	31	255	1.73	1.91	2.88	1.91	1.78	2.08
Transketolase	9	AT3G60750	80/5.94	36	57	655	1.66	1.80	2.86	1.85	2.20	2.89
Transketolase	9	AT2G45290	80/6.12	9	11	77	1.66	1.80	2.86	2.05	2.20	2.89
Luminal binding protein BIP1	10	AT5G28540	74/5.08	34	39	343	-1.70	-1.76	-2.07	-1.72	-1.97	-2.67
Luminal binding protein BIP2	10	AT5G42020	74/5.11	35	40	336	-1.70	-1.76	-2.07	-1.72	-1.97	-2.67
Phosphoglucomutase 2	11	AT1G70730	64/5.56	23	35	330	1.49	1.72	2.30	1.16	1.40	2.01
Phosphoglucomutase 3	11	AT1G23190	63/5.92	15	20	178	1.49	1.72	2.30	1.16	1.40	2.01
Large subunit of RUBISCO	11	ATCG00490	53/5.88	12	24	90	1.49	1.72	2.30	1.16	1.40	2.01
Phosphoglycerate mutase 1	12	AT1G09780	6/5.32	25	33	241	1.28	2.54	2.67	1.35	2.50	2.07
NAD-Dependent malic enzyme 1	13	AT2G13560	70/5.31	17	18	130	1.43	1.74	2.21	1.14	1.37	2.04
Nitrite reductase 1	14	AT2G15620	66/5.95	27	37	347	1.12	1.32	2.02	1.12	1.41	2.24
Epithiospecifier protein	14	AT1G54040	37/5.56	14	37	108	1.12	1.32	2.02	1.12	1.41	2.24
Large subunit of RUBISCO	14	ATCG00490	53/5.88	12	23	70	1.12	1.32	2.02	1.12	1.41	2.24
RUBISCO activase	15	AT2G39730	52/5.87	23	37	255	1.53	1.72	2.11	1.76	2.21	2.32

Supplementary Table 2 continues…

a) Protein Name	b) Spot No.	c) Accession Number	d) Mass/pI	e) Mascot Score			f) Avg ratio (WT)			g) Avg ratio (*gsnor*)		
				Unique Peptide	Seq. Cover	Protein Score	0.8 ppm	1.5 ppm	3 ppm	0.8 ppm	1.5 ppm	3 ppm
RUBISCO activase	16	AT2G39730	52/5.87	29	51	574	1.47	2.83	2.46	1.40	3.11	2.17
CC-NBS-LRR class protein	16	AT1G58410	105/6.62	20	21	83	1.47	2.83	2.46	1.40	3.11	2.17
Glutamine synthetase 2	17	AT5G35630	48/6.43	12	30	154	1.15	2.05	2.15	1.67	2.66	2.72
ATP synthase subunit beta	17	ATCG00480	54/5.38	17	37	118	1.15	2.05	2.15	1.67	2.66	2.72
ADP glucose pyrophosphorylase 1	17	AT5G48300	57/6.13	12	29	64	1.15	2.05	2.15	1.67	2.66	2.72
Glutamine synthetase 2	18	AT5G35630	48/6.43	21	42	506	1.27	2.25	2.41	1.98	2.30	2.91
Glutamine synthase clone F 11	18	AT1G66200	39/5.14	7	13	98	1.27	2.25	2.41	1.98	2.30	2.91
Glutamine synthetase 1.3	18	AT3G17820	39/5.72	3	9	74	1.27	2.25	2.41	1.98	2.30	2.91
Phosphoglycerate kinase	19	AT1G56190	43/5.39	24	60	469	1.48	2.52	2.01	1.68	2.54	2.06
Phosphoglycerate kinase 1	19	AT3G12780	50/5.91	15	30	258	1.48	2.52	2.01	1.68	2.54	2.06
Phosphoglycerate kinase 1	20	AT3G12780	50/5.91	23	42	507	1.32	1.43	1.51	1.63	1.90	2.18
Phosphoglycerate kinase	20	AT1G56190	43/5.39	17	35	315	1.32	1.43	1.51	1.63	1.90	2.18
Phosphoglycerate kinase 1	21	AT3G12780	50/5.91	19	32	343	1.31	2.06	2.04	1.62	1.89	2.31
Phosphoglycerate kinase	21	AT1G56190	43/5.39	12	22	200	1.31	2.06	2.04	1.62	1.89	2.31
GAPDH B subunit	22	AT1G42970	48/6.33	24	44	485	1.95	2.55	3.07	2.70	3.39	4.30
Phosphoribulokinase	24	AT1G32060	45/5.71	28	68	718	2.71	3.10	2.75	2.65	2.89	2.13
Adenosine kinase 1	25	AT3G09820	38/5.29	11	33	166	1.50	1.60	2.20	1.94	2.14	2.00
Adenosine kinase 2	25	AT5G03300	38/5.14	10	28	153	1.50	1.60	2.20	1.94	2.14	2.00
Sedoheptulose-1,7-bisphosphatase	26	AT3G55800	43/6.17	23	46	434	1.75	1.71	2.32	1.42	1.94	2.54
Fructose-bisphosphate aldolase	27	AT3G52930	39/6.05	20	48	329	1.66	1.87	2.59	1.83	1.86	2.86
Fructose-bisphosphate aldolase	27	AT2G36460	39/7.01	8	26	101	1.66	1.87	2.59	1.83	1.86	2.86
Fructose-bisphosphate aldolase	27	AT5G03690	39/7.60	4	11	78	1.66	1.87	2.59	1.83	1.86	2.86
Chloroplast stem-loop binding protein	28	AT3G63140	44/8.54	24	44	494	1.21	2.27	2.29	1.50	2.74	3.03
Sedoheptulose-1,7-bisphosphatase	29	AT3G55800	43/6.17	21	33	229	1.24	2.16	2.97	1.50	1.75	2.09
Malate dehydrogenase	30	AT1G04410	36/6.11	20	51	325	1.19	1.32	2.48	1.27	1.31	2.58
Malate dehydrogenase	30	AT5G43330	36/6.33	9	24	123	1.19	1.32	2.48	1.27	1.31	2.58
Isoflavone reductase	31	AT1G75280	34/5.66	11	23	197	1.62	1.83	2.65	1.61	1.71	2.69
NADH/NADPH-binding oxidoreductase	31	AT1G75290	35/5.83	2	4	68	1.62	1.83	2.65	1.61	1.71	2.69

Supplementary Table 2 continous

a) Protein Name	b) Spot No.	c) Accession Number	d) Mass/pI	e) Mascot Score			f) Avg ratio (WT)			g) Avg ratio (*gsnor*)		
				Unique Peptide	Seq. Cover	Protein Score	0.8 ppm	1.5 ppm	3 ppm	0.8 ppm	1.5 ppm	3 ppm
PM associated cation-binding protein 1	32	AT4G20260	25/4.99	12	45	121	-1.20	-1.52	-3.85	-1.05	-1.25	-3.41
Protein binding	33	AT1G55480	38/8.19	21	37	188	1.59	1.80	2.26	1.98	2.58	2.54
Ferredoxin:NADP(H) oxidoreductase 1	34	AT5G66190	41/8.32	22	48	297	1.20	1.75	2.05	1.09	1.81	2.13
Reduced sugar response 4	34	AT5G01410	33/5.79	11	24	68	1.20	1.75	2.05	1.09	1.81	2.13
Ferredoxin:NADP(H) oxidoreductase 2	34	AT1G20020	40/8.65	11	17	62	1.20	1.75	2.05	1.09	1.81	2.13
Phosphoglycolate phosphatase	35	AT5G36790	40/6.89	22	49	546	-1.01	1.35	2.08	1.03	1.53	2.14
2-phosphoglycolate phosphatase 1	35	AT5G36700	40/6.89	22	49	546	-1.01	1.35	2.08	1.03	1.53	2.14
2-phosphoglycolate phosphatase 2	35	AT5G47760	33/5.05	2	3	104	-1.01	1.35	2.08	1.03	1.53	2.14
PSII-Oxygen evolving complex 1	36	AT5G66570	35/5.55	21	53	393	2.02	2.31	2.21	1.89	2.22	2.05
Photosystem subunit O2	36	AT3G50820	35/5.92	15	38	248	2.02	2.31	2.21	1.89	2.22	2.05
Carbonic anhydrase 2	37	AT5G14740	29/5.36	19	53	309	1.40	1.53	2.16	1.42	1.45	1.45
Carbonic anhydrase 1	37	AT3G01500	30/5.54	12	30	141	1.40	1.53	2.16	1.42	1.45	1.45
Haloacid dehalogenase-like hydrolase	38	AT3G48420	35/8.31	15	40	171	1.21	1.67	2.34	1.35	1.65	2.47
Nudix hydrolase homolog 3	38	AT1G79690	87/5.27	13	16	60	1.21	1.67	2.34	1.35	1.65	2.47
Ribulose-phosphate 3-epimerase	39	AT5G61410	30/8.24	10	32	113	1.74	1.98	2.21	2.25	1.98	2.56
Glutathione S-transferase F 2	40	AT4G02520	24/5.92	18	65	472	1.36	1.70	2.17	1.32	1.61	1.80
Glutathione S-transferase F 3	40	AT2G02930	24/6.25	9	29	226	1.36	1.70	2.17	1.32	1.61	1.80
Photosystem II subunit P1	41	AT1G06680	24/7.71	14	47	292	1.37	1.58	1.76	1.61	1.84	2.32
Photosystem II subunit P2	41	AT2G30790	28/9.01	7	28	150	1.37	1.58	1.76	1.61	1.84	2.32
Glutathione S-transferase F 2	42	AT4G02520	24/5.92	21	78	634	1.64	2.34	3.16	1.73	2.23	2.38
Glutathione S-transferase F 3	42	AT2G02930	24/6.25	9	29	255	1.64	2.34	3.16	1.73	2.23	2.38
Ferretin 1	43	AT5G01600	28/5.73	13	20	196	-2.11	-2.37	-2.42	-1.37	-1.53	-1.24
Fe-superoxide dismutase 1	44	AT4G25100	21/6.16	6	17	94	-1.32	-1.35	-1.93	1.37	1.38	1.47
Cyclophilin 20-3	46	AT3G62030	29/8.83	20	52	474	-1.64	-1.81	-2.45	-1.71	-1.96	-2.53
Chloroplast stem-loop binding protein	47	AT3G63140	44/8.54	11	18	146	1.41	1.49	1.18	1.81	2.24	2.08
Ascorbate peroxidase 1	48	AT1G07890	28/5.85	10	31	104	1.30	1.35	-1.11	-1.88	-3.64	-3.68
Ascorbate peroxidase 1	49	AT1G07890	28/5.85	15	45	200	-1.48	-1.86	-2.51	-1.77	-3.91	-3.22

Supplementary Table 2 continous

a) Protein Name	b) Spot No.	c) Accession Number	d) Mass/p*I*	e) Mascot Score			f) Avg ratio (WT)			g) Avg ratio (*gsnor*)		
				Unique Peptide	Seq. Cover	Protein Score	0.8 ppm	1.5 ppm	3 ppm	0.8 ppm	1.5 ppm	3 ppm
Type VII myosin 2	50	AT5G54280	118/8.83	19	19	60	1.22	2.27	2.71	1.96	2.21	2.27
Large subunit of RUBISCO	51	ATCG00490	53/5.88	23	41	219	1.87	2.10	2.66	2.57	2.66	3.84
ATPase alpha subunit	52	ATCG00120	55/5.19	19	33	291	1.20	1.89	2.22	1.91	2.26	3.25
Galacturonosyltransferase 3	52	AT4G38270	78/7.27	15	29	74	1.20	1.89	2.22	1.91	2.26	3.25
Phosphoribulokinase	53	AT1G32060	45/5.71	16	49	190	1.29	1.92	3.46	1.08	2.40	2.25
Adenosine kinase 2	53	AT5G03300	38/5.14	12	33	118	1.29	1.92	3.46	1.08	2.40	2.25
Ribonuclease III family protein	53	AT4G37510	63/9.35	12	30	59	1.29	1.92	3.46	1.08	2.40	2.25
RAB GTPase homolog E1B	54	AT4G20360	52/5.84	11	23	62	-1.17	-1.38	-2.46	-1.20	-1.40	-2.79
Glutathione S-transferase F 2	55	AT4G02520	24/5.92	10	33	71	1.33	1.77	2.61	1.40	1.78	2.47
ATP-dep Clp protease proteolytic subunit	55	AT4G17040	34/9.34	7	18	66	1.33	1.77	2.61	1.40	1.78	2.47
Cyclophilin 20-3	57	AT3G62030	35/9.24	12	25	73	-1.77	-2.01	-2.12	-1.73	-2.06	-1.97

The table shows list of identified proteins from *Arabidopsis thalina* leaves with a significant change in their abundance due to NO exposure. Using Decyder BVA module change in the average standardized abundance from three independent experiment was estimates. Proteins were identified using MALDI-TOF/TOF MS.

a) Identified proteins with a significant protein score set to 58 against TAIR peptide database; b) Number assigned for the identified spot on 2D gel; c) Protein accession number that best matches identified peptides on the TAIR database; d) Molecular mass in Da and isoelectric point (p*I*); e) MASCOT software was used to parse MS data to identify proteins from primary sequence databases. Number of unique peptides, sequence coverage and protein score are given; f) Average ratio of the protein abundance between WT control and NO treated plants (0.8ppm, 1.5ppm and 3.0ppm). The values highlighted in blue represents a significant change in the average ratio =>2.0 with *p*-value of ANOVA analysis set to 0.1; f) Average ratio of the protein abundance between *gsnor* control and NO treated plants (0.8ppm, 1.5ppm and 3.0ppm). The values highlighted in blue represents a significant change in the average ratio =>2.0 with p-value of ANOVA analysis set to 0.1

Supplementary Table 3 – Protein and transcripts with similar regualtion.

Locus Tag	Name	Transcripts		Protein	
		WT	KO	WT	KO
AT1G06680	Photosystem II Subunit P-1	2.4	3.8	1.8	2.3
AT1G20020	Ferredoxin-NADP(+)-Oxidoreductase 2	2.0	3.5	2.1	2.1
AT1G32060	Phosphoribulokinase	1.9	3.3	2.8	2.1
AT1G42970	Glyceraldehyde-3-phosphate dehydrogenase	1.9	3.0	3.1	4.3
AT1G54040	Epithiospecifier Protein	1.9	1.9	2.0	2.2
AT1G55480	Binding (protein binding)	1.4	1.8	2.3	2.5
AT1G56190	Phosphoglycerate kinase (putative)	2.0	2.5	2.0	2.3
AT1G62750	Snowy Cotyledon 1	1.2	1.5	2.1	2.6
AT1G75280	Isoflavone reductase (putative)	1.4	1.8	2.7	2.7
AT2G02930	Glutathione-S-transferase F3	2.2	1.6	2.2	1.8
AT2G15620	Nitrite reductase 1	2.6	3.5	2.0	2.2
AT2G30790	Photosystem II subunit P-2	1.8	2.0	1.8	2.3
AT2G39730	Rubisco activase	1.6	2.5	2.1	2.3
AT3G01500	Carbonic anhydrase 1	12.5	7.7	2.2	1.5
AT3G12780	Phosphoglycerate kinase 1	1.9	2.6	2.0	2.3
AT3G12915	GTP binding / GTPase	-1.6	-1.5	2.2	2.3
AT3G17820	ATGSKB6	-1.1	-1.4	2.4	2.9
AT3G19050	Phragmoplast orienting kinesin 2	1.8	1.3	2.8	2.2
AT3G48420	Haloacid dehalogenase-like hydrolase protein	1.4	2.0	2.3	2.5
AT3G50820	Photosystem II Subunit oxygen evolving	2.4	3.9	2.2	2.1
AT3G52930	Fructose-bisphosphate aldolase (putative)	1.4	1.1	2.6	2.9
AT3G55800	Sedoheptulose bisphosphatase	1.4	2.3	2.3	2.5
AT3G60750	Transketolase (putative)	2.1	3.1	2.9	2.9
AT3G62030	Peptidyl-prolyl cis-trans isomerase	1.6	2.4	-2.1	-2.0
AT3G63140	Chloroplast stem-loop binding protein 41KDA	1.8	2.7	2.3	3.0
AT4G02520	Glutathione-S-transferase PHI 2	2.6	2.2	2.6	2.5
AT4G20260	DREPP PM polypeptide family protein	-1.6	-2.6	-3.9	-3.4
AT4G25100	Fe Superoxide dismutase 1	1.5	4.3	-1.9	1.5
AT4G30710	Hypothetical protein	1.0	1.5	2.8	2.2
AT4G33010	Glycine decarboxylase P-protein 1	1.2	1.7	2.1	2.1
AT5G01410	Reduced sugar response 4	-1.0	1.3	2.1	2.1
AT5G01600	ATFER1; ferric iron binding / iron ion binding	-1.8	-1.5	-2.4	-1.2
AT5G14740	Carbonic anhydrase 2	4.0	6.5	2.2	1.5
AT5G35630	Glutamine synthetase 2	1.6	2.4	2.4	2.9
AT5G36700	2-Phosphoglycolate phosphatase 1	1.4	2.7	2.1	2.1
AT5G42020	BIP2; ATP binding	-1.2	-1.2	-2.1	-2.7
AT5G43330	Malate dehydrogenase (putative)	1.0	-1.3	2.5	2.6
AT5G47760	2-Phosphoglycolate phosphatase	-1.2	-1.3	2.1	2.1
AT5G61410	Ribulose-phosphate 3-epimerase	1.2	1.6	2.2	2.6
AT5G66190	Ferredoxin-NADP(+)-oxidoreductase 1	1.4	2.0	2.1	2.1
AT5G66570	PS II oxygen-evolving complex 1	1.9	2.8	2.2	2.1

A fold change of 1.5 or above

A fold change of 2.0 or above in transcript level and protein level for WT and *atgsnor*-KO plants

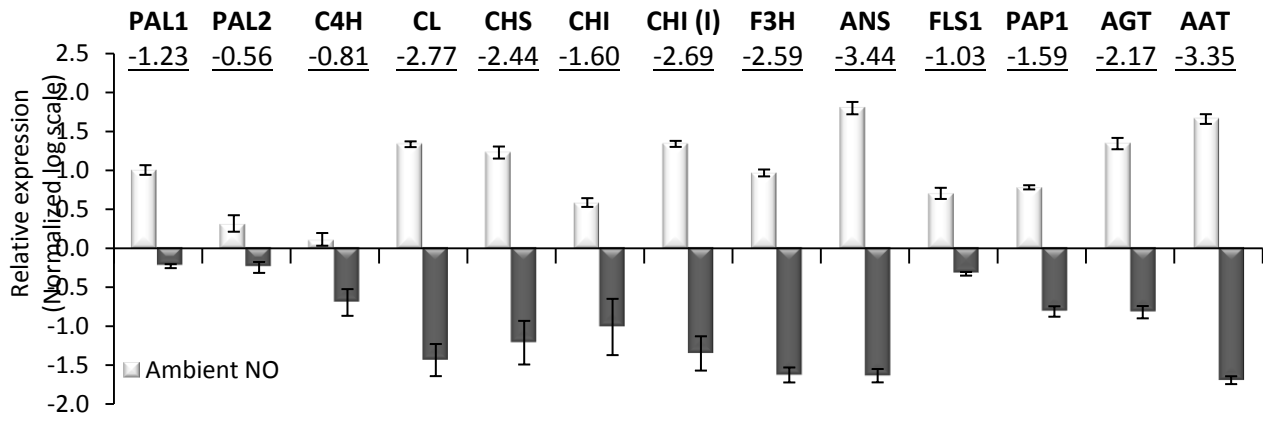

Supplementary Figure 1- Regulated genes in the phenylpropanoid pathway.
The graph shows the microarray results of differential regulation pattern of some of the important genes involved in the phenylpropanoid pathway by long-term NO exposure of *Arabidopsis thaliana*. Name of the gene and the fold change of the regulation in log scale are shown in the graph just above corresponding bar. Data is from four-week old WT plants. ±SD determined from three independent microarray experiments. *Gsnor*-KO plants too showed a similar regulation pattern. Full names of the genes are given in Figure 24.

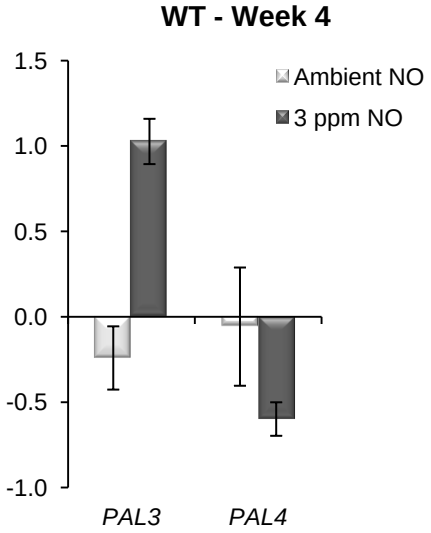

Supplementary Figure 2 – Regulation of *PAL3* and *PAL4* genes (microarray)

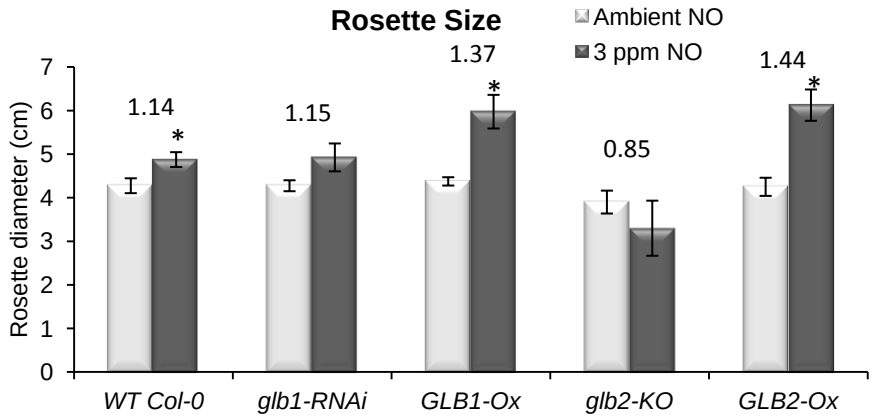

Supplementary Figure 3 - Rosette size of the NO treated plants

Four-week old rosettes were excised out and the diameter of circle that perfectly fits the rosette was measured. ±SD determined from four biological repeats. Number above the measurement bar in each plant line represents the rosette size ratio of 3 ppm NO plants to ambient NO plants. * denotes significant difference in the rosette size after NO treatment ($p \leq 0.01$).

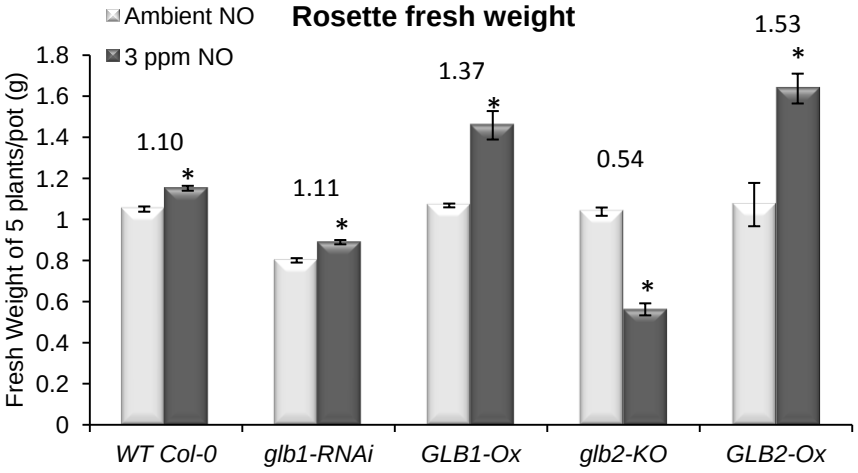

Supplementary Figure 4 – Rosette fresh weight of NO treated plants.

Four-week old rosettes were excised to remove root and shoot and weighed immediately. All the five rosettes grown on a single pot were weighed together and were treated as a single reading. Four such readings were taken from one biological repeat. Number above the measurement bar in each plant line represents the fresh weight ratio of 3 ppm NO plants to ambient NO plants. * denotes significant difference in the rosette size after NO treatment ($p \leq 0.01$).

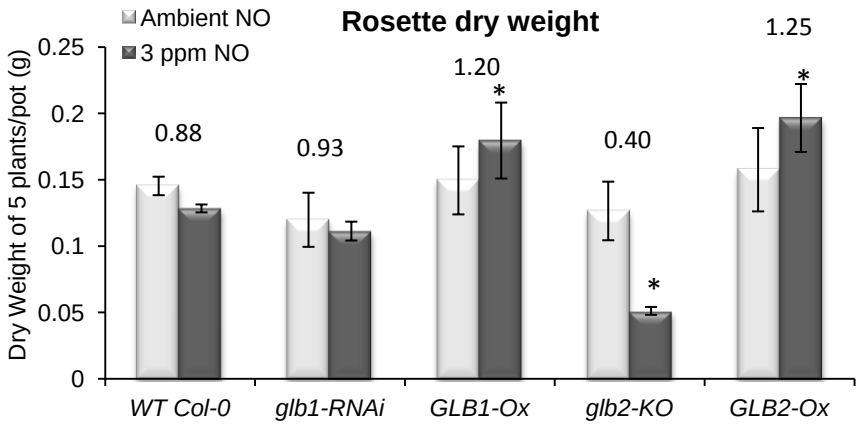

Supplementary Figure 5 – Rosette dry weight of NO treated plants.

Four-week old rosettes were excised to remove root and shoot and were dried by overnight incubation at 60 °C and weighed. All the five rosettes grown on a single pot were weighed together and were treated as a single reading. Four such readings were taken from one biological repeat. Number above the measurement bar in each plant line represents the dry weight ratio of 3 ppm NO plants to ambient NO plants. . * denotes significant difference in the rosette size after NO treatment ($p \leq 0.01$).

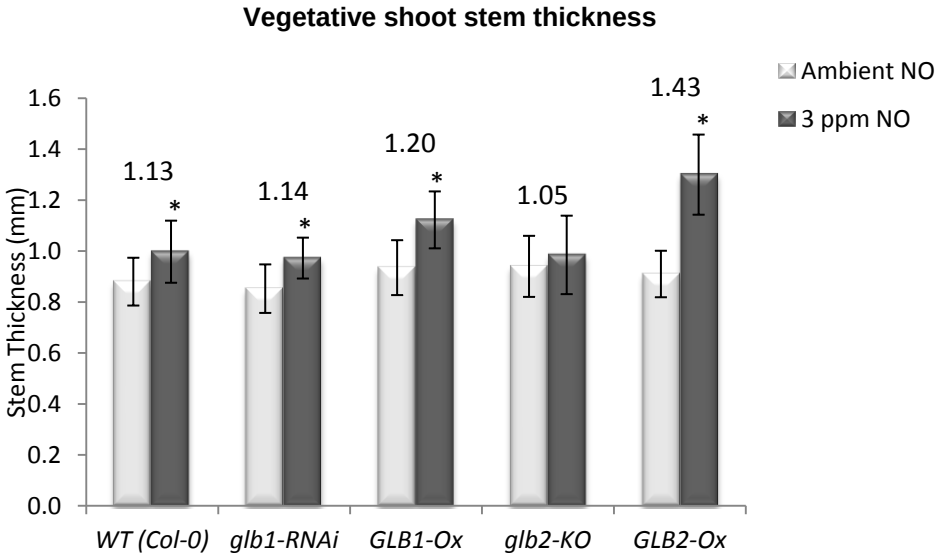

Supplementary Figure 6 – Vegetative shoot stem thickness of NO treated plants

Thickness of vegetative shoot stem of the six week old plants (n = 20) was measured using vernier calipier. Number above the measurement bar in each plant line represents the fresh weight ratio of 3 ppm NO plants to ambient NO plants. * denotes significant difference in the rosette size after NO treatment ($p \leq 0.01$).

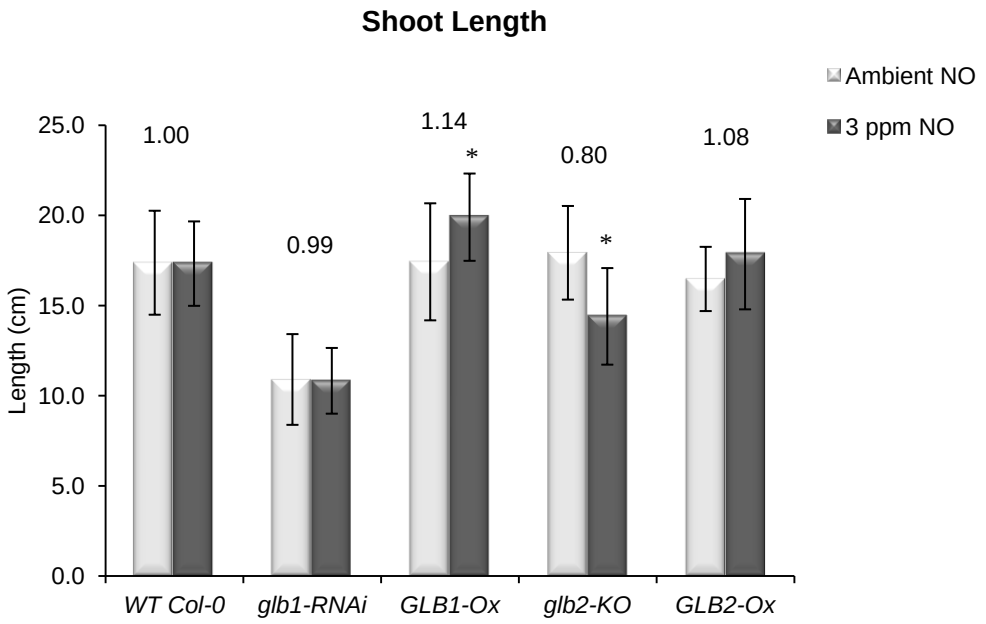

Supplementary Figure 7 – Shoot length of NO treated plants

Shoot length of the six week old plants (n = 20) was measured. Number above the measurement bar in each plant line represents the fresh weight ratio of 3 ppm NO plants to ambient NO plants. * denotes significant difference in the rosette size after NO treatment ($p \leq 0.01$).

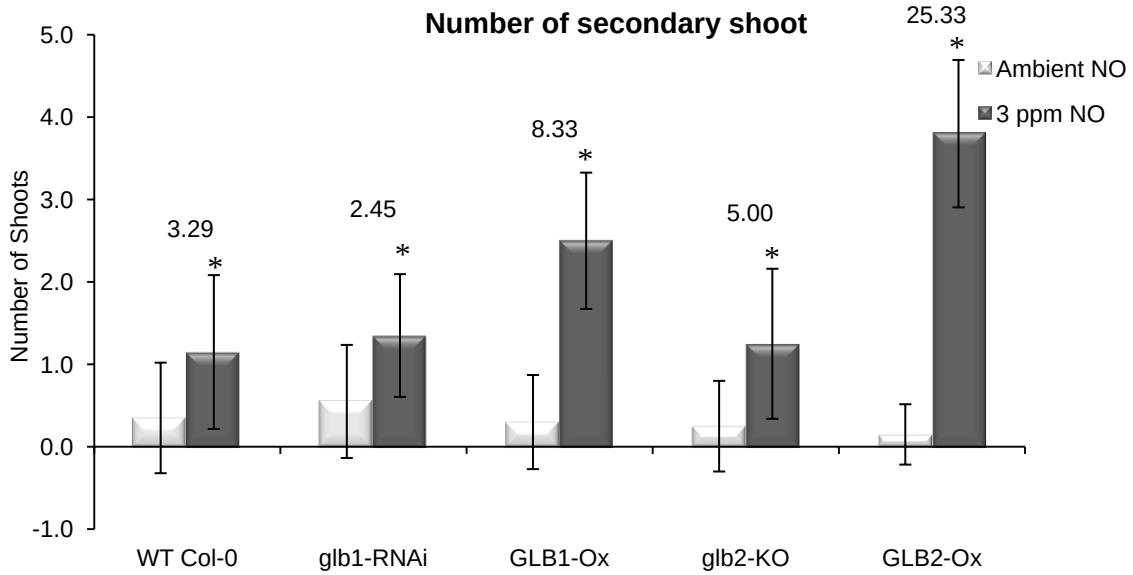

Supplementary Figure 8 – Number of shoots on NO treated plants

Shoot length of the six week old plants (n = 20) was measured. Number above the measurement bar in each plant line represents the fresh weight ratio of 3 ppm NO plants to ambient NO plants. * denotes significant difference in the rosette size after NO treatment ($p \leq 0.01$).

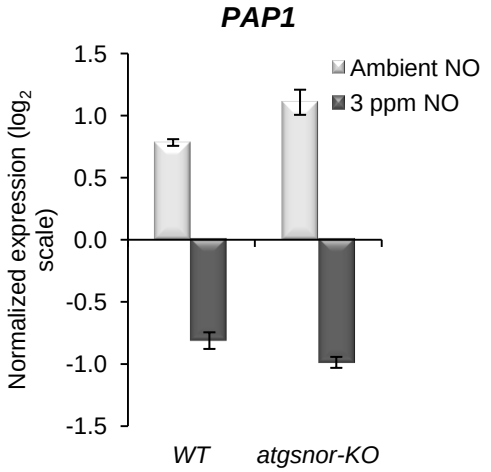

Supplementary Figure 9 - Regulation of *PAP1* transcript (microarray).

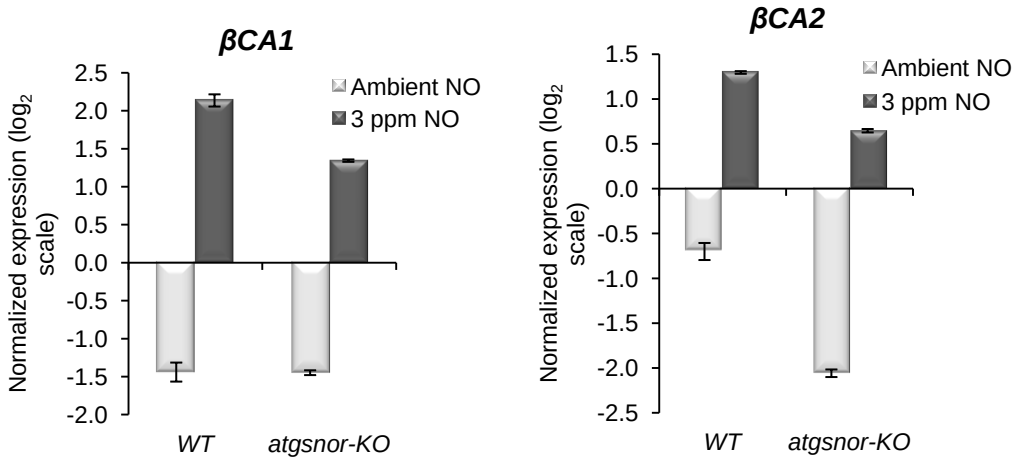

Supplementary Figure 10 - Regulation of *βCA1* and *βCA2* transcripts (microarray).

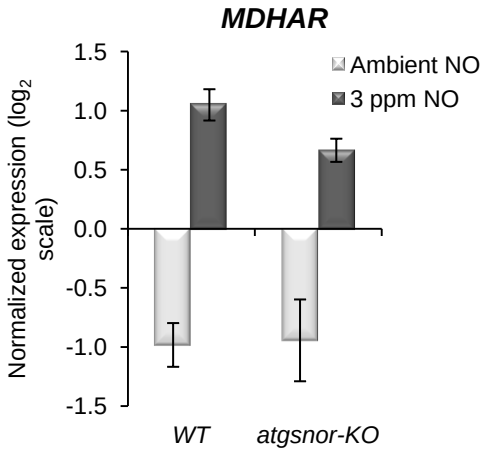

Supplementary Figure 11 – Regulation of *MDHAR* transcripts (microarray)

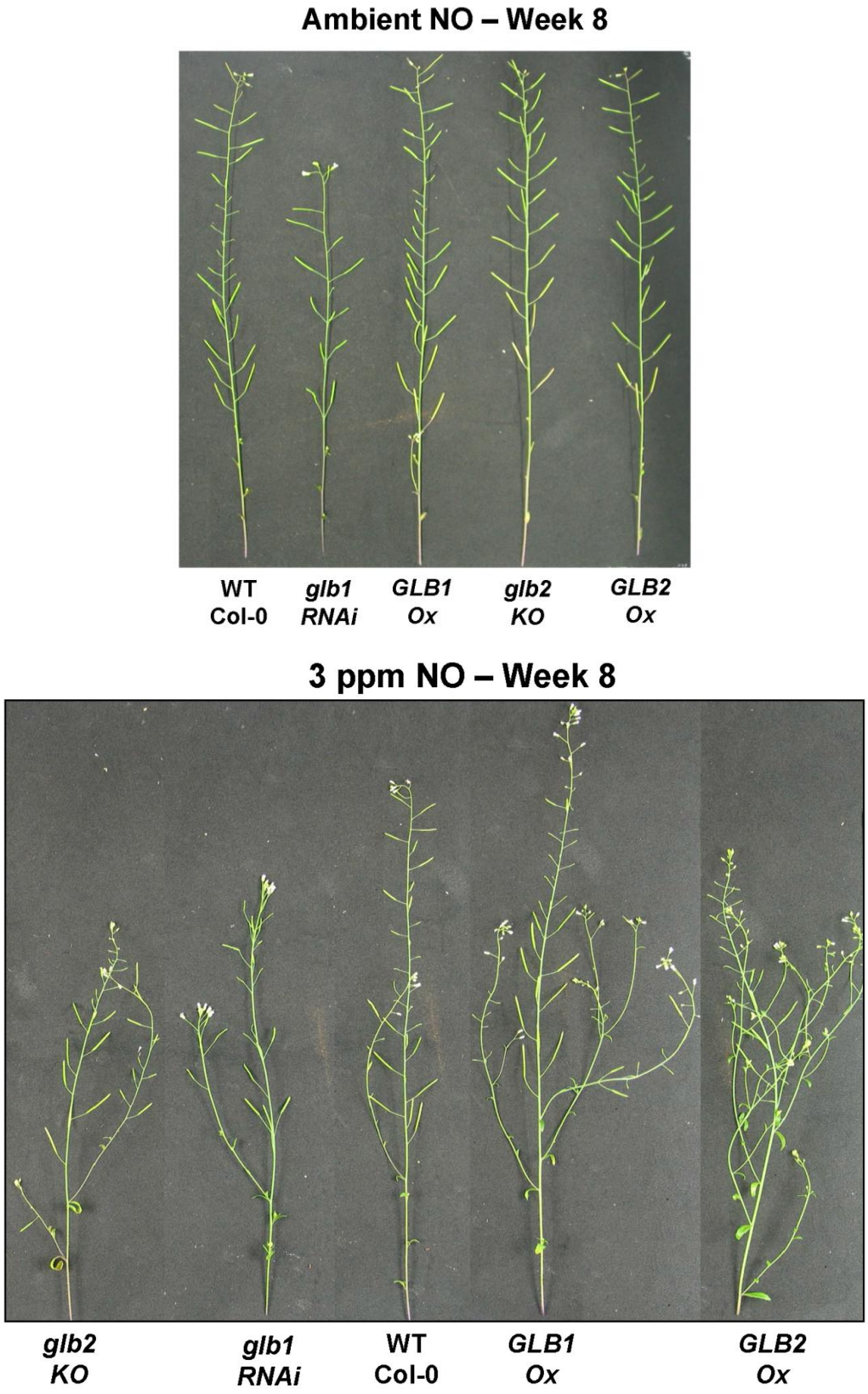

Supplementary Figure 12 – Vegetative shoot of NO fumigated plants.

9 ACKNOWLEDGEMENTS

First, I would like to thank my PhD supervisors Prof. Dr. Jörg Durner and Dr. Christian Lindermayr for providing me the opportunity to do my PhD project work in their laboratory at Helmholtz Zentrum München, Germany. Guidance and mentorship of Prof. Dr. Jörg Durner made my PhD work a thoughtful and rewarding journey. Dr. Christian Lindermayr intellectual heft is matched only by his genuinely good nature and down-to-earth humility, and I am truly fortunate to have had the opportunity to work with him.

I am highly obliged to Prof. Dr. Claus Schwechheimer for appearing as the second examiner and Prof. Dr. Ralph Hückelhoven for accepting the chairmanship in my doctoral examination.

I would like to thank Asst. Prof. Dr. Kim Hebelstrup from Aarhus University, Denmark for generously providing me with the *Arabidopsis* seeds for my thesis work.

I feel grateful to Prof. Dr. Jörg-Peter Schnitzler and his colleagues from EUS (Research Unit Environmental Simulation), Helmholtz Zentrum München for their constant help in setting up the plant growth chambers and NO fumigation facility. Also, I would like to thank Mr. Rüdiger Kuhnke from EUS for helping me in quantifying plant pigments using HPLC.

I would also like to express my gratitude to ‘protein core facility’ in Helmholtz Zentrum München for performing MALDI-TOF MS-MS, Prof. Dr Michalke Bernhard for performing soil analysis and Dr. Werner Heller and Ms. Susanne Stich for analyzing secondary metabolites.

I want to thank Dr. Frank Gaupels, Dr. Andreas Fröhlich, Mr. Christian Holzmeister, Ms. Elke Mattes, Ms. Rosina Ludwig, Ms. Lucia Gößl, Ms. Birgit Geist, Ms. Evi Bieber, and all the members in our group for their technical suggestions and help during my work.

Also, I would like to thank all the staff and colleagues in BIOP, especially Dr. Malay Das, Dr. Veronica von Saint Paul, Dr. Stephan Dräxl and Ms. Wei Zhang for providing a pleasant working atmosphere at the institute.

Last but not least, I am grateful to all my family members in India, especially my wife Jency, father, mother and brother for their encouragement which enable me to complete my thesis work on time.